NACA TN 3940

NATIONAL ADVISORY COMMITTEE FOR AERONAUTICS

TECHNICAL NOTE 3940

IMPACT-LOADS INVESTIGATION OF CHINE-IMMERSED MODELS HAVING CONCAVE-CONVEX TRANSVERSE SHAPE AND STRAIGHT OR CURVED KEEL LINES

By Philip M. Edge, Jr.

Langley Aeronautical Laboratory
Langley Field, Va.

FOR REFERENCE

NOT TO BE TAKEN FROM THIS ROOM

Washington
February 1957

NATIONAL ADVISORY COMMITTEE FOR AERONAUTICS

TECHNICAL NOTE 3940

IMPACT-LOADS INVESTIGATION OF CHINE-IMMERSED MODELS HAVING CONCAVE-CONVEX TRANSVERSE SHAPE AND STRAIGHT OR CURVED KEEL LINES

By Philip M. Edge, Jr.

SUMMARY

As part of an investigation of hydrodynamic impact loads on chine-immersed bodies of heavy beam loading, three narrow-beam models of concave-convex transverse shape and having, respectively, a straight keel, a curved bow, and a curved stern were tested at the Langley impact basin. The tests were made over a wide range of trim and initial-flight-path angles. Most of the landing impacts were made at a beam-loading coefficient of 18.77 with a few impacts at beam-loading coefficients of 27.39 and 36.15. The investigation was conducted primarily in smooth water; however, a few impacts with the curved bow were made in rough water.

The impact-loads data are presented in tables, and the derived coefficients of loads and motions are presented in figures as the variation with initial-flight-path angle. The experimental effects of transverse and longitudinal curvatures agree reasonably well with those predicted by theory. The concave-convex bottom, which was similar to shapes considered as being of constant-force type, yields slightly higher peak loads than a narrow-beam model having conventional vee bottom of equivalent angle of dead rise, with the possible exception of certain rough-water-impact conditions. The effect of stern curvature for the configurations tested is greater than the effect of bow curvature. The rough-water loads were found to be much greater than smooth-water loads for similar initial impact conditions and were in reasonable agreement with loads obtained from theory when the flight-path angle, velocity, and trim angle relative to the wave slope were used.

INTRODUCTION

In previous investigations of hydrodynamic impact loads on chine-immersed bodies of heavy beam loading, experimental data were obtained for straight-keel models of flat and vee transverse shapes. These data were presented in reference 1 for a model having 0° angle of dead rise

(flat bottom) and in reference 2 for the vee-shape model with 30° angle of dead rise. A theoretical method for predicting the impact loads on chine-immersed models having straight keel lines was developed and presented in reference 3. The values predicted by this method, which is based on the application of planing data, were shown to be in fairly good agreement with the experimental data for 0° and 30° angles of dead rise.

The present investigation extends the study of impact loads on chine-immersed prismatic bodies to transversely curved models with and without longitudinal curvature and includes a brief study of impacts in rough water.

The models used in the investigation were of concave-convex cross section, being convex near the keel with a reversal in curvature toward the chine. This shape was based on designs for which planing data were available. It so happened that this shape closely approximates configurations which have long been of interest as a possible approach to a constant-force time history during certain impact processes, particularly full-length zero-trim impacts of non-chine-immersed bodies. Studies of such impacts and configurations were made by Wagner in 1932 (ref. 4) and were continued in 1950 by Bisplinghoff and Doherty at the Massachuetts Institute of Technology (ref. 5) and in 1954 by Schulz at the Colorado Agricultural and Mechanical College (ref. 6). Since the transverse shape used in the present investigation is similar to those developed as constant-force-type bottoms, the data obtained in these tests may be considered to be indicative of the loads experienced by a chine-immersed model having a constant-force-type bottom tested with forward speed over a range of trim angles and flight-path angles. A brief discussion of some factors involved in such a comparison is included in this paper.

Three different configurations were tested with the same concave-convex transverse shape but with different longitudinal profiles - a straight keel, a curved bow, and a curved stern. The investigation consisted of a series of hydrodynamic impacts at the Langley impact basin for each of the models tested. The impacts were made over a range of trim and initial-flight-path angles at a beam-loading coefficient of 18.77 in smooth water; however, a few smooth-water impacts were made at beam-loading coefficients of 27.39 and 36.15 on the straight-keel and curved-bow models and a few rough-water impacts were made on the curved-bow model at a beam-loading coefficient of 18.77.

This paper presents the data obtained in this impact-loads investigation of chine-immersed models having concave-convex transverse shape and straight or curved keel lines. The maximum loads obtained are compared with those predicted by theory for the straight-keel case. The effects of transverse and longitudinal curvature are indicated, and a brief analysis is made of the rough-water impacts.

SYMBOLS

γ	flight-path angle relative to undisturbed water surface, deg
ρ	mass density of water, 1.938 slugs/cu ft
τ	trim angle, deg
τ_e	equivalent trim angle, deg
b	model beam, ft
θ	wave slope at point of contact, deg
g	acceleration due to gravity, 32.2 ft/sec^2
t	time after contact, sec
W	dropping weight, lb
n_i	impact load factor normal to undisturbed water surface, $\frac{F_v}{W}$
$\dot{x}$	velocity of model parallel to undisturbed water surface, fps
z	draft of model normal to undisturbed water surface, ft
$\dot{z}$	velocity of model normal to undisturbed water surface, fps
M_Y	pitching moment referred to step, lb-ft
F_n	hydrodynamic force normal to keel, lb
V	resultant velocity of model, fps
F_v	vertical component of hydrodynamic force, lb
C_L	impact lift coefficient, $\frac{n_i W}{\frac{1}{2}\rho V_o^2 b^2} = \frac{F_v}{\frac{1}{2}\rho V_o^2 b^2}$
C_d	draft coefficient, $\frac{z}{b}$
C_V	vertical-velocity coefficient, $\frac{\dot{z}}{\dot{z}_o}$

C_t time coefficient, $\frac{V_o t}{b}$

C_{cp} center-of-pressure coefficient, $\frac{\text{Center of pressure measured from step}}{b}$

C_m pitching-moment coefficient, $\frac{M_Y}{\frac{1}{2}\rho V_o^2 b^3}$

C_Δ beam-loading coefficient, $\frac{W}{\rho g b^3}$

Subscripts:

o at water contact

s referred to step (stern of model)

max maximum

w referred to surface of wave

APPARATUS

The impact-loads investigation reported herein was conducted in the Langley impact basin. A description of this facility and its equipment is given in reference 7.

Models

Two basic models were used in the tests: a longitudinally straight model 12 feet long and a model 10 feet long with the aft 5 feet straight and the forward 5 feet pulled up along an arc of 10-foot radius. The basic models were of light-sheet-metal construction with a bottom of wood covered with fiber glass being installed for this investigation. The models were equipped with a concave-convex transversely curved bottom with a beam of 1 foot. This bottom section consisted of a rounded keel of 3.4-inch radius and a concave curvature extending to the chine. Profiles of these models are presented in figure 1 and a cross-sectional view of the concave-convex bottom is shown in figure 2. Although the shape tested in this investigation was not developed as a constant-force-type bottom, its shape curve is between those for shapes developed as constant-force bottoms by M.I.T. and Colorado A. & M. College (fig. 3).

The models as tested are shown mounted on the impact-basin carriage in figure 4. Figure 4(a) shows the longitudinally straight model. Figures 4(b) and 4(c) show the longitudinally curved model mounted, respectively, as a curved-stern model and as a curved-bow model. The model was attached rigidly to the carriage beam through a load measuring dynamometer and was held fixed at each trim angle throughout the impact by this mounting.

Instrumentation

The instrumentation used consisted of a multi-channel oscillograph, accelerometers, a dynamometer, water-contact indicators, an optical wave-height recorder, and electrical pickups for measuring displacements and velocities. All measurements were recorded on the oscillograph except the wave height which was recorded separately.

Accelerations in the vertical direction were measured by three oil-damped strain-gage-type accelerometers having undamped natural frequencies of 60, 75, and 120 cycles per second. The outputs from these accelerometers were recorded on three galvanometers having frequencies of 17, 100, and 800 cycles per second, respectively. The values obtained with these accelerometers were compared, and, in tests in which there was no evidence of attenuation due to frequency response, the measurements from the lower frequency accelerometer were considered valid. In this manner, extraneous structural vibrations were eliminated by electrical fairing. Loads normal to the deck of the model and pitching moments about the forward attachment point were obtained from a strain-gage dynamometer mounted between the model and carriage boom. These measurements were corrected for the distribution of mass and center of gravity of the parts located below the dynamometer and those for the pitching moment were referred to the step. Only the corrected values of loads and moments about the step are presented. The initial contact of the model with the water and the rebound of the model from the water were determined by means of an electrical circuit completed by the water. Horizontal velocity was computed from photoelectric-cell measurements of horizontal displacement. Vertical velocity was obtained by electrical differentiation of a slide-wire output which measured vertical displacement.

The wave-height measurements were obtained from an NACA optical wave-height recorder which consists of a mercury arc lamp and a standard NACA film drum mounted in an instrument housing. The light from the mercury arc lamp is passed through a lens system which focuses a small image on the water surface. The image formed on the water surface is recorded by the film drum which is located so that the rise and fall of the water surface result in the trace moving across the film. The wave-height recorder was mounted in the nose of the carriage and measured the wave height just forward of the model. The wave-height record was correlated

with the oscillograph record by means of a common timing impulse on each record. The NACA optical wave-height recorder is described in detail in reference 8.

TEST PROCEDURE

This investigation consisted of a series of impacts in smooth water with each of the three models (straight keel, curved bow, and curved stern) and a few impacts in rough water with the curved-bow model. The smooth-water impacts were made at fixed trim angles and under conditions covering a wide range of trim angles and flight-path angles at a beam-loading coefficient of 18.77. Impacts were made at beam-loading coefficients of 27.39 and 36.15 at 8° trim over a range of flight-path angles for the straight-keel and curved-bow models only. The five rough-water tests were made at a fixed trim angle of 8° at flight-path angles from 1.5° to 7° for the curved-bow model at a beam-loading coefficient of 18.77 in waves $1\frac{1}{4}$ feet by 40 feet. The test conditions covered by the investigation are given in table I. The forward speeds ranged from 20 feet per second to 95 feet per second and the initial vertical velocity ranged from approximately 3 feet per second to 13 feet per second. Throughout the immersion a lift force equal to the total weight of the model and drop linkage was exerted on the model by means of the lift engine described in reference 7.

In order to check the consistency of the behavior of the instrumentation and equipment, at frequent intervals during the investigation repeat impacts were made with the test conditions as nearly identical as possible. The data obtained from these repeat impacts showed that no significant change occurred in the performance of the equipment and instrumentation during the investigation. The data obtained in these repeat impacts were averaged for each model and only these average values for each model are presented.

THEORETICAL COMPUTATIONS

In order to obtain theoretical impact loads for comparison with the data obtained in this investigation, the maximum impact loads were computed over the range of test conditions of this investigation by means of procedure 3 of reference 3. Procedure 3 is a theoretical method for determining smooth-water landing loads on bodies of arbitrary cross section for which experimental planing data are available. Planing data obtained at Langley tank no. 2 with a straight-keel model having the same cross section as the model of this investigation were used in these computations. Therefore, the impact loads determined in this manner were for the same conditions as the straight-keel runs of this investigation. The maximum

impact lift coefficients predicted by this method are shown in figures 5 and 6. Figure 5 shows the maximum impact lift coefficient plotted against angle of trim for each of five flight-path angles for the straight-keel model at a beam-loading coefficient of 18.77. Since planing data were available only for trim angles of 4° to 20°, the theoretical curves of figure 5 were extrapolated below 4° to 2°, as indicated by the dashed portion of the curves. By means of this extrapolation, theoretical values were obtained for comparison with the data obtained at 3° trim. Further extrapolation of these curves was considered too inaccurate to be of use at trim angles below 3° or appreciably above 20°.

From figure 5 several interesting observations can be made in regard to the variation of maximum impact load as predicted by theory with flight-path angle and trim angle. At low flight-path angles (10° and below), the angle of trim has little effect on the maximum impact load. At high flight-path angles (above 15°), the load increases rapidly as the angle of trim is reduced below 8°. At higher angles of trim (above 8°), the impact load is affected very little by changes in trim angle.

The effect of beam loading on maximum impact lift coefficient is shown in figure 6, wherein maximum impact lift coefficient is plotted against initial-flight-path angle for the straight-keel model at 8° trim for beam-loading coefficients of 18.77, 27.39, and 36.15. This figure shows that, as the beam loading is increased, the maximum impact lift coefficient becomes less sensitive to increases of initial-flight-path angle.

Since theoretical predicted loads are not available for curved-bow and curved-stern models, the curves of figures 5 and 6 for the straight-keel model were used throughout this analysis for comparisons with experimental data obtained for each model.

EXPERIMENTAL RESULTS AND COMPARISONS WITH THEORY

The experimental data obtained in this investigation are presented in tables II and III for each series of impacts made. As a means of analyzing these results, the data were converted into dimensionless coefficient form. In this manner the results obtained for each impact can be compared with results of all the other impacts, with trim and flight-path angles being the only variables for a given bottom shape, beam loading, and seaway condition. The maximum impact lift coefficient, the impact lift coefficient at the instant of maximum draft, the draft coefficients at the instants of maximum acceleration and maximum draft, the vertical-velocity coefficients at maximum acceleration and at rebound, the time coefficients at maximum acceleration, maximum draft, and rebound, and the

pitching-moment coefficient and the center-of-pressure coefficient at maximum acceleration were computed from the experimental data. These experimental coefficients were plotted against initial-flight-path angle for each angle of trim, and typical variations for each series of impacts made are presented.

Straight-Keel Model

Experimental values of the aforementioned coefficients were calculated for each of the impacts with the straight-keel model, and these coefficients are plotted against the initial-flight-path angle in figures 7 to 18. These data are presented for five trim angles (3°, 8°, 15°, 20°, and 30°) of the six trim angles tested at $C_{\Delta} = 18.77$ and for the only trim angle (8°) tested at $C_{\Delta} = 27.39$ and 36.15. The trend of each coefficient with initial-flight-path angle is shown by a line faired through the data points on each of the figures.

In addition to the experimental data, the maximum impact lift coefficient as predicted by theory (fig. 5) is shown in figures 7 and 8. The curves of figures 7 and 8 indicate that the agreement between loads obtained in this investigation and those predicted by theory is excellent for 8° angle of trim at all three beam loadings tested; however, the loads predicted by theory for 3° and 20° trim angles are somewhat low, the theoretical data at 20° trim being almost 10 percent less than the experimental data. It is noted that the data obtained at 3° trim angle are limited to flight-path angles below 14° and that the theoretical variation at 3° trim angle was taken from the extrapolated portion of the curves in figure 5.

Several observations can be noted from these variations of the coefficients with initial-flight-path angle. From figures 7, 9, and 13 it is observed that, as the angle of trim is increased from 3° to 30°, the coefficients of impact lift, draft, and time approach the same values for the instants of maximum acceleration and maximum draft; that is, as the trim angle is increased toward 30°, the instants of maximum acceleration approach the instants of maximum draft during the impact process. This observation is also apparent in figure 11 where the velocity at maximum acceleration is slightly reduced and the rebound velocity is increased (negatively) as the trim angle is increased to 30°. It is further observed from figures 15 and 17 that, as the trim angle is increased from 3° to 30°, the center of pressure at the instant of maximum acceleration moves toward the step, and the pitching moment about the step is reduced. The effects of beam loading can be observed from figures 8, 10, 12, 14, 16, and 18. These figures show that, as the beam-loading coefficient is increased from 27.39 to 36.15, all the coefficients increase in value with the exception of the impact lift coefficient at maximum draft (fig. 8)

and the vertical-velocity coefficients at maximum acceleration and at rebound (fig. 12); for these coefficients little effect of beam loading is indicated over the range of initial-flight-path angle tested.

Curved-Stern Model

Experimental values of the coefficients were calculated for each of the impacts made with the curved-stern model in smooth water at five trim angles tested, the trim angle being measured as the angle of the tangent at the stern. It is noted from figure 1 that the angle of the tangent at the stern is 30° to the angle of the bow half of the bottom. However, the angle of the bow portion of the model is of little consequence over the range tested since only the curved stern is involved during most of the immersion process. Because the profile of the curved stern is that of a circular arc, the various angles of trim tested are of significance primarily from the standpoint of the effect of the location of the termination of the circular-arc profile. The point of termination was varied from 22° aft of vertical to 16° forward of vertical with impact being made at corresponding angles of trim of -22°, -14°, 0°, 8°, and 16°.

Variations of the coefficients with initial-flight-path angle are presented in figures 19 to 24 for the curved-stern model. In general, these variations indicate that the scatter among the experimental data is very small for most of the trim angles. In parts (d) and (e) of figure 19, a comparison is made between the values of maximum impact lift coefficient for the curved-stern model and the experimental and theoretical values for the straight-keel model. Inasmuch as the maximum load is not significantly affected by a 1° change in trim (fig. 5), the curved-stern data are for an angle of trim of 16° and the straight-keel data are for an angle of trim of 15° (fig. 19(e)). These comparisons indicate reductions in maximum load at high initial-flight-path angles for the curved-stern model at angles of trim of 8° and 16°; however, these figures show that at maximum draft the loads on the curved-stern model are greater at 8° trim and about the same at 16° trim as those on the straight-keel model. It is noted from figure 19 that, as the trim angle is increased from -14° to 16°, the variation of maximum impact lift with initial-flight-path angle remains about the same; however, the impact lift at maximum draft increases and approaches the maximum lift at 16° trim.

The variation of draft coefficient with initial-flight-path angle is shown in figure 20 to be insignificant as the trim angle is increased to 16°. In figures 20(d) and 20(e) the draft coefficients obtained for the curved-stern model are compared with those of the straight-keel model and fairly close agreement is shown.

Figure 21 shows that the vertical-velocity coefficient at maximum acceleration is only slightly affected at high flight-path angles by trim angle; whereas, a reduction in vertical-velocity coefficient is indicated at low flight-path angles as the trim is increased to 16°. Increased (negatively) rebound velocities are indicated, however, as the trim is increased to 16°. From figure 22 it is observed that as the trim is increased there is little effect on time at maximum acceleration, a slight decrease in time at maximum draft, and a definite decrease in time at rebound.

Figure 23 shows that the center of pressure moves toward the step as the trim is increased to 16°; whereas, in figure 24 a decrease in pitching moment about the step is indicated only as the trim is increased from -14° to 0°.

Curved-Bow Model in Smooth Water

Experimental values of the coefficients were calculated for each of the impacts made with the curved-bow model in smooth water; these coefficients are plotted against the initial-flight-path angle in figures 25 to 36. These data are presented for four trim angles (-3°, 3°, 8°, and 16°) of the seven trim angles tested at $C_{\Delta} = 18.77$ and for the only trim angle (8°) tested at $C_{\Delta} = 27.39$ and 36.15.

The experimental values of maximum impact lift coefficient for the curved-bow model are compared in figures 25 and 26 with the variation for the straight-keel model as predicted by theory (figs. 5 and 6) and as obtained experimentally (figs. 7 and 8). These data show that the experimental loads tend to lie slightly below the variation obtained for the straight-keel model. This reduction in maximum load is believed to be caused by the immersion of the curved bow. The effect of bow immersion can be analyzed from the variation of draft coefficient with initial-flight-path angle as shown in figures 27 and 28. Included in these figures is the draft coefficient at which geometric bow immersion occurs for each angle of trim. It is observed from figure 27 that at a beam-loading coefficient of 18.77 bow immersion occurred before maximum acceleration for all impacts made at or below 3° trim angle; whereas, bow immersion occurred before maximum acceleration for those impacts made at 8° trim angle above an initial-flight-path angle of 12°. Although bow immersion occurred before maximum acceleration at or below 8° trim angle, figure 27 shows that less than one-half of the immersion before maximum acceleration at 3° trim involved the bow and even less than one-half was involved at 8° trim. The effects of bow immersion on maximum load at these trims, therefore, are expected to be small, as shown in figures 25(b) and (c). The experimental data plotted in figure 25(d) show that values of maximum impact lift coefficient for the curved-bow model at 16°

trim lie a little below the experimental variation obtained for the straight-keel model at 15° trim and a little above the variation predicted by theory for the straight-keel model at 16° trim. With this experimental scatter, agreement with the values obtained for the straight-keel model appears reasonable since there should be no effect of bow immersion present.

From figure 28 it can be observed that, at beam-loading coefficients of 27.39 and 36.15 at 8° angle of trim, geometric bow immersion occurred before maximum acceleration at initial-flight-path angles of about 6.5° and 5.4°, respectively.

Several observations can be made from the variation of vertical-velocity coefficient, time coefficient, center-of-pressure coefficient, and pitching-moment coefficient with initial-flight-path angle as shown in figures 29, 31, 33, and 35, respectively, for the curved-bow model in smooth water at several trim angles at a beam-loading coefficient of 18.77. As the trim angle is increased from 3° to 16°, the time coefficient at maximum draft and at rebound (fig. 31) and the pitching moment about the step (fig. 35) decrease and the center of pressure moves toward the step (fig. 33). For this same range of trim angle, the vertical-velocity coefficient at maximum acceleration decreases, and at rebound C_V increases negatively (fig. 29).

In general, the effect of increasing the beam-loading coefficient from 27.39 to 36.15 for the curved-bow model in smooth water at 8° trim is shown to be an increase in time, in location of center of pressure from the step, and in pitching moment about the step. (See figs. 30, 32, 34, and 36.) The vertical-velocity coefficient is affected less and shows only a slight increase at maximum acceleration and very little change at rebound.

Curved-Bow Model in Rough Water

Experimental values of the coefficients were calculated for each of the impacts made with the curved-bow model in $1\frac{1}{4}$- by 40-foot waves; these coefficients are plotted against the initial-flight-path angle in figure 37. This figure shows that in rough water there is wide scatter of the data and that a simple variation with initial-flight-path angle is not established. The scatter shown can be attributed largely to the variation of the location of the impacts along the wave profile. The variation of maximum impact lift coefficient with location of the impact along the wave profile is illustrated in figure 38 wherein the location of the stern at the instant of water contact on an average wave profile is shown. Although there were small localized variations in wave profile from impact to impact, the wave sizes and shapes were essentially the same.

The locations of the impacts along the wave profile were taken into account by using the slope of the wave surface at the point contacted by the model. When the values of these slopes were subtracted from the fixed trim angle of 8°, the angle of trim relative to the water surface was found to range from 3.0° to 6.9°. In order to obtain the initial-flight-path angle relative to the surface of the moving wave, the velocity of the wave was added to the model velocity and the flight-path angle computed by using this total velocity was obtained relative to the wave surface by addition of the wave slope.

The maximum impact lift coefficient was recomputed by using the velocity relative to the wave and these values of maximum impact lift coefficient are plotted against the initial-flight-path angle relative to the wave in figure 39. These values of maximum impact lift coefficient are compared in this figure with the variations of maximum lift predicted by theory for the straight keel at the upper and lower limits of trim angle (3.0° and 6.9°) relative to the water surface. This comparison shows that, although only a few tests were made over a small range of initial-flight-path angle, the variations predicted by theory for the maximum and minimum angles of trim relative to the wave are in fair agreement with the experimental values.

DISCUSSION OF RESULTS

The primary purpose of this investigation is to extend previous studies of impact loads on chine-immersed bodies of flat or vee cross section to the case of transversely curved bodies with and without longitudinal curvature. The data are of interest also to the problem of loads on constant-force-type bottoms. As already noted, the studies of references 4, 5, and 6 were concerned with the special case of full-length zero-trim impacts without chine immersion; however, the results of the present tests deal with quite different landing conditions of trimmed impacts involving appreciable chine immersion. Therefore, the results of the present investigation and those of the aforementioned studies are not directly comparable.

In the following sections, a discussion of some of the effects of transverse and longitudinal curvature on maximum hydrodynamic loads measured in this investigation is presented along with a brief discussion of the loads measured in the few rough-water impacts.

Transverse Curvature

Previous impact-basin investigations of transverse shapes on narrow-beam models have dealt only with flat-bottom models and vee-bottom models

having 30° angles of dead rise. These loads data were given in references 1 and 2 and were shown in reference 3 to be in reasonable agreement with loads predicted by theory. The present investigation in the Langley impact basin is the first with models having bottoms of transverse curvature. A comparison of the results presented in this report indicates reasonable agreement between loads predicted by theory and loads measured during actual impacts with forward speed for the constant-force-type transverse shape tested.

Inasmuch as experimental verification of the theory has been obtained for the flat bottom, vee bottom, and the constant-force-type bottom, the maximum loads as predicted by theory can be used as a means of comparing the loads for the three bottom shapes. The maximum loads predicted by theory for these three transverse shapes are presented in figure 40 as the variation of maximum impact lift coefficient with angle of trim for each of three initial-flight-path angles. The theoretical curves were obtained from computational procedures in reference 3. The solution for the vee bottom was for 17° dead rise, which is the approximate average angle of dead rise of the constant-force-type bottom tested. The comparison shown in figure 40 indicates that, at the low initial-flight-path angle of 5.5°, the maximum load on the constant-force-type bottom is almost the same as that on the vee-bottom model having 17° dead rise except at very low angles of trim. At high initial-flight-path angles and at high trim angles (above approximately $\tau = 7^\circ$ at 25° γ_o), the constant-force-type bottom yields greater loads than those predicted for a vee bottom of 17° dead rise. This figure indicates that, when compared with the vee bottom, the constant-force-type bottom shows a reduction in maximum load only at low angles of trim. This reduction at low trim angle appears more pronounced at the higher initial-flight-path angles. When the flight-path angle and trim angle are referred to the water surface, the high-flight-path-angle and low-trim-angle portion of figure 40 represents the landing conditions of rough-water landings where the seaplane is landing on the inclined surface of a relatively long wave; whereas, the low-flight-path-angle and high-trim-angle portion of this figure represents smooth-water landings or impacts on the back surface of a long wave. This comparison (fig. 40), therefore, indicates that, although slightly greater peak loads would be experienced by the constant-force-type bottom in smooth water than by the vee bottom with an equivalent angle of dead rise, a reduction in peak load might be expected under certain conditions of rough-water landings.

Longitudinal Curvature

The incorporation of longitudinal curvature especially in the bow region of seaplane hulls has been widely used; however, little experimental data have been obtained in order to isolate and to determine the effect of longitudinal curvature on maximum impact loads. Results

obtained from impact-basin tests of a narrow-beam model having a curved bow and straight stern and of the same model with a straight bow and curved stern are presented in this section. Also presented are results obtained from impact-basin tests of a narrow-beam straight-keel model of the same type bottom. If the loads data or the theoretically predicted values of maximum load for the straight-keel model are compared with the maximum loads obtained on the longitudinally curved models, the effect of longitudinal curvature can be indicated.

The results presented for the curved-bow model showed the maximum loads to be slightly less than the maximum loads obtained for the straight-keel model (fig. 25). However, the results presented for the curved-stern model showed the maximum-load data to be appreciably less than the loads predicted by theory for the straight-keel model having the same value for the trim angle as that for the angle of the tangent at the stern (fig. 19). The small effect of bow curvature on the maximum impact load is explained by the fact that most of the impact process involves only the straight portion of the model and the curved portion becomes involved too late to affect greatly the maximum load (figs. 27 and 28); however, since the curved portion of the curved-stern model is involved from the instant of water contact, the load is affected throughout the impact process.

An effort was made to analyze the effect of longitudinal curvature on maximum impact load. It was apparent that longitudinal curvature can be compared to landing at an increased angle of trim. From the characteristic variation of maximum impact load with trim angle (fig. 5), it is observed that longitudinal curvature (increased trim angle) would be of greater consequence in the low trim-angle range than at the high trim-angle range.

As a means of comparing the maximum loads on a longitudinally curved model with those on a longitudinally straight model, an equivalent angle of trim was chosen for each trim angle except for -22°, the angle at which the range of flight-path angle was too small to obtain a comparison (fig. 19). This equivalent trim angle was taken as the average of the trim angles along the immersed portion at the instant of maximum load. For -14° angle of trim, the equivalent trim angle was the average of the trim angles of the immersed portion from the forward water line to the point of maximum draft. In this manner, the negative curvature at the rear of the model was considered to have little effect on the load. The maximum loads are shown in figure 41; in this figure maximum impact lift coefficient is plotted against initial-flight-path angle for four of the trim angles tested. These experimental values are compared with those of maximum impact lift coefficient predicted by theory for a straight-keel model at the average equivalent trim angle for each trim angle shown. For most of the impacts, the equivalent trim angle was approximately the same as the given angle of trim except for $\tau_s = -14^\circ$, the angle at which

the equivalent trim angle varied between approximately 7° and 11°. Although the scatter is large at $\tau_s = -14°$, the general agreement of these experimental loads with the maximum impact loads predicted by theory indicates that these loads can be approximated by use of the average trim angle of the curved portion at the time of maximum load.

Rough Water

The resulting maximum impact loads from the five rough-water impacts were presented in figure 37 as the variation of maximum impact lift coefficient with the initial-flight-path angle and in figure 39 as the variation of maximum impact lift coefficient relative to the wave surface with the initial-flight-path angle relative to the wave surface. These figures show that the maximum impact loads are greatly dependent upon the seaway and that, by taking into account the wave velocity and slope, a trend of the load with initial-flight-path angle can be established relative to the wave.

If the wave velocities are assumed to be approximately the same for each of the impacts at 8° trim angle, the slope of the wave at the point where the impact occurs becomes an important parameter in determining the maximum impact load. In order to illustrate the effect of rough water in terms of wave slope, the maximum impact lift coefficient obtained from the experimental data was divided by the maximum impact lift coefficient predicted by theory for smooth water under identical landing-approach conditions and this ratio was plotted against wave slope at the point of contact (fig. 42). This figure shows that the increase in load due to rough water can be several times that due to smooth water and that the amount of load increase varies with wave slope for the conditions of these impacts. In regard to the landing conditions of these impacts, it is noted that the ratio of wave length to model length is 4, that all the impacts occur on the forward flank of the wave, and that the wave slopes approach the trim angle of the model (8°). This increase in load as the trim angle of the model approaches the slope of the water surface is in general agreement with the theoretical variation of maximum load with trim angle as shown in figure 5.

If the flight-path angle, trim angle, and velocity relative to the sloping wave surface are used, the impact process is rotated and treated as smooth-water-impact conditions for the purpose of predicting the maximum impact loads. In figure 43, load coefficients relative to the wave are plotted against load coefficients calculated for these smooth-water-impact conditions for each impact from theory. Considering the limited data and wide scatter, this figure indicates that the maximum loads predicted by rotating the axis and applying smooth-water theory are in substantial agreement with the measured loads of this investigation.

Observations on the Constant-Force-Type Bottom

The close similarity of the model tested to shapes derived to obtain constant-force impact loads for the idealized conditions of zero trim, vertical drop, and no chine immersion permits speculation on the maximum impact loads that might be expected on such configurations under the more realistic conditions of forward-speed landings with trim angle and chine immersion. The data of this investigation have shown that at low trim angles and high flight-path angles (i.e., conditions almost the same as those for the idealized case) lower maximum impact loads are indicated than would be predicted for a vee bottom of the same average dead-rise angle. However, for other landing conditions more representative of those that would be encountered in normal seaplane operations, the maximum loads experienced by the constant-force-type bottom are greater than those which would be predicted for the vee-bottom hull. Although it might be possible to design a shape to give a substantially constant impact force for any given landing condition, for routine seaplane operations such a design might result in an irregular load time history for many types of impacts, with the possibility of higher peak loads than for the conventional-vee-bottom hull.

CONCLUSIONS

An analysis of experimental data obtained in an impact-basin investigation of a concave-convex transverse-shape bottom mounted on narrow-beam models having straight and curved keel lines leads to the following conclusions:

1. For conditions of this investigation, the maximum impact loads experienced by the concave-convex or constant-force-type bottom are greater than those predicted for the conventional-vee-bottom model of equivalent dead-rise angle for typical smooth-water conditions. Although there are indications of possible load reductions under certain rough-water conditions, the results obtained show that, in general, the curved surface of the bottom tested yields maximum loads that are similar to the maximum loads to be expected with the vee bottom of equivalent angle of dead rise.

2. Load on irregular-shaped narrow-beam models of the constant force type tested can be computed with reasonable accuracy by using procedure 3 of NACA Technical Report 1152 provided that the necessary planing data are available. The loads predicted by theory, however, are less than those obtained in experiment for high angles of trim, by almost 10 percent at 20° angle of trim.

3. The effect of longitudinal curvature of the forward half of the model was a slight reduction in loads for tests in which the curved bow was immersed.

4. Longitudinal curvature of the stern half of the model results in a significant reduction in maximum impact loads as compared with loads obtained for the straight-keel model. The maximum loads obtained were approximately the same as those that would be predicted for a straight-keel model at the average trim angle of the curved portion involved at the time of maximum load.

5. Maximum impact loads obtained in the five rough-water impacts indicate possible maximum loads several times those experienced in smooth water for the same approach conditions. The severity of these loads was shown to vary with the slope of the portion of the wave contacted by the model. Theoretical approximation of loads of the type experienced by these impacts was shown to be possible by using the flight-path angle, velocity, and trim angle relative to the slope of the wave surface contacted.

Langley Aeronautical Laboratory,
National Advisory Committee for Aeronautics,
Langley Field, Va., November 13, 1956.

REFERENCES

1. McArver, A. Ethelda: Water-Landing Investigation of a Model Having Heavy Beam Loadings and 0° Angle of Dead Rise. NACA TN 2330, 1951.

2. Batterson, Sidney A., and McArver, A. Ethelda: Water Landing Investigation of a Model Having a Heavy Beam Loading and a 30° Angle of Dead Rise. NACA TN 2015, 1950.

3. Schnitzer, Emanuel: Theory and Procedure for Determining Loads and Motions in Chine-Immersed Hydrodynamic Impacts of Prismatic Bodies. NACA Rep. 1152, 1953. (Supersedes NACA TN 2813.)

4. Wagner, Herbert: Über Stoss- und Gleitvorgänge an der Oberfläche von Flüssigkeiten. Z.a.M.M., Bd. 12, Heft 4, Aug. 1932.

5. Bisplinghoff, R. L., and Doherty, C. S.: A Two-Dimensional Study of the Impact of Wedges on a Water Surface. Contract No. NOa(s)-9921, Dept. Aero. Eng., M.I.T., Mar. 20, 1950.

6. Schulz, E. F.: Development of a Constant-Force Bottom Contour for Seaplane Hulls. Rep. No. 54EFS31 (Contract No. NOas52-332-c, Bur. Aero.), Dept. Civil Eng., Colorado A. & M. College, Nov. 1954.

7. Batterson, Sidney A.: The NACA Impact Basin and Water Landing Tests of a Float Model at Various Velocities and Weights. NACA Rep. 795, 1944. (Supersedes NACA WR L-163.)

8. Edge, Philip M., Jr.: Instrumentation for Investigation of Seaplane Impact Loads in Waves. Proc. First Conf. on Coastal Eng. Instruments (Berkeley, Calif., Oct. 31 - Nov. 2, 1955), Council on Wave Res., The Eng. Foundation, 1956, pp. 213-226.

TABLE I

TEST CONDITIONS

Beam-loading coefficient, C_{Δ}	Weight, W, lb	Trim angle, τ, deg	Initial-flight-path angle, γ, deg	Number of runs
Straight-keel model in smooth water				
18.77	1170	3, 6, 8, 15, 20, 30	2.75 to 28.63	76
27.39	1707	8	3.41 to 19.00	5
36.15	2253	8	3.29 to 19.16	8
Curved-bow model in smooth water				
18.77	1170	-3, 0, 3, 4, 8, 12, 16	3.13 to 23.62	78
27.39	1707	8	3.35 to 21.63	8
36.15	2253	8	3.39 to 19.14	8
Curved-bow model in rough water ($1\frac{1}{4}$' x 40' waves)				
18.77	1170	8	1.62 to 6.96	5
Curved-stern model in smooth water				
18.77	1170	-22, -14, 0, 8, 16	2.96 to 23.89	35

TABLE II

IMPACT-LOADS DATA FROM TESTS OF NARROW-BEAM MODELS WITH A CONSTANT-FORCE-TYPE BOTTOM

Run	τ, deg	At contact: $\dot{z}_o$, fps	$\dot{x}_o$, fps	γ_o, deg	At $n_{1,max}$: t, sec	n_1	F_n, lb	z, ft	$\dot{z}$, fps	M_Y, lb-ft	At z_{max}: t, sec	n_1	z, ft	At rebound: t, sec	$\dot{z}$, fps
Straight-keel model in smooth water; C_Δ = 18.77															
1		4.40	80.00	3.15	0.090	0.90	1087	0.317	2.78	2,823	0.222	0.40	0.444	0.627	-1.12
2		10.15	68.26	8.46	.058	2.64	3184	.521	7.23	13,335	.235	.87	.964	.649	-2.78
3	3	10.19	60.42	9.57	.053	2.63	3136	.473	7.77	11,362	.250	.88	1.017	.680	-2.65
4		10.15	51.41	11.17	.061	2.36	2976	.537	7.68	12,321	.266	.83	1.112	.732	-2.96
5		11.54	47.39	13.68	.054	2.94	3523	.524	8.71	14,557	.295	.68	1.273	.794	-3.19
6		4.71	80.00	3.37	.095	1.09	1362	.388	2.83	2,418	.176	.47	.479	.454	-2.33
7		4.56	78.74	3.39	.124	.96	1079	.378	1.82	3,151	.174	.67	.419	.457	-2.22
8		10.42	69.69	8.50	.075	2.41	3047	.608	6.91	7,870	.212	.83	.930	.608	-3.28
9		10.51	66.89	8.93	.072	2.24	2778	.676	6.42	6,503	.197	1.01	.943	.577	-3.55
10		11.31	49.02	12.99	.078	2.32	2739	.679	7.72	8,899	.264	.67	1.172	.844	-2.47
11		10.96	46.84	13.17	.075	2.02	2388	.642	8.04	5,984	.265	.54	1.168	.855	-2.67
12		12.68	51.68	13.79	.064	2.63	3165	.675	8.82	8,846	.249	.74	1.189	.777	-3.52
13		5.57	20.96	14.88	.101	.54	555	.467	4.45	1,548	.447	.24	1.046	1.362	-1.26
14		12.80	47.28	15.15	.064	2.50	3062	.670	9.25	8,607	.264	.65	1.255	.854	-3.10
15		5.66	20.65	15.33	.109	.55	571	.488	4.45	2,032	.439	.25	1.016	1.319	-1.26
16		12.75	44.35	16.04	.065	2.57	3159	.694	9.11	9,644	.285	.59	1.324	.910	-2.92
17		12.75	44.15	16.11	.067	2.49	3056	.694	9.20	9,544	.287	.58	1.317	.901	-2.92
18		11.05	38.10	16.17	.072	1.87	2228	.662	8.40	5,857	.312	.49	1.337	.979	-2.74
19	6	12.71	39.99	17.63	.069	2.30	2821	.716	9.47	8,288	.314	.42	1.413	1.006	-3.01
20		11.05	34.42	17.80	.072	1.90	2363	.679	8.53	6,919	.357	.39	1.448	1.094	-2.33
21		12.66	39.29	17.86	.090	2.34	2916	.692	9.38	8,876	.227	.42	1.416	1.032	-2.92
22		12.75	34.84	20.10	.068	2.18	2646	.688	9.71	7,435	.356	.44	1.551	1.034	-3.14
23		9.34	24.75	20.68	.047	1.28	1443	.661	4.85	5,254	.388	.33	1.384	1.194	-3.23
24		9.34	24.45	20.91	.082	1.24	1406	.627	7.18	3,896	.404	.34	1.390	1.271	-3.05
25		10.87	27.87	21.31	.073	1.60	1987	.641	8.53	5,542	.292	.35	1.502	1.189	-2.78
26		11.23	28.57	21.46	.075	1.70	2112	.710	8.53	6,579	.395	.42	1.636	1.122	-2.83
27		11.00	27.93	21.50	.069	1.55	1848	.607	8.71	4,916	.386	.39	1.469	1.236	-3.01
28		12.80	31.25	22.27	.072	2.22	2719	.690	9.65	7,956	.355	.43	1.529	1.033	-3.14
29		11.18	26.85	22.61	.081	1.67	1898	.726	8.13	6,738	.381	.43	1.532	1.139	-2.69
30		8.80	21.10	22.64	.081	1.08	1271	.593	6.87	3,744	.420	.34	1.419	1.275	-1.89
31		8.94	20.86	23.20	.083	1.00	1165	.614	6.56	3,178	.437	.32	1.472	1.313	-1.80
32		12.08	28.17	23.21	.073	1.86	2507	.713	9.25	9,045	.383	.47	1.624	1.093	-3.28
33		8.89	20.66	23.28	.079	1.10	1312	.596	6.94	3,666	.429	.32	1.432	1.269	-1.84
34		4.98	93.02	3.06	.095	1.56	1911	.345	2.20	3,337	.133	1.30	.373	.303	-3.42
35		4.40	81.63	3.09	.112	1.11	1313	.382	1.93	2,635	.162	.90	.410	.367	-2.96
36		3.28	51.15	3.67	.133	.51	510	.302	1.57	985	.218	.42	.326	.532	-1.57
37		3.28	46.62	4.03	.151	.47	550	.371	1.80	882	.246	.41	.442	.619	-1.71
38		3.77	47.62	4.53	.087	.55	1000	.307	2.78	3,345	.232	.45	.482	.622	-1.75
39	8	10.19	47.62	12.08	.078	1.89	2366	.661	7.45	5,248	.260	.71	1.153	.776	-2.96
40		11.31	49.02	12.99	.076	2.14	2783	.714	8.08	6,654	.192	.76	1.206	.780	-2.96
41		10.51	33.67	17.34	.074	1.49	1777	.663	8.31	3,597	.324	.51	1.400	1.040	-2.51
42		11.36	34.48	18.24	.072	1.78	2279	.682	9.11	5,114	.327	.49	1.482	1.038	-2.22
43		11.40	29.41	21.19	.072	1.72	2237	.687	9.34	5,478	.366	.46	1.606	1.192	-1.89
44		11.36	27.40	22.52	.086	1.59	1868	.765	8.31	6,140	.379	.43	1.599	1.153	-2.87
(a)		10.42	67.64	8.77	.081	2.38	2946	.649	6.51	7,183	.185	1.29	.865	.526	-4.16
45		3.77	78.43	2.75	.120	1.25	1533	.297	.94	2,191	.135	1.17	.301	.289	-2.92
46		9.43	61.54	8.71	.094	2.18	2663	.695	5.16	5,243	.167	1.65	.852	.419	-5.30
47		9.43	42.46	11.97	.050	1.53	1775	.792	8.62	4,079	.240	.93	1.141	.648	-4.04
48		12.35	44.05	15.66	.092	2.21	2690	.900	8.31	6,507	.207	1.12	1.347	.606	-5.07
49		5.61	19.55	16.10	.180	.44	463	.763	3.59	1,150	.475	.24	1.175	1.450	-1.44
50	15	9.38	28.40	18.28	.106	1.17	1325	.880	6.60	3,474	.331	.55	1.476	.992	-3.01
51		12.39	34.72	19.64	.088	1.89	2298	.914	9.09	5,217	.292	.60	1.581	.868	-4.09
52		12.44	34.78	19.68	.087	1.92	2321	.872	9.14	5,118	.300	.68	1.546	.855	-4.04
53		7.63	20.28	20.62	.163	.67	761	.925	6.96	2,048	.447	.32	1.528	1.415	-2.93
54		9.52	17.44	28.63	.116	.88	1301	.925	7.36	5,171	.494	.33	1.957	.149	-1.98
55		3.64	78.13	2.67	.121	1.32	1669	.288	.81	2,166	.128	1.31	.292	.270	-3.05
56		9.43	62.11	8.63	.116	2.23	2743	.728	4.53	4,858	.174	1.85	.842	.396	-6.02
57	20	9.34	43.48	12.12	.116	1.60	1935	.862	5.52	4,590	.230	1.12	1.135	.573	-4.94
58		8.94	27.62	18.97	.137	1.05	1256	1.000	5.79	2,995	.347	.60	1.489	.945	-3.50
59		8.89	17.54	26.88	.150	.76	902	1.141	6.38	2,281	.500	.35	2.009	1.523	-2.29
60		4.13	79.05	2.99	.124	1.70	2352	.303	4.50	2,665	.119	1.68	.307	.244	-4.04
61		8.89	62.50	8.10	.115	2.21	2937	.730	3.64	4,291	.159	2.03	.803	.353	-6.82
62		8.80	55.25	9.05	.117	2.01	2696	.770	4.18	4,475	.171	1.85	.871	.388	-6.69
63		11.65	54.35	12.10	.126	2.56	3276	.822	6.02	5,104	.132	2.27	1.044	.396	-8.04
64	30	9.43	43.86	12.13	.122	1.65	2184	.898	4.53	3,805	.217	1.48	1.110	.508	-4.89
65		12.48	43.48	16.01	.106	2.12	2763	1.027	7.86	4,838	.230	1.57	1.372	.527	-7.27
66		8.44	28.17	16.68	.174	.95	1284	1.172	4.67	2,437	.337	.70	1.507	.868	-4.18
67		12.39	39.22	17.53	.114	1.93	2439	1.107	7.97	4,790	.240	1.43	1.497	.597	-6.82
68		8.94	24.63	19.95	.177	.89	1265	1.239	5.34	2,502	.371	.60	1.668	.980	-3.95
Straight-keel model in smooth water; C_Δ = 27.39															
69		4.85	81.30	3.41	.116	.98	1791	.444	2.65	4,277	.191	.91	.535	.448	-3.19
70		10.42	71.43	8.30	.091	2.08	3708	.775	6.51	12,622	.225	.94	1.116	.633	-3.95
71	8	11.00	52.91	12.00	.088	1.85	3256	.842	7.68	11,136	.298	.69	1.465	.900	-3.05
72		10.96	42.46	14.96	.100	1.59	2830	.912	8.04	9,752	.357	.59	1.690	1.134	-2.69
73		10.32	32.84	19.00	.089	1.39	2445	.852	8.35	8,866	.453	.32	1.907	1.398	-2.29

[a] Average of eight consistency runs.

TABLE II - Continued

IMPACT-LOADS DATA FROM TESTS OF NARROW-BEAM MODELS WITH A CONSTANT-FORCE-TYPE BOTTOM

Run	τ, deg	At contact: $\dot{z}_o$, fps	$\dot{x}_o$, fps	γ_o, deg	At $n_{1,max}$: t, sec	n_1	F_n, lb	z, ft	$\dot{z}$, fps	M_r, lb-ft	At z_{max}: t, sec	n_1	z, ft	At rebound: t, sec	$\dot{z}$, fps
Straight-keel model in smooth water; C_Δ = 36.15															
74	8	4.49	78.13	3.29	0.143	0.68	1592	0.489	2.33	3,776	0.248	0.50	0.578	0.613	-2.11
75		5.03	79.37	3.63	.104	.87	2074	.428	3.10	5,127	.222	.65	.569	.552	-2.70
76		10.10	69.97	8.33	.097	1.64	3809	.824	6.87	13,568	.277	.78	1.304	.758	-3.52
77		10.33	69.44	8.46	.100	1.72	4017	.883	6.60	15,843	.273	.80	1.337	.768	-3.46
78		10.87	52.36	11.73	.098	1.48	3426	.897	8.04	13,495	.358	.50	1.679	1.054	-3.19
79		11.05	51.55	12.10	.096	1.54	3607	.907	8.22	14,875	.361	.49	1.696	1.084	-2.74
80		10.91	39.19	15.29	.099	1.26	2944	.925	8.44	11,726	.473	.30	2.075	1.602	-2.07
81		10.96	31.55	19.16	.095	1.15	2669	.941	8.80	10,815	.554	.31	2.383	1.622	-2.50
Curved-bow model in smooth water; C_Δ = 28.77															
82	-3	5.52	90.91	3.47	.114	1.24	1415	.448	2.52	11,418	.159	1.12	.497	.416	-2.35
83		12.48	84.75	8.38	.037	2.78	3251	.427	10.09	20,283	.154	2.12	.912	.430	-3.65
84		12.22	82.64	8.41	.085	3.00	3530	.399	10.01	20,926	.128	2.11	.928	.364	-4.96
85		12.14	70.43	9.78	.039	2.82	3234	.392	10.09	18,772	.180	1.64	1.014	.483	-4.26
86		11.70	66.67	9.95	.036	2.58	3007	.374	9.83	17,089	.178	1.38	1.063	.499	-4.00
87		11.79	59.00	11.30	.036	2.64	2970	.374	10.18	16,287	.213	1.00	1.085	.589	-3.52
88		10.57	49.26	12.11	.033	2.31	2662	.356	9.66	14,585	.272	.56	1.184	.765	-3.48
89	0	5.57	87.72	3.63	.046	1.36	1652	.219	4.52	6,894	.153	.93	.414	.399	-1.96
90		12.22	83.33	8.34	.045	3.70	4269	.325	9.92	17,499	.160	1.84	.813	.408	-4.48
91		12.18	74.35	9.30	.029	3.28	3858	.305	10.01	15,293	.187	1.14	.918	.553	-2.44
92		12.35	62.70	11.14	.029	3.25	3895	.300	9.79	15,397	.183	1.25	.906	.595	-3.70
93		12.40	58.48	11.97	.024	3.24	3760	.322	9.87	15,006	.190	1.17	1.005	.594	-2.78
94		12.31	51.02	13.57	.029	3.06	3601	.318	9.96	13,633	.230	.91	1.150	.706	-2.39
95		12.44	42.19	16.43	.030	3.00	3418	.307	10.27	12,578	.279	.72	1.213	.864	-2.09
96	3	5.50	89.29	3.53	.065	1.58	1960	.278	3.44	5,123	.172	.81	.473	.674	-.39
97		11.87	80.65	8.37	.044	3.40	3998	.482	7.78	14,097	.164	1.57	.994	.584	-1.20
98		12.05	59.17	11.51	.048	3.03	3337	.513	9.31	11,870	.215	1.10	1.432	.739	-1.48
99		12.56	61.35	11.57	.050	3.24	3677	.532	8.43	13,734	.216	1.16	1.282	.709	-1.98
100		12.44	42.37	16.36	.043	2.71	3234	.358	10.51	11,377	.286	.69	1.218	1.185	-.22
101		6.44	21.83	16.44	.075	.89	929	.423	5.39	3,006	.415	.29	1.107	----	----
102		7.18	23.70	16.85	.063	.89	----	.399	6.00	----	.423	.34	1.240	----	----
103		10.14	32.47	17.34	.048	1.79	2188	.331	8.79	7,056	.353	.42	1.252	----	----
104		12.66	40.49	17.36	.049	2.61	2757	.551	10.18	9,865	.293	.61	1.379	----	----
105		9.96	31.65	17.47	.051	1.74	1891	.430	8.31	6,189	.358	.44	1.327	----	----
106		11.61	33.33	19.20	.049	2.49	2917	.504	9.16	9,959	.327	.62	1.497	----	----
107	4	5.48	90.91	3.45	.080	1.46	1772	.352	3.18	4,414	.160	.85	.436	.433	-2.13
108		11.53	86.96	7.55	.050	3.04	3737	.492	8.44	11,151	.170	1.35	.835	.557	-2.31
109		12.18	58.82	11.70	.050	2.60	3212	.597	9.22	9,594	.215	.93	1.092	.790	-1.48
110		10.53	47.96	12.38	.058	2.00	2444	.532	8.13	7,706	.265	.80	1.128	.982	-1.09
111		11.79	42.19	15.61	.055	2.24	2697	.541	9.48	8,528	.280	.60	1.298	1.061	-1.22
112		9.44	33.11	15.91	.065	1.33	1582	.528	7.40	4,649	.348	.39	1.307	----	----
113		6.66	22.52	16.48	.080	.80	845	.479	5.48	3,038	.452	.26	1.212	----	----
114		10.79	32.47	18.38	.053	2.15	2626	.584	9.83	8,083	.328	.53	1.582	----	----
115	8	5.03	86.96	3.31	.099	1.30	1646	.334	2.20	2,704	.138	1.184	.396	.321	-3.28
116		10.33	74.63	7.88	.082	2.43	2937	.631	5.79	7,959	.162	1.359	.737	.448	-4.58
117		11.85	82.64	8.16	.069	2.89	3686	.637	7.36	8,441	.154	1.682	.844	.526	-4.71
118		11.18	50.20	12.56	.076	1.95	2400	.662	7.77	6,348	.238	.789	1.110	.816	-3.59
119		9.79	34.13	16.01	.081	1.24	1514	.633	7.41	3,939	.340	.445	1.329	1.120	-1.75
120		12.21	42.37	16.08	.072	1.97	2461	.723	8.89	6,920	.272	.733	1.342	.899	-3.01
121		6.70	21.61	17.22	.123	.61	505	.662	5.00	1,272	.485	.210	1.332	----	----
122		6.33	18.12	19.26	.105	.49	537	.547	4.98	1,372	.500	.221	1.263	----	----
123		12.08	33.78	19.68	.071	1.78	2181	.723	9.29	6,275	.325	.540	1.558	----	----
124		12.01	31.35	20.92	.081	1.72	2171	.745	9.27	6,554	.347	.470	1.583	----	----
125		7.09	14.93	25.40	.136	.53	562	.751	4.94	1,809	.512	.232	1.472	----	----
(a)		12.27	59.80	11.60	.070	2.54	3176	.691	8.40	8,473	.205	1.05	1.093	.625	-3.82
126	12	4.53	82.61	3.14	.103	1.52	1894	.269	.99	2,525	.120	1.489	.269	.239	-3.59
127		9.92	71.94	7.85	.089	2.28	2761	.606	5.21	5,668	.158	1.721	.730	.393	-4.98
128		11.90	83.33	8.13	.085	3.12	4071	.671	5.97	8,109	.141	2.318	.788	.349	-6.87
129		10.60	72.99	8.26	.071	2.58	3254	.544	6.24	6,290	.143	1.765	.708	.362	-5.52
130		11.54	79.37	8.27	.061	3.05	3806	.627	5.07	8,541	.128	2.234	.727	.325	-6.29
131		10.87	58.82	10.47	.085	2.18	2642	.708	6.11	6,055	.276	1.355	.912	.484	-4.67
132		12.62	62.89	11.35	.077	2.59	3230	.507	7.72	7,032	.186	1.435	1.070	.489	-5.61
133		11.90	58.82	11.44	.081	2.42	2982	.717	7.45	6,477	.190	1.357	.996	.509	-4.71
134		11.94	39.68	16.75	.086	1.84	2132	.667	9.52	3,609	.265	.765	1.348	1.032	-3.41
135		10.96	34.72	17.52	.087	1.50	1715	.770	7.63	4,420	.300	.581	1.357	1.053	-2.56
136		12.21	30.96	21.52	.091	1.61	1841	.866	8.76	5,195	.324	.547	1.567	1.610	-2.11
137	16	5.16	94.34	3.13	.095	1.77	2318	.309	1.53	2,682	.112	1.72	.315	.260	-3.50
138		5.25	88.50	3.49	.094	1.87	2417	.309	1.44	2,896	.104	1.84	.312	.235	-4.40
139		10.28	70.42	8.31	.091	2.49	3065	.652	5.03	5,597	.142	1.98	.752	.316	-6.38
140		10.28	69.44	8.42	.085	2.67	3427	.622	5.12	5,786	.131	2.04	.714	.321	-6.29
141		12.26	59.17	11.71	.088	2.62	3284	.757	7.09	6,762	.176	1.62	.971	.452	-5.79
142		12.39	58.48	11.96	.089	2.58	3202	.785	7.27	6,905	.173	1.67	1.023	.458	-6.05
143		12.35	58.14	11.99	.086	2.56	3201	.815	7.32	6,970	.169	1.75	1.039	.439	-6.24
144		9.43	33.11	15.90	.107	1.18	1384	.307	6.42	3,185	.307	.61	1.296	.933	-2.56
145		11.94	41.67	15.99	.089	1.89	2243	.959	7.99	5,224	.238	1.00	1.292	.684	-4.45
146		12.67	39.22	16.57	.096	1.78	2008	.857	7.86	4,823	.258	.90	1.298	.840	-3.41
147		6.91	23.04	16.69	.162	.53	652	.669	4.62	1,267	.464	.28	1.388	----	----
148		9.29	30.67	16.85	.102	1.03	1174	.773	6.69	2,575	.322	.55	1.336	1.017	-2.29
149		11.99	35.84	18.50	.095	1.54	1786	.884	8.44	4,395	.334	.63	1.527	1.014	-2.74
150		12.12	30.86	21.44	.095	1.53	1782	.931	8.49	4,610	.324	.68	1.598	.997	-3.10
151		6.11	13.97	23.62	.166	.41	425	.452	5.75	1,003	.596	.18	1.477	----	----

[b] Average of eight consistency runs.

TABLE II - Concluded

IMPACT-LOADS DATA FROM TESTS OF NARROW-BEAM MODELS WITH A CONSTANT-FORCE-TYPE BOTTOM

Run	τ, deg	At contact			At $n_{1,max}$						At z_{max}			At rebound	
		$\dot{z}_o$, fps	$\dot{x}_o$, fps	γ_o, deg	t, sec	n_1	F_n, lb	z, ft	$\dot{z}$, fps	M_Y, lb-ft	t, sec	n_1	z, ft	t, sec	$\dot{z}$, fps
Curved-bow model in smooth water; C_Δ = 27.39															
152	8	5.09	86.96	3.35	0.106	1.07	1956	0.417	2.78	3,926	0.180	0.87	0.501	0.456	-2.44
153		11.48	80.65	8.10	.076	2.43	4496	.727	5.96	13,587	.191	1.28	1.079	.582	-3.26
154		10.83	64.10	9.59	.074	1.98	3553	.674	8.22	10,105	.247	.85	1.172	.704	-3.13
155		12.60	58.14	12.23	.071	2.17	3793	.754	8.56	11,591	.255	.90	1.403	1.817	-2.75
156		6.53	21.93	16.58	.160	.45	786	1.079	4.87	2,851	.605	.19	1.703	-----	-----
157		11.92	39.68	16.72	.067	1.66	2876	.788	9.79	9,465	.361	.53	1.775	1.38	-.74
158		9.74	30.86	17.52	.081	1.03	1838	.705	8.13	5,542	.446	.32	1.799	-----	-----
159		12.47	31.45	21.63	.075	1.46	2586	.776	9.68	8,353	.443	.37	2.052	-----	-----
Curved-bow model in smooth water; C_Δ = 36.15															
160	8	5.13	86.58	3.39	.107	.93	2283	.414	3.00	5,386	.208	.68	.532	.498	-2.61
161		11.40	76.92	8.43	.080	1.98	4535	.727	8.22	14,131	.235	.95	1.209	.695	-2.91
162		11.48	63.69	10.22	.082	1.78	4010	.776	9.14	13,004	.287	.85	1.499	.920	-2.13
163		11.75	56.82	11.68	.077	1.62	3747	.761	9.40	11,979	.310	.72	1.623	1.019	-1.87
164		5.39	21.10	14.33	.185	.28	742	.869	4.22	2,770	.759	.16	1.864	-----	-----
165		12.73	45.66	15.58	.077	1.57	3562	.810	9.76	12,072	.373	.59	1.967	1.326	-.99
166		9.48	33.90	15.63	.083	.85	2095	.739	7.87	6,643	.493	.31	2.000	-----	-----
167		11.61	33.39	19.14	.075	1.20	2677	.807	9.92	8,882	.483	.37	2.263	-----	-----
Curved-bow model in rough water; C_Δ = 18.77															
168	8	6.70	76.92	4.98	.043	3.24	4071	.207	4.13	11,537	.088	1.68	.251	.260	-2.81
[c]169		6.87	73.20	5.36	.043	1.39	1836	.267	5.63	2,712	.403	2.23	1.032	.708	-3.83
[d]169		2.00	70.70	1.62	.077	2.67	3422	.079	0	12,607	.394	.21	1.519	-----	-----
170		6.70	65.79	5.82	.040	2.91	3625	.214	4.61	10,534	.150	.56	.369	.640	-2.91
171		6.26	60.06	5.95	.104	1.90	2326	.459	2.96	8,660	.134	1.68	.490	.304	-4.44
172		6.46	52.91	6.96	.048	2.57	3099	.242	5.00	10,028	.118	1.18	.328	.323	-1.91
Curved-stern model in smooth water; C_Δ = 18.77															
173	-22	5.00	83.33	3.43	.092	1.08	1277	.352	2.83	7,602	.164	.78	.436	.462	-1.44
174		7.83	67.57	6.61	.082	1.29	1575	.532	5.05	10,085	.220	.70	.785	.625	-1.57
175		8.79	54.35	9.19	.065	1.34	1553	.485	6.70	9,105	.295	.30	.992	.957	-1.22
176		7.13	43.86	9.23	.049	.73	802	.303	6.35	3,743	.379	.18	1.023	1.670	-.30
177	-14	5.00	83.33	3.43	.095	1.24	1166	.347	2.48	6,733	.140	1.10	.387	.348	-2.44
178		5.05	78.74	3.67	.085	.97	1021	.325	3.26	4,743	.170	.85	.442	.411	-2.44
179		7.53	74.91	5.74	.102	1.52	1920	.637	3.65	10,272	.167	1.35	.720	.441	-3.26
180		9.53	76.92	7.06	.080	1.99	2454	.606	6.22	11,688	.160	1.66	.816	.424	-4.09
181		9.48	66.67	8.09	.078	1.80	2156	.547	5.87	11,343	.168	1.31	.745	.423	-4.26
182		11.44	78.74	8.27	.085	2.45	3089	.714	6.66	16,471	.159	1.95	.912	.414	-4.83
183		11.53	53.76	12.11	.023	1.62	1933	.247	10.70	7,448	.213	1.13	1.072	.586	-3.87
184		12.01	42.74	15.70	.023	1.74	2066	.262	11.01	7,345	.262	.74	1.277	.769	-3.13
185		12.01	38.76	17.22	.034	1.81	2106	.392	11.14	6,891	.312	.65	1.262	.981	-2.35
186		12.09	33.33	19.94	.024	2.39	2227	.262	10.96	7,509	.339	.50	1.502	1.093	-1.61
187		12.44	28.09	23.89	.033	1.81	2193	.387	11.18	6,972	.393	.39	1.827	1.648	-.39
188	0	4.74	91.74	2.96	.087	1.04	1140	.325	2.91	3,552	.156	.93	.408	.400	-2.22
189		6.35	80.00	4.54	.089	1.33	1788	.445	3.61	5,579	.163	1.07	.566	.424	-2.65
190		12.18	72.99	9.47	.063	2.63	3546	.649	8.44	10,294	.155	2.00	.986	.442	-4.79
191		12.31	72.46	9.64	.065	2.59	3533	.674	8.27	10,373	.165	1.85	1.005	.442	-4.61
192		12.01	67.11	10.15	.070	2.44	3193	.683	8.57	8,675	.190	1.43	1.092	.503	-4.48
193		12.09	43.10	15.67	.064	1.82	2382	.692	9.74	6,234	.264	.84	1.434	.816	-3.00
194		12.31	34.25	19.77	.060	1.68	2104	.696	9.92	5,344	.320	.69	1.660	.503	-1.87
[e]		12.27	53.96	12.91	.064	2.18	2871	.570	9.45	8,149	.215	1.28	1.235	.602	-3.92
195	8	6.83	92.59	4.23	.092	1.84	2378	.473	2.83	4,761	.131	1.66	.513	.304	-4.52
196		10.44	65.79	9.02	.071	2.31	3218	.624	7.35	7,311	.160	1.77	.890	.421	-5.18
197		11.66	54.95	11.98	.077	2.07	2841	.739	8.44	6,648	.198	1.33	1.175	.543	-4.61
198		12.35	41.32	16.64	.071	1.80	2528	.779	9.74	6,201	.261	.92	1.466	.747	-3.70
199		12.48	33.33	20.53	.066	1.56	2210	.739	10.18	5,560	.301	.77	1.703	.985	-2.48
200	16	6.13	83.33	4.21	.098	2.04	2661	.405	1.78	4,377	.108	2.03	.411	.251	-5.00
201		10.40	66.67	8.87	.083	2.59	3580	.674	6.13	7,174	.144	2.21	.819	.328	-6.83
202		11.83	54.35	12.28	.078	2.23	3208	.757	7.87	6,721	.187	1.52	1.103	.458	-6.35
203		12.57	40.98	17.05	.084	1.79	2568	.658	10.27	5,472	.242	1.19	1.379	.627	-5.26
204		12.66	33.11	20.93	.078	1.51	2219	.857	10.05	4,931	.304	.87	1.775	.853	-4.18

[c] First impact.
[d] Second impact.
[e] Average of three consistency runs.

TABLE III

ADDITIONAL DATA FOR CURVED-BOW MODEL IN ROUGH WATER

Run	Impact location, in.	Wave slope, θ, deg	$\dot{x}_{o,w}$, fps	$\gamma_{o,w}$, deg	τ_w, deg
168	340	5.0	88.20	4.37	3.0
[a]169	440	1.1	84.48	4.45	6.9
[b]169	287	4.0	81.58	1.34	4.0
170	392	3.5	77.07	4.87	4.5
171	332	2.1	71.34	5.16	5.9
172	320	4.6	64.19	5.70	3.4

[a]First impact.
[b]Second impact.

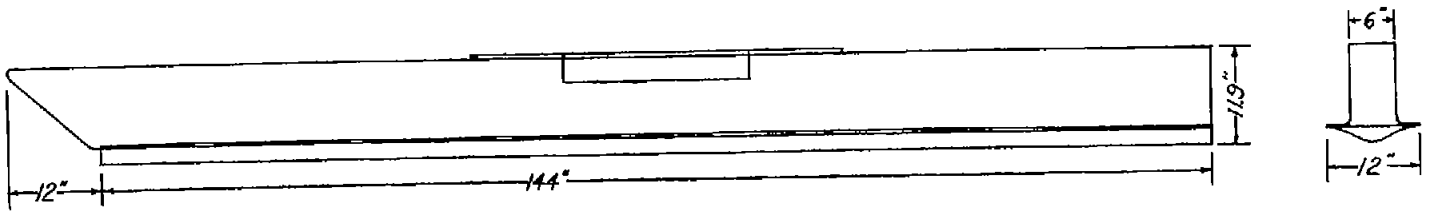

(a) Straight-keel model.

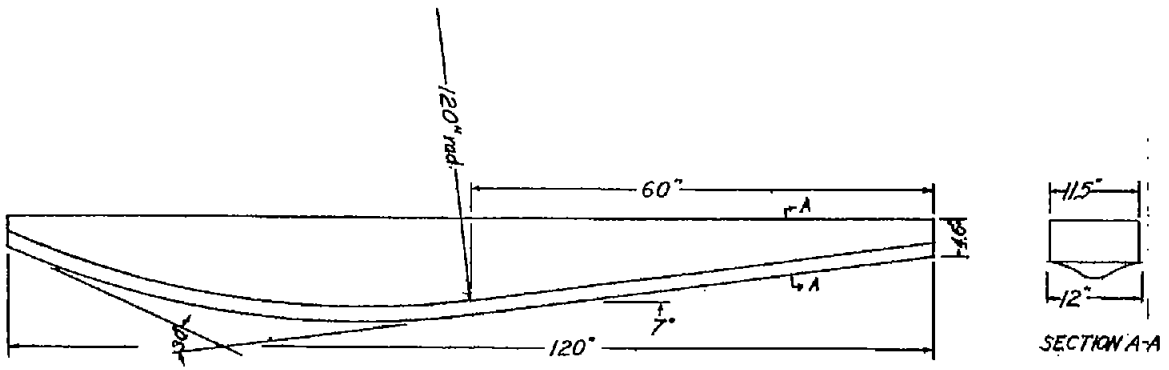

(b) Longitudinally curved model.

Figure 1.- Profiles of models.

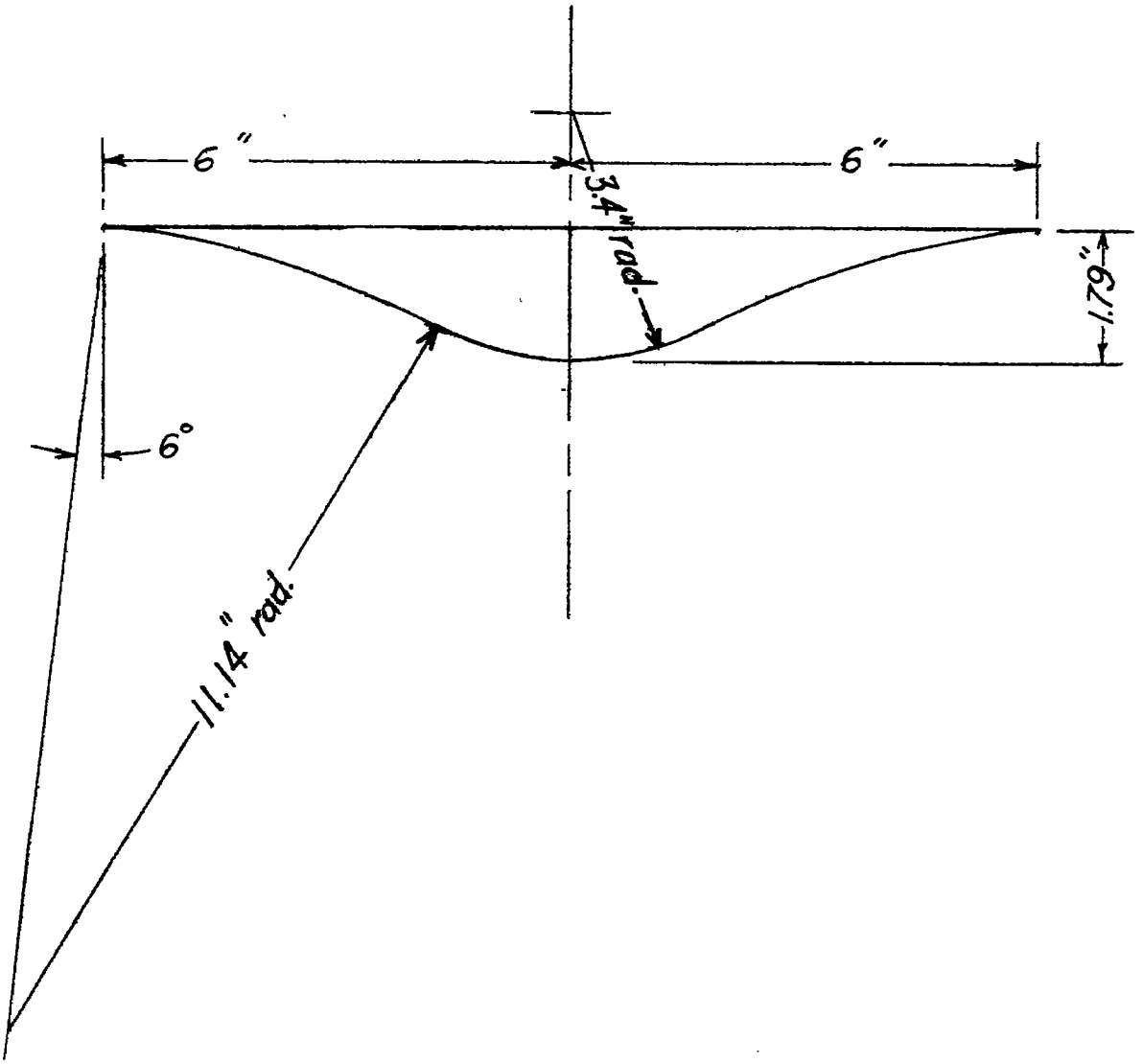

Figure 2.- Cross section of concave-convex bottom.

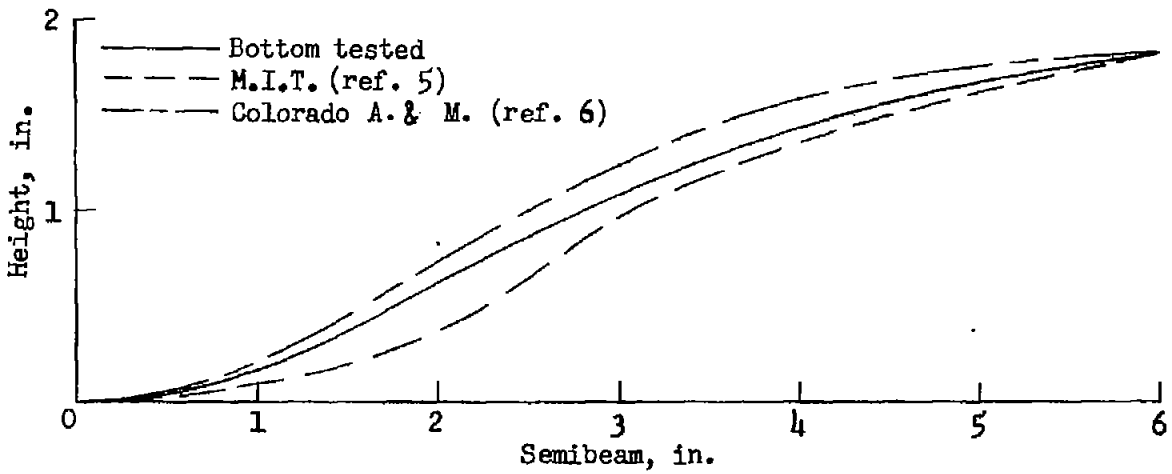

Figure 3.- Comparison of the cross section of the bottom tested with the constant-force shapes of M.I.T. and Colorado A. & M. College.

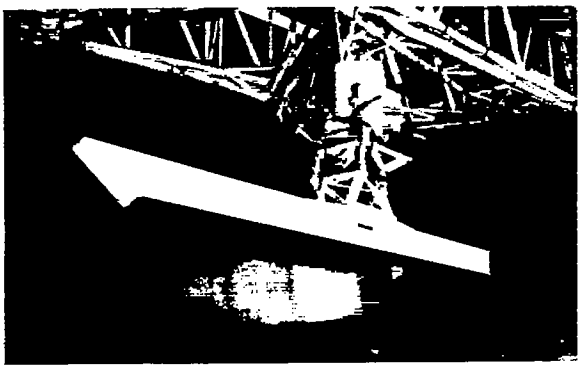

(a) Straight-keel model. L-95886

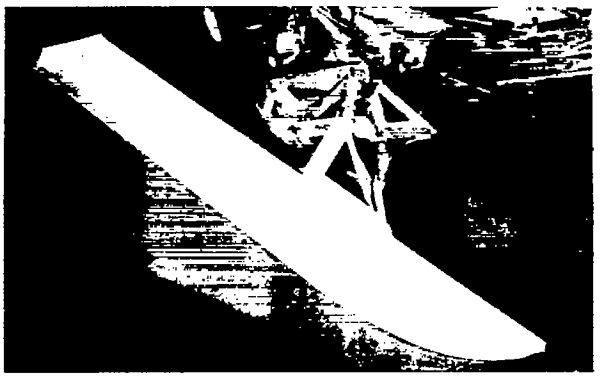

(b) Curved-stern model. L-95887

(c) Curved-bow model. L-95888

Figure 4.- Models mounted on carriage in Langley impact basin.

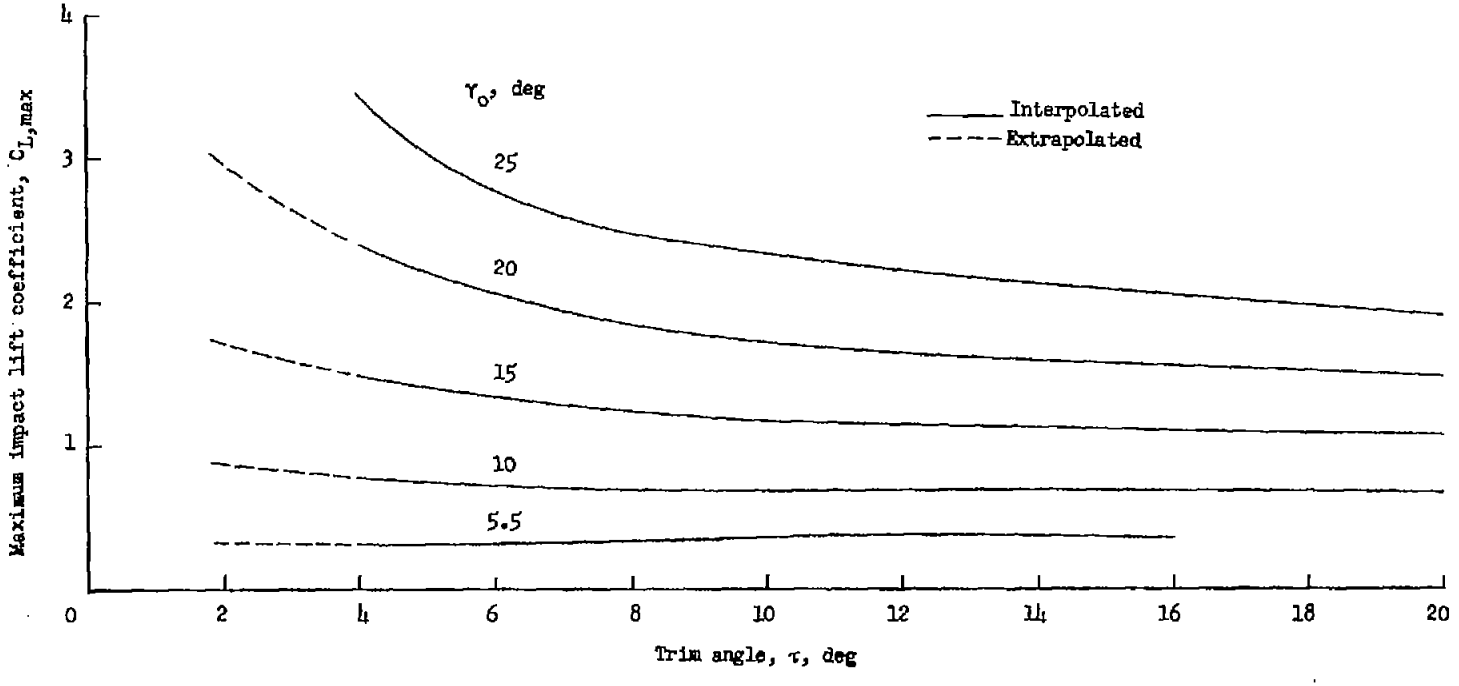

Figure 5.- Theoretical variation of maximum impact lift coefficient with trim angle for straight-keel model. $C_\Delta = 18.77$.

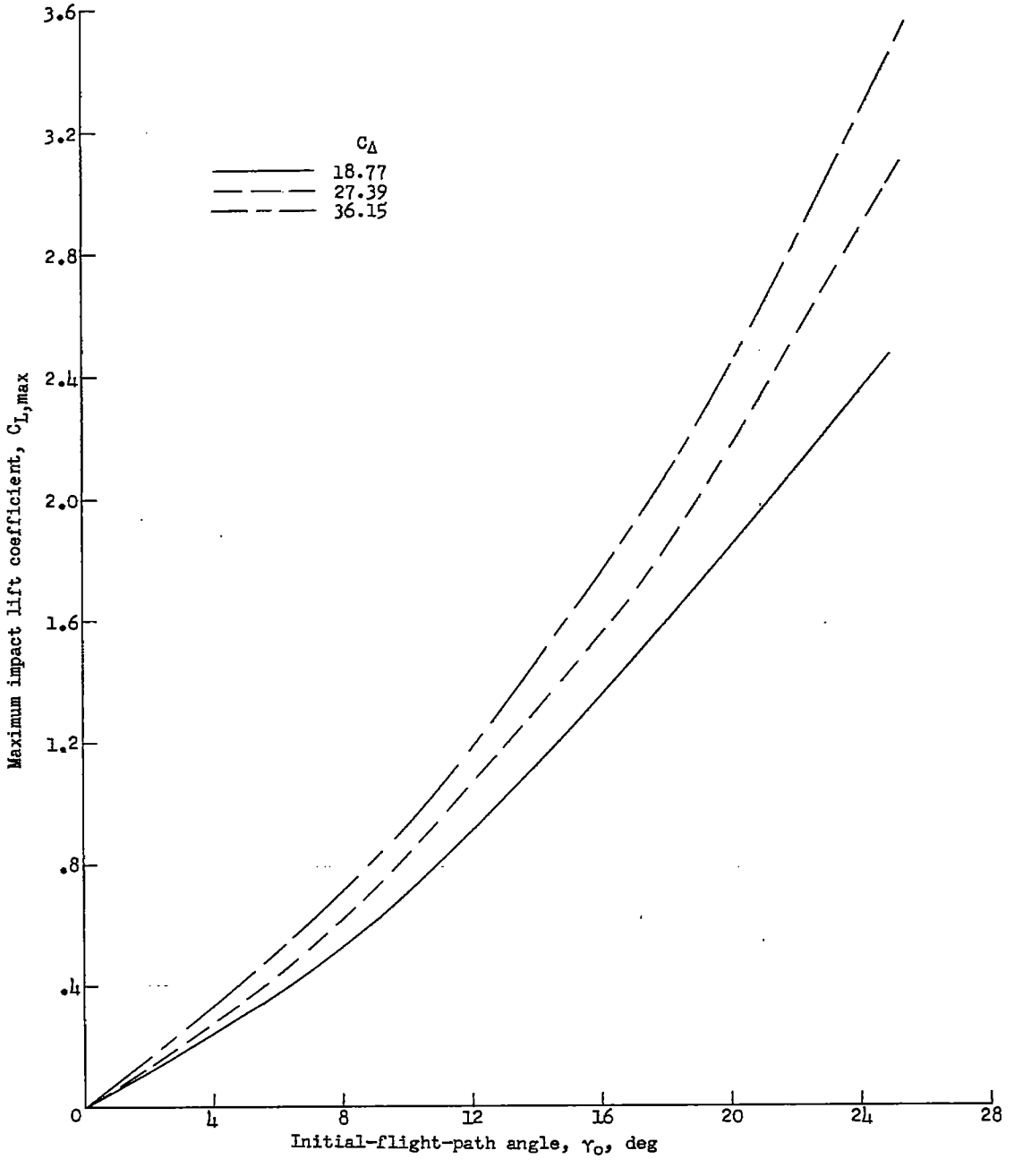

Figure 6.- Theoretical variation of maximum impact lift coefficient with initial-flight-path angle for three beam loadings for straight-keel model. $\tau = 8^\circ$.

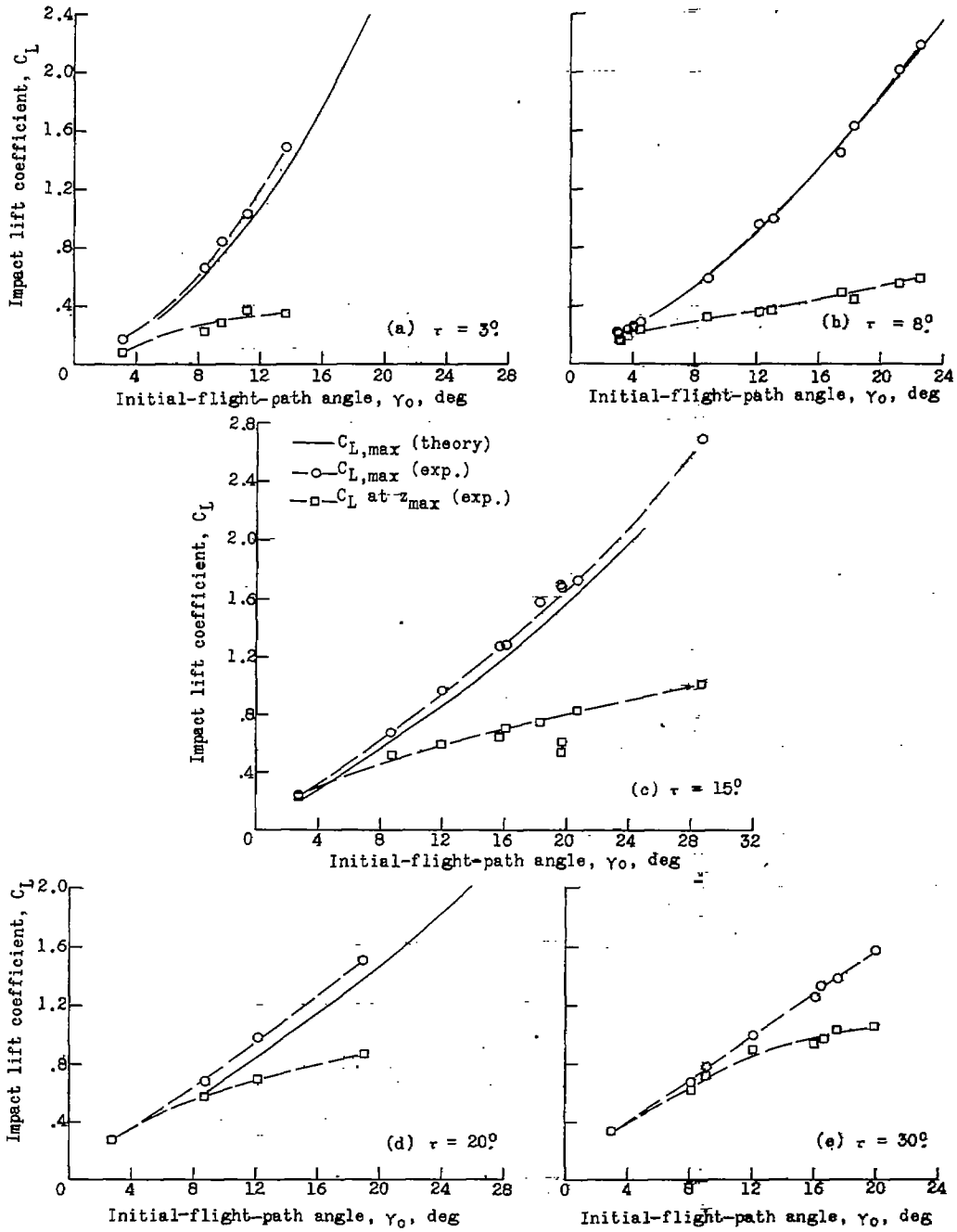

Figure 7.- Variation of impact lift coefficient with initial-flight-path angle for straight-keel model. $C_\Delta = 18.77$.

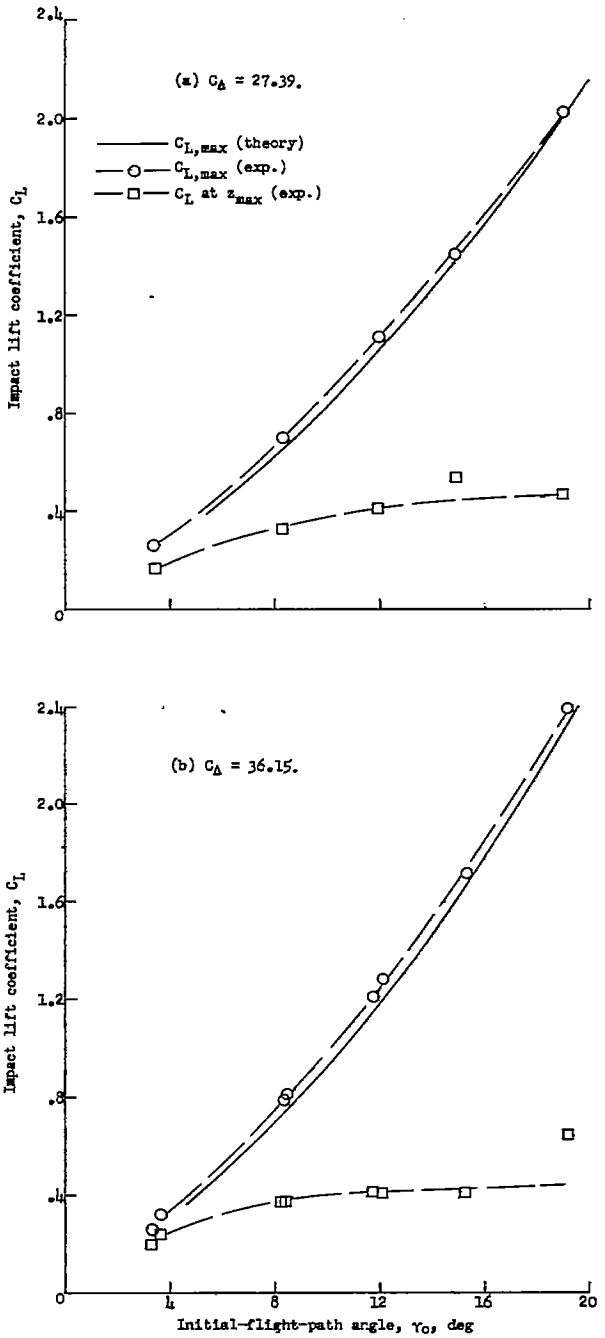

Figure 8.- Variation of impact lift coefficient with initial-flight-path angle for straight-keel model. $\tau = 8^o$; $C_\Delta = 27.39$ and 36.15.

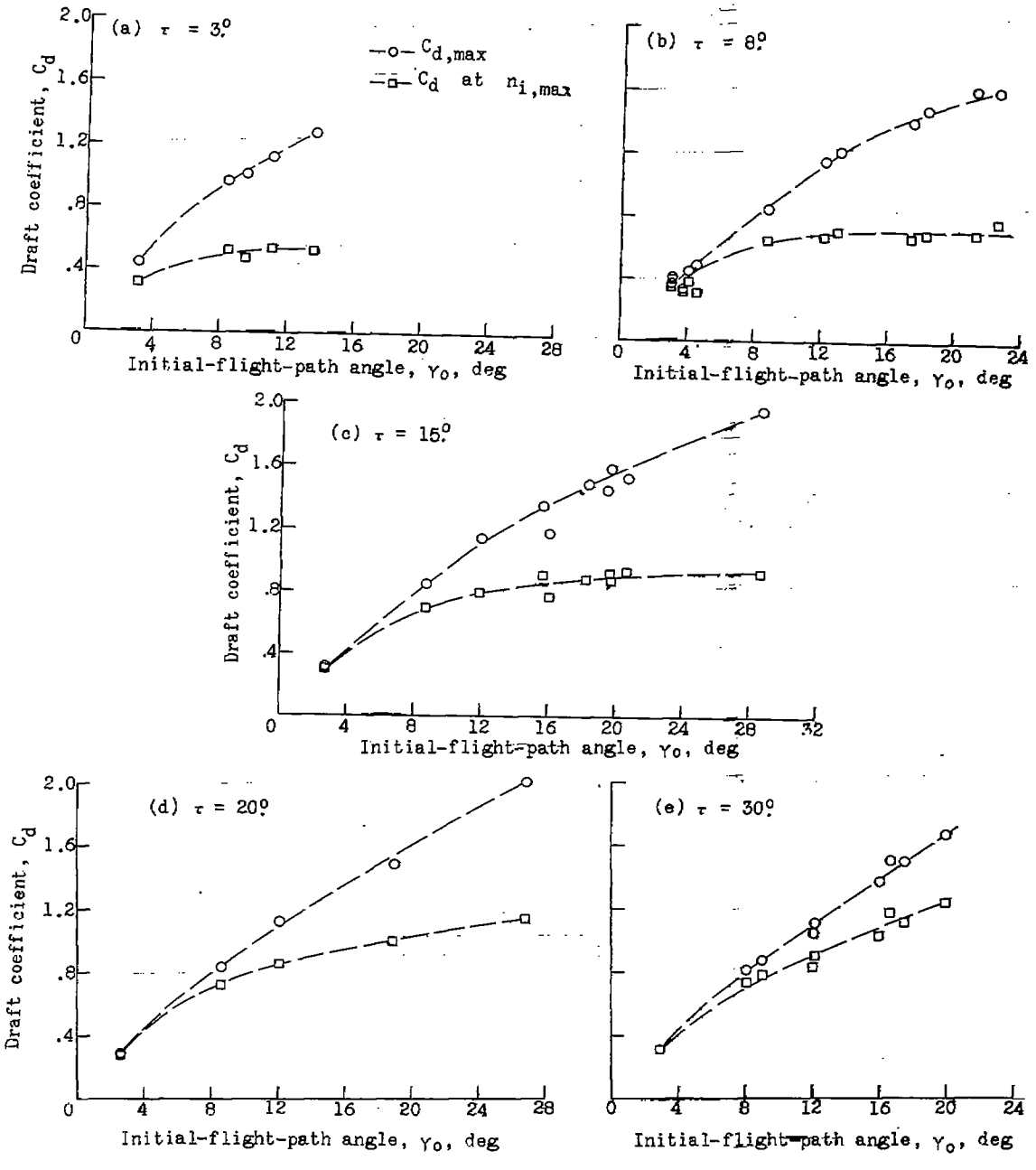

Figure 9.- Experimental variation of draft coefficient with initial-flight-path angle for straight-keel model. $C_\Delta = 18.77$.

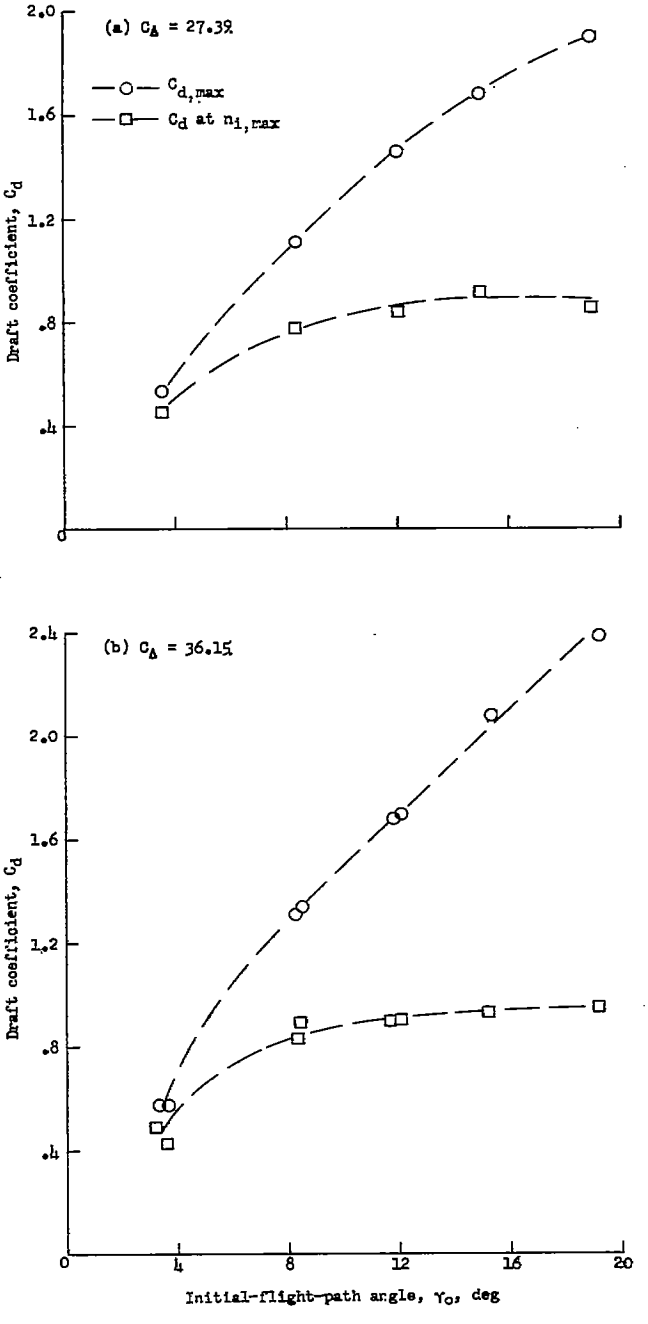

Figure 10.- Experimental variation of draft coefficient with initial-flight-path angle for straight-keel model. $\tau = 8^\circ$; $C_\Delta = 27.39$ and 36.15.

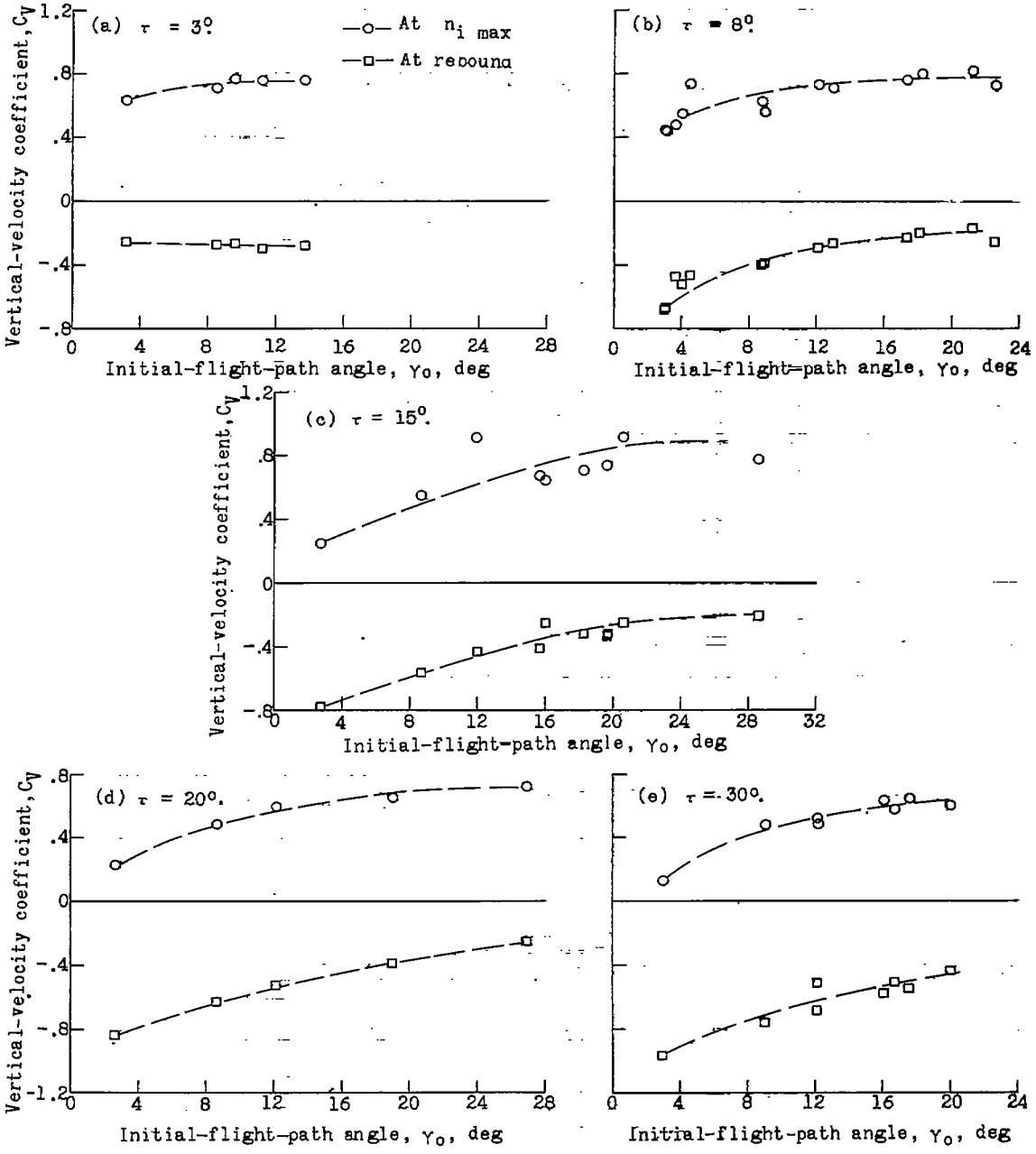

Figure 11.- Experimental variation of vertical-velocity coefficient with initial-flight-path angle for straight-keel model. $C_\Delta = 18.77$.

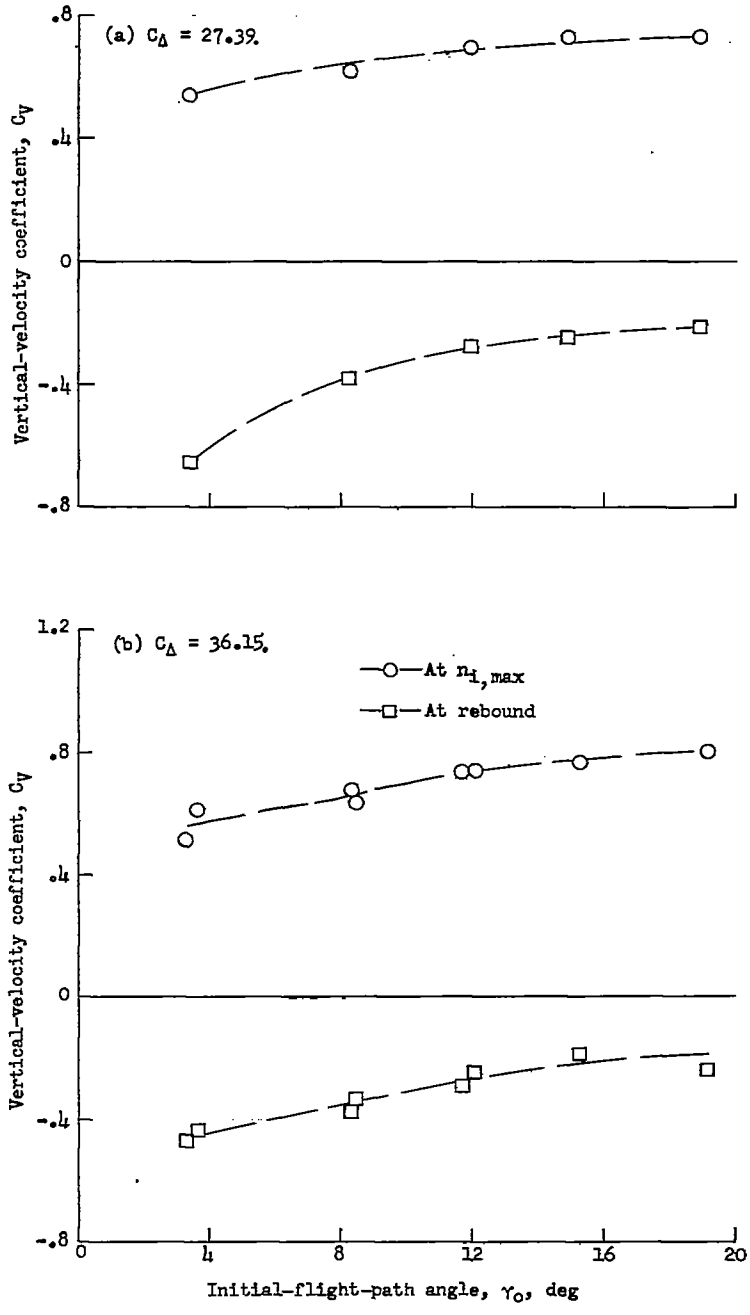

Figure 12.- Experimental variation of vertical-velocity coefficient with initial-flight-path angle for straight-keel model. $\tau = 8^\circ$; $C_\Delta = 27.39$ and 36.15.

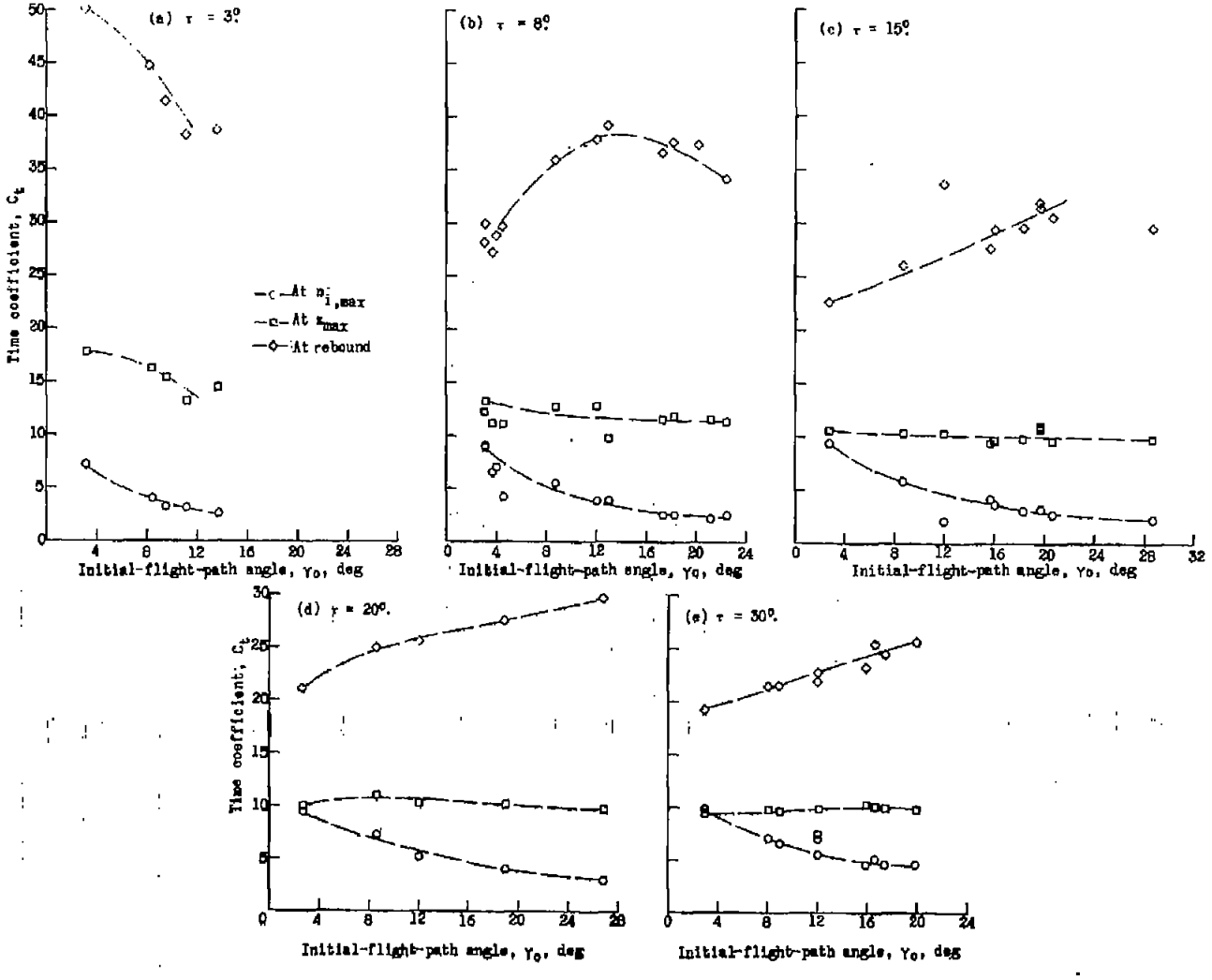

Figure 13.- Experimental variation of time coefficient with initial-flight-path angle for straight-keel model. $C_\Delta = 18.77$.

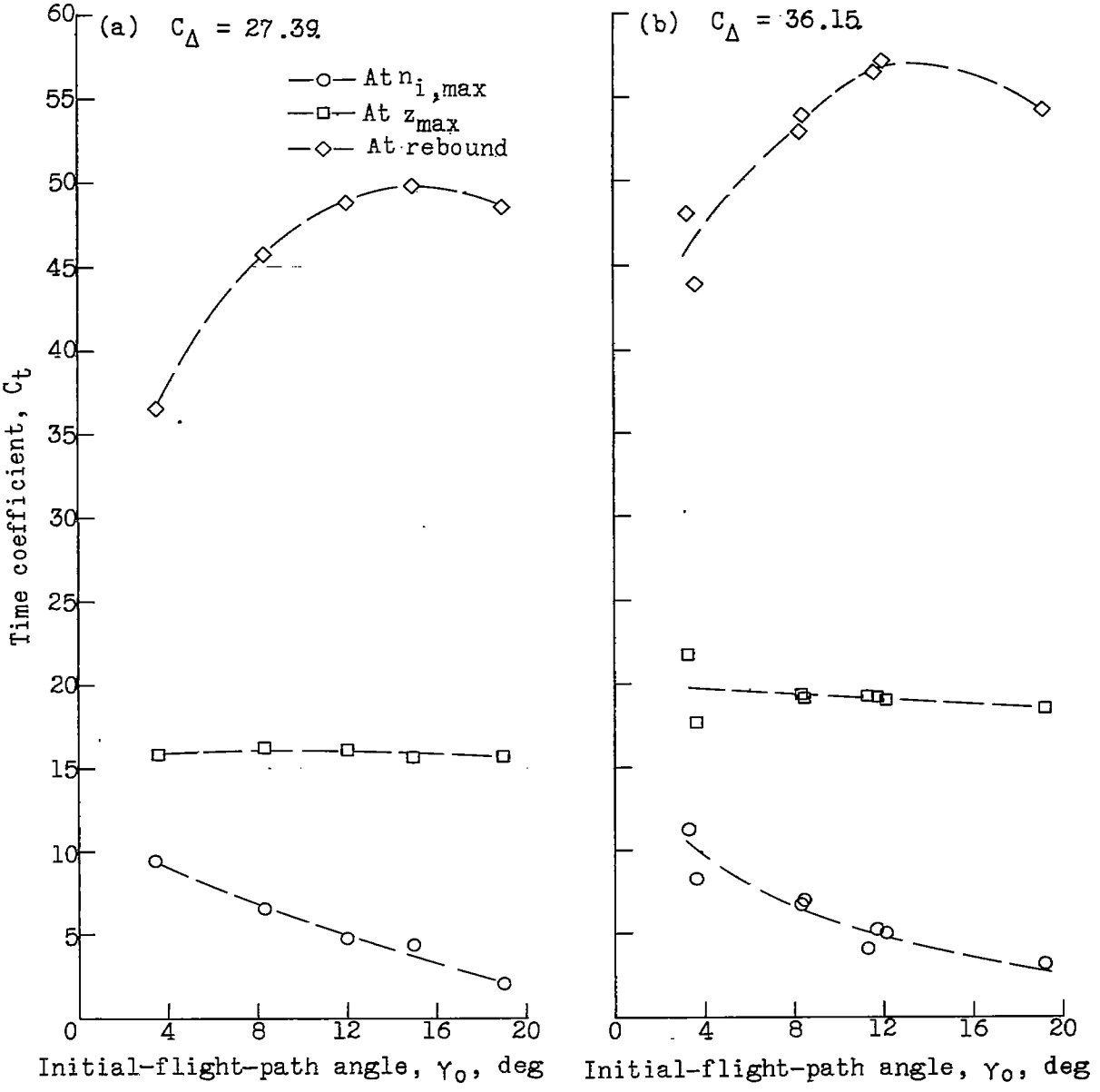

Figure 14.- Experimental variation of time coefficient with initial-flight-path angle for straight-keel model. $\tau = 8^\circ$; C_Δ = 27.39 and 36.15.

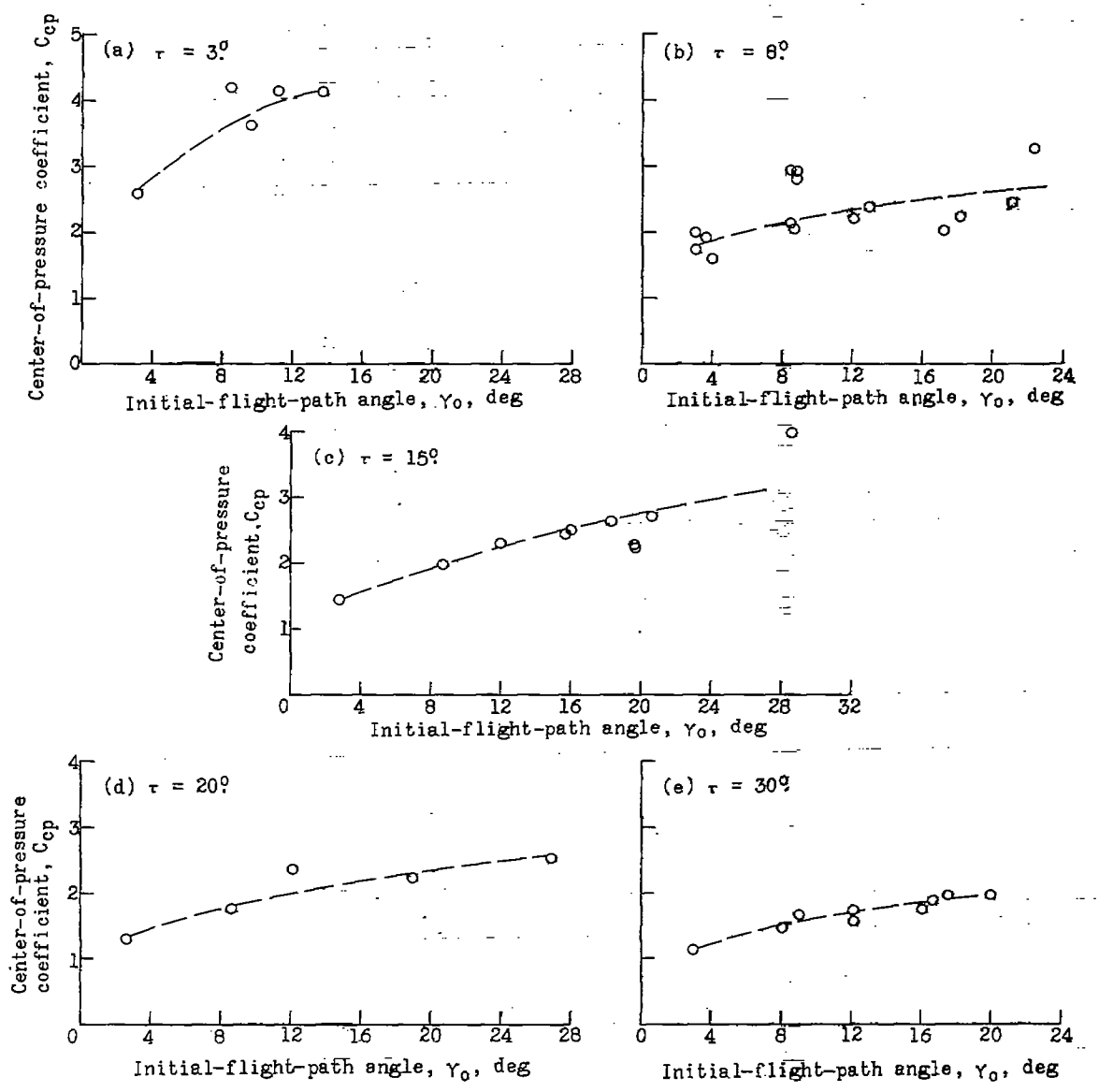

Figure 15.- Experimental variation of center-of-pressure coefficient at $n_{i,max}$ with initial-flight-path angle for straight-keel model. $C_\Delta = 18.77$.

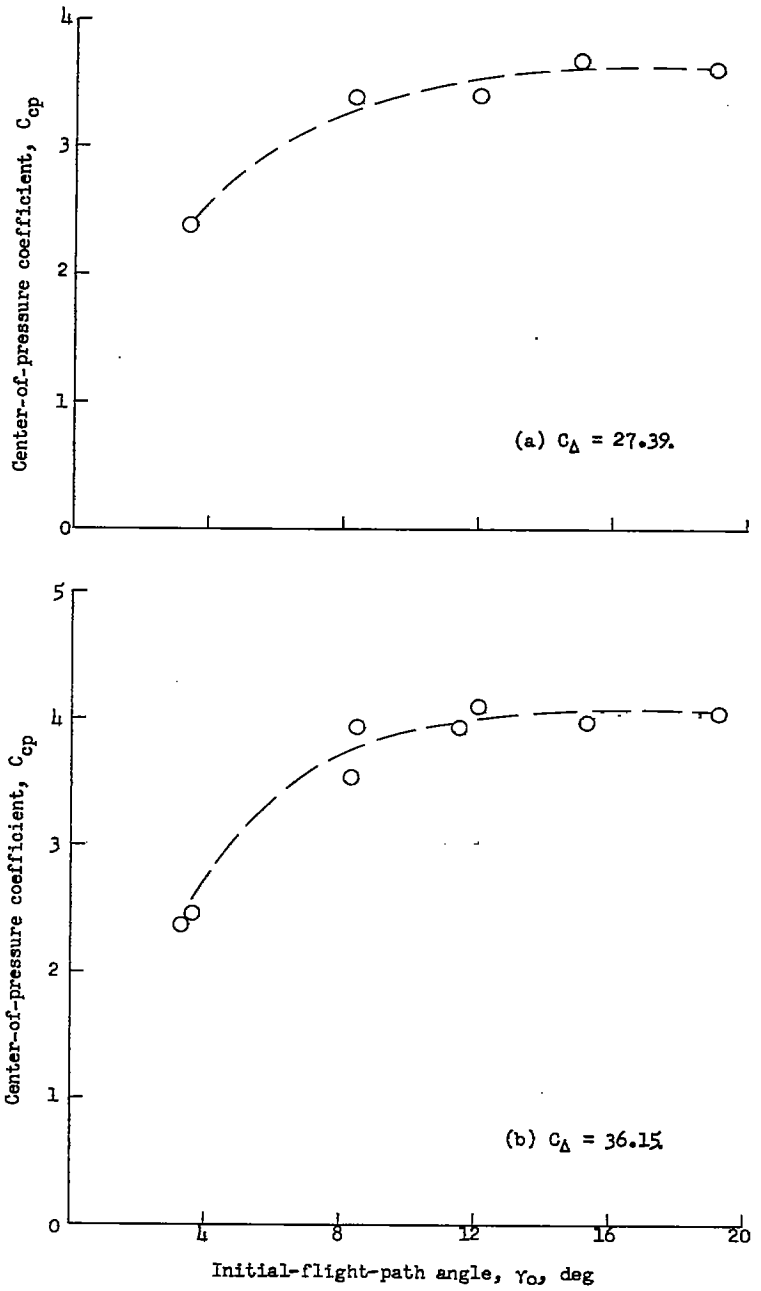

Figure 16.- Experimental variation of center-of-pressure coefficient at $n_{i,max}$ with initial-flight-path angle for straight-keel model. $\tau = 8^\circ$; C_Δ = 27.39 and 36.15.

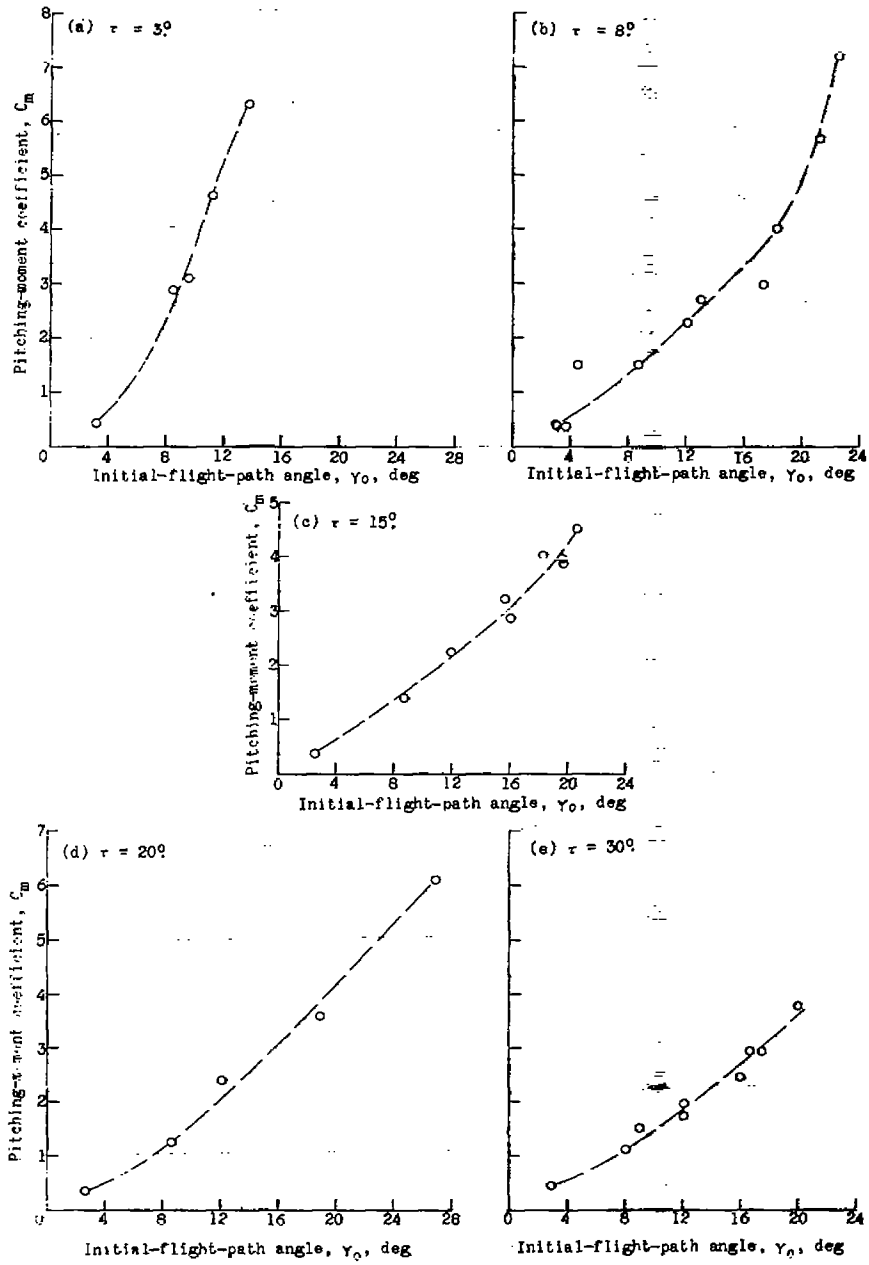

Figure 17.- Experimental variation of pitching-moment coefficient at $n_{i,max}$ with initial-flight-path angle for straight-keel model. C_Δ = 18.77.

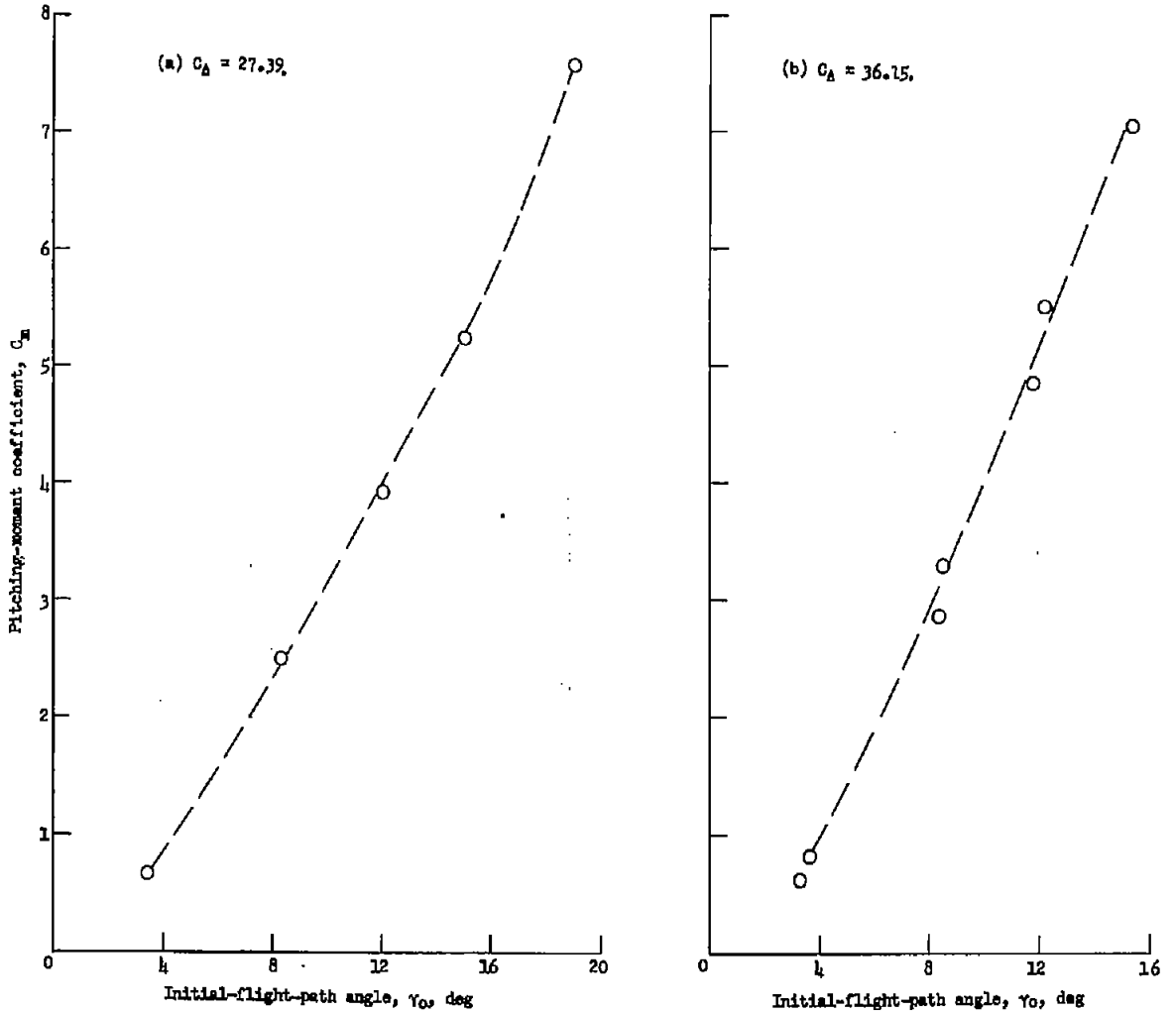

Figure 18.- Experimental variation of pitching-moment coefficient at $n_{1,max}$ with initial-flight-path angle for straight-keel model. $\tau = 8^\circ$; $C_\Delta = 27.39$ and 36.15.

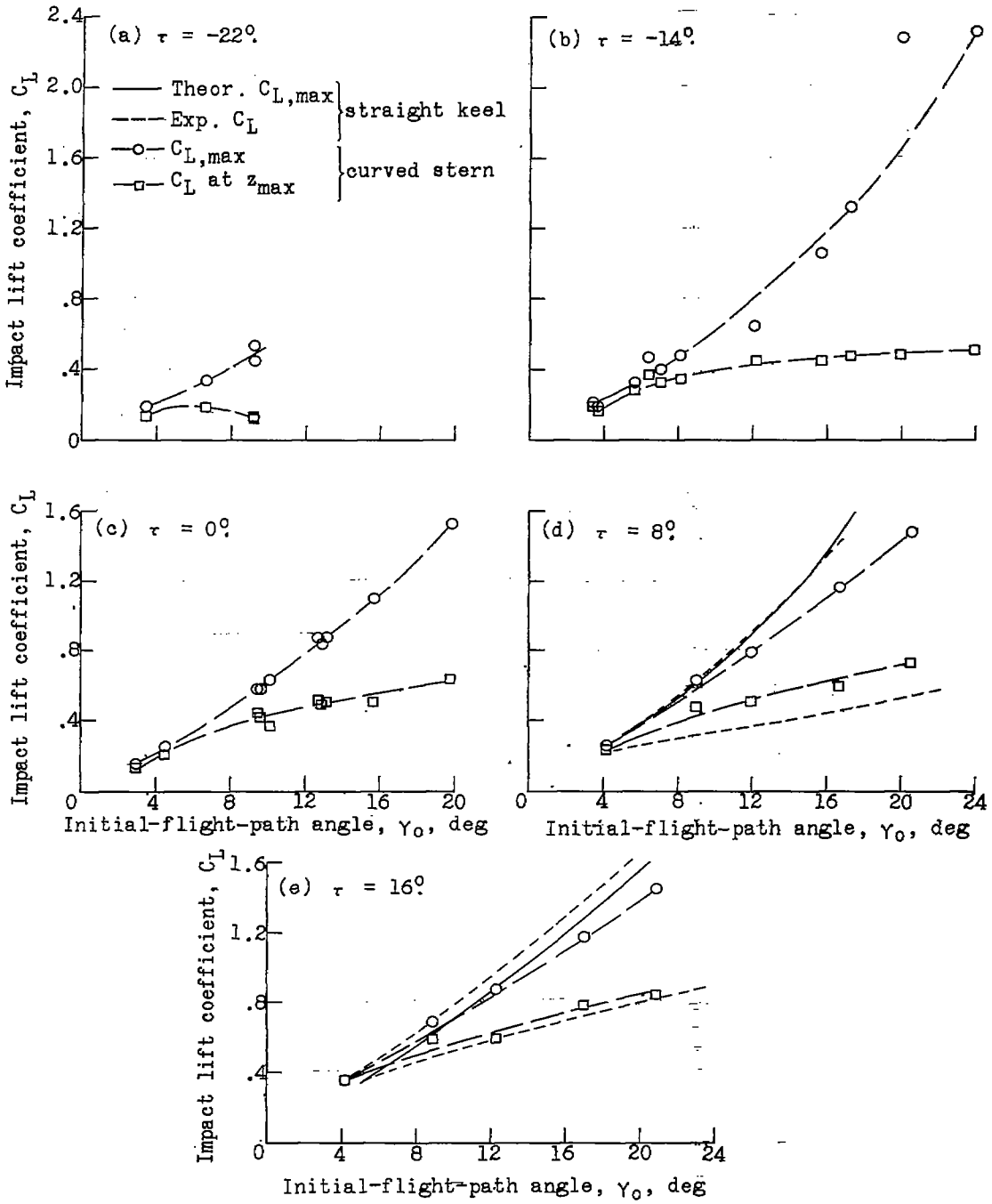

Figure 19.- Experimental variation of impact lift coefficient with initial-flight-path angle for the curved-stern model.

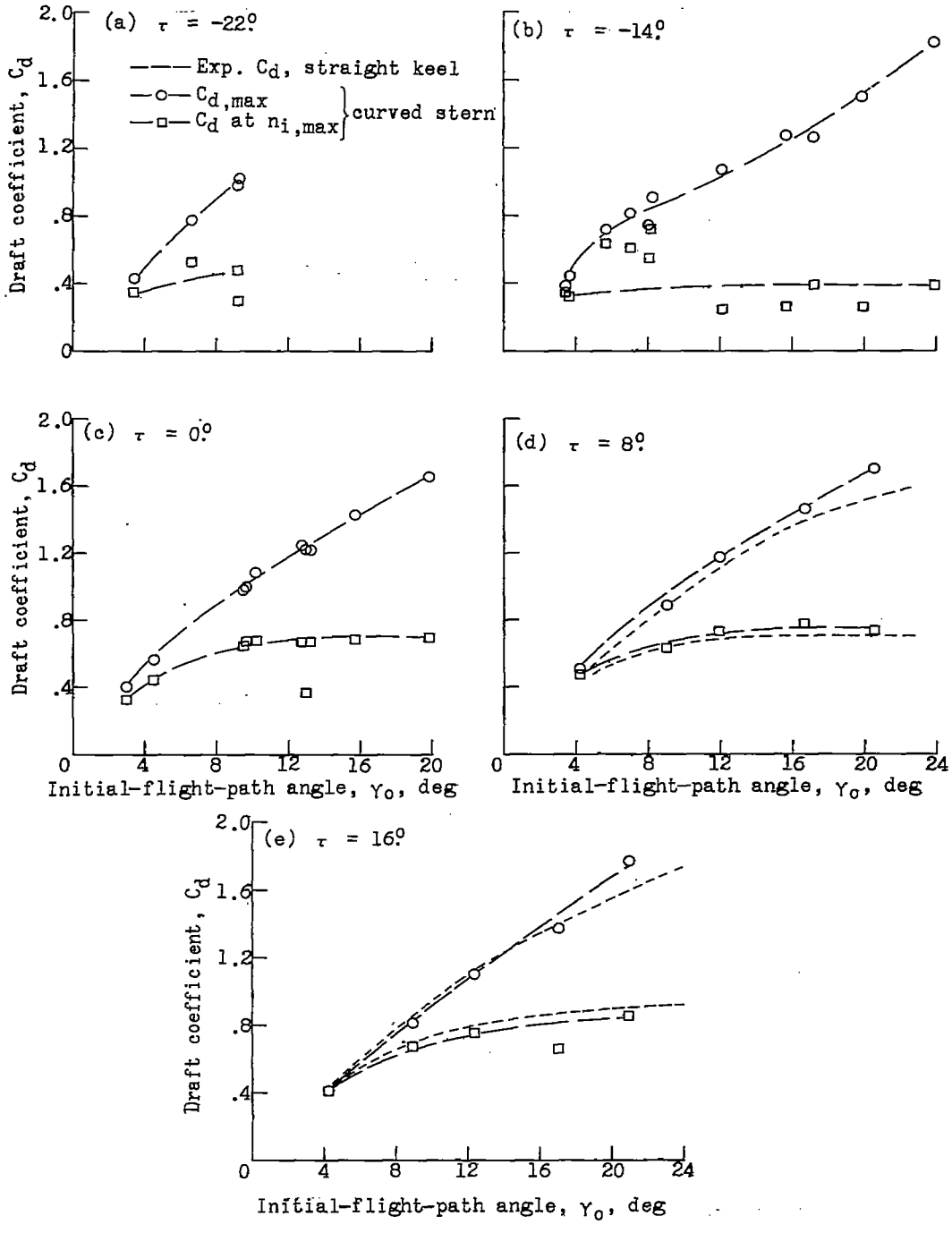

Figure 20.- Experimental variation of draft coefficient with initial-flight-path angle for the curved-stern model.

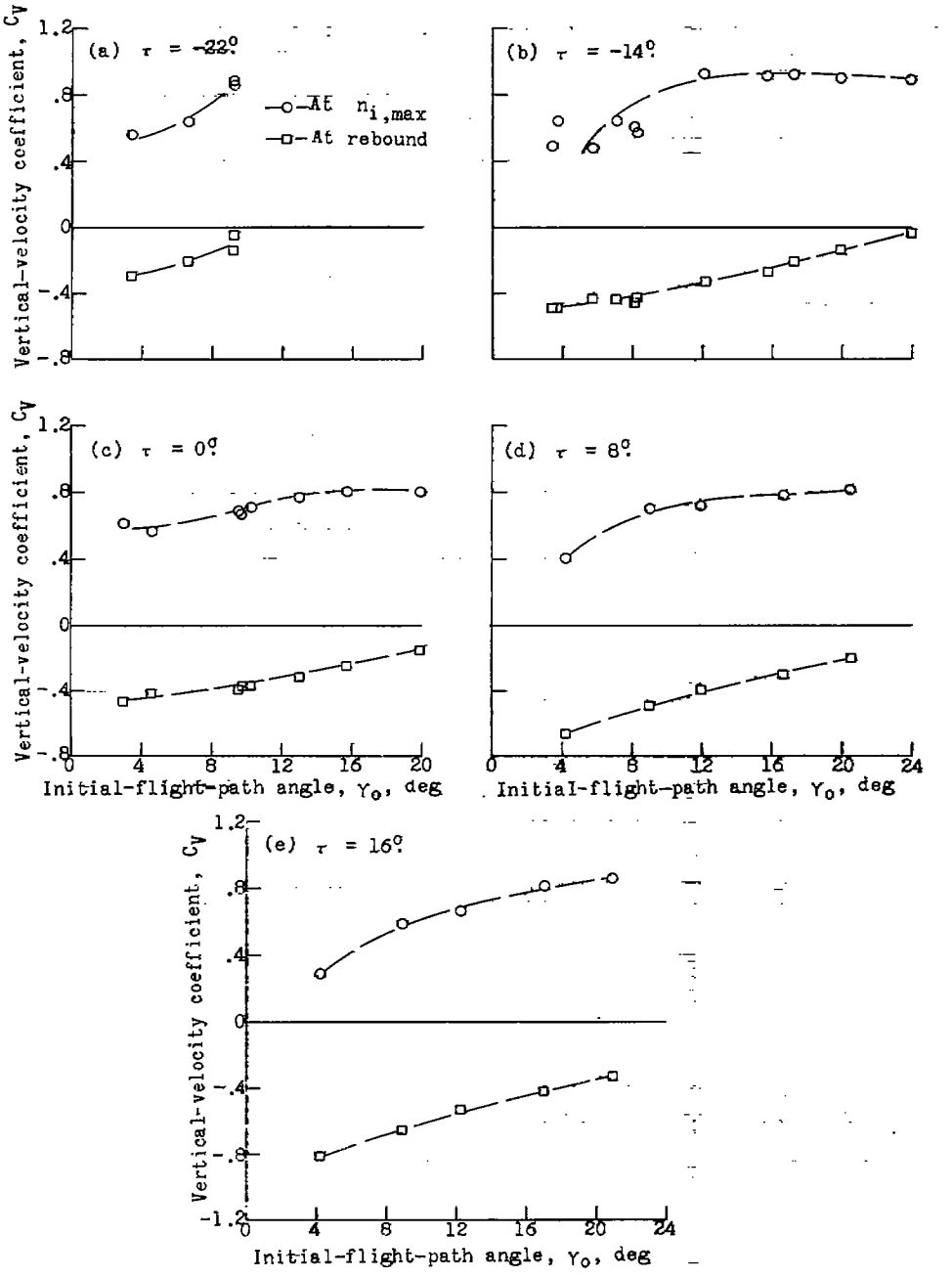

Figure 21.- Experimental variation of vertical-velocity coefficient with initial-flight-path angle for the curved-stern model.

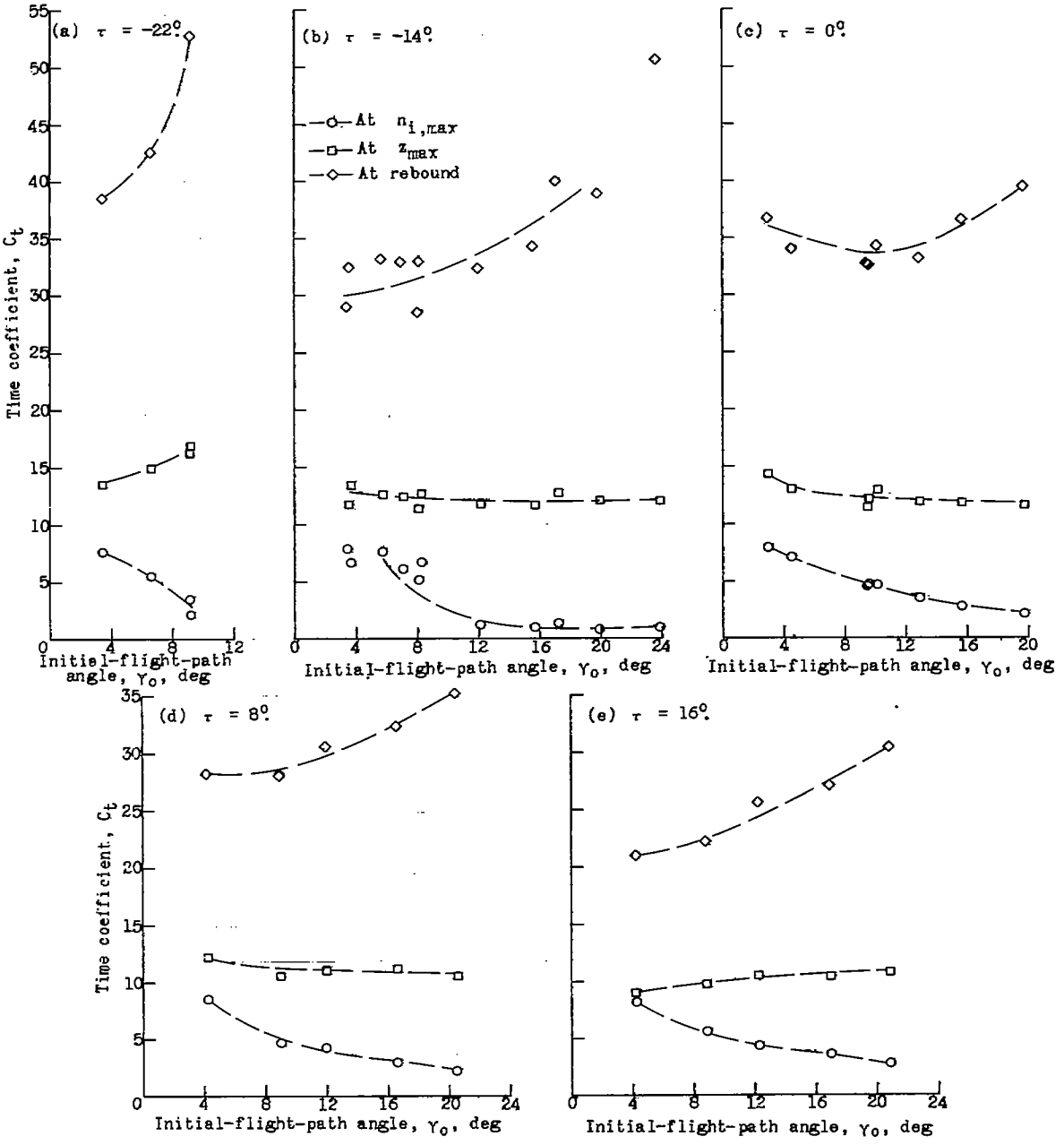

Figure 22.- Experimental variation of time coefficient with initial-flight-path angle for the curved-stern model.

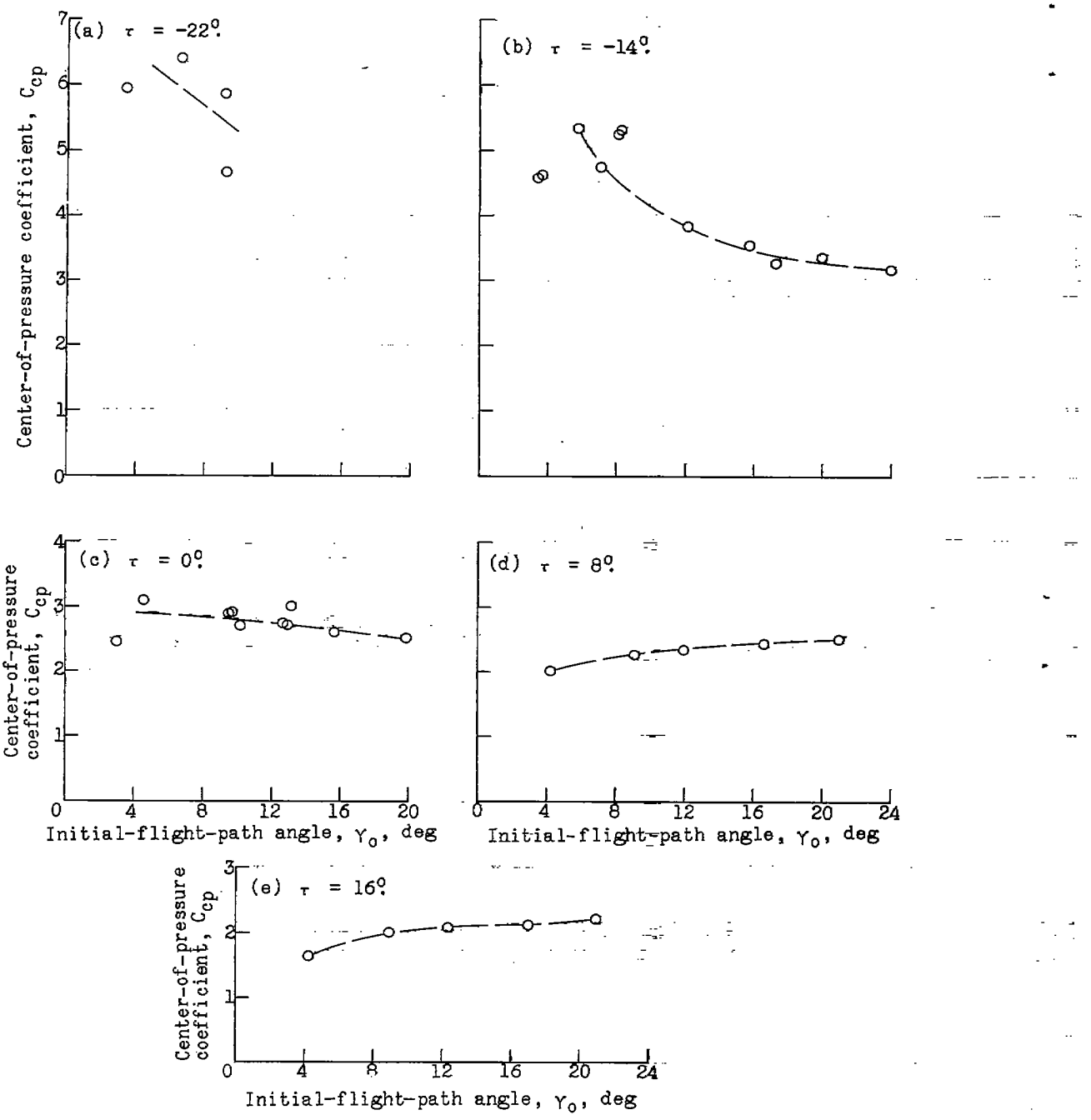

Figure 23.- Experimental variation of center-of-pressure coefficient at $n_{i,max}$ with initial-flight-path angle for the curved-stern model.

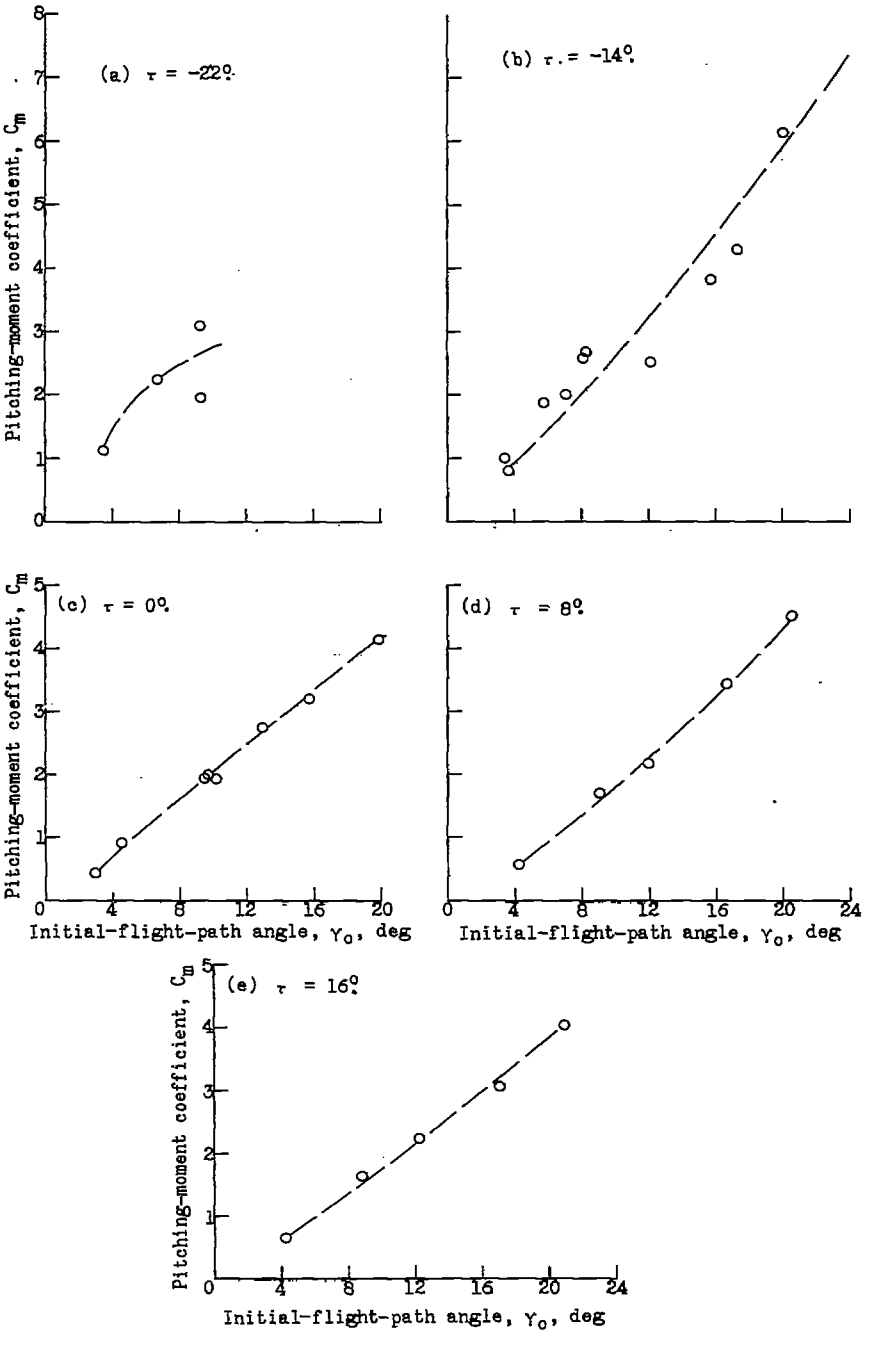

Figure 24.- Experimental variation of pitching-moment coefficient at $n_{1,max}$ with initial-flight-path angle for the curved-stern model.

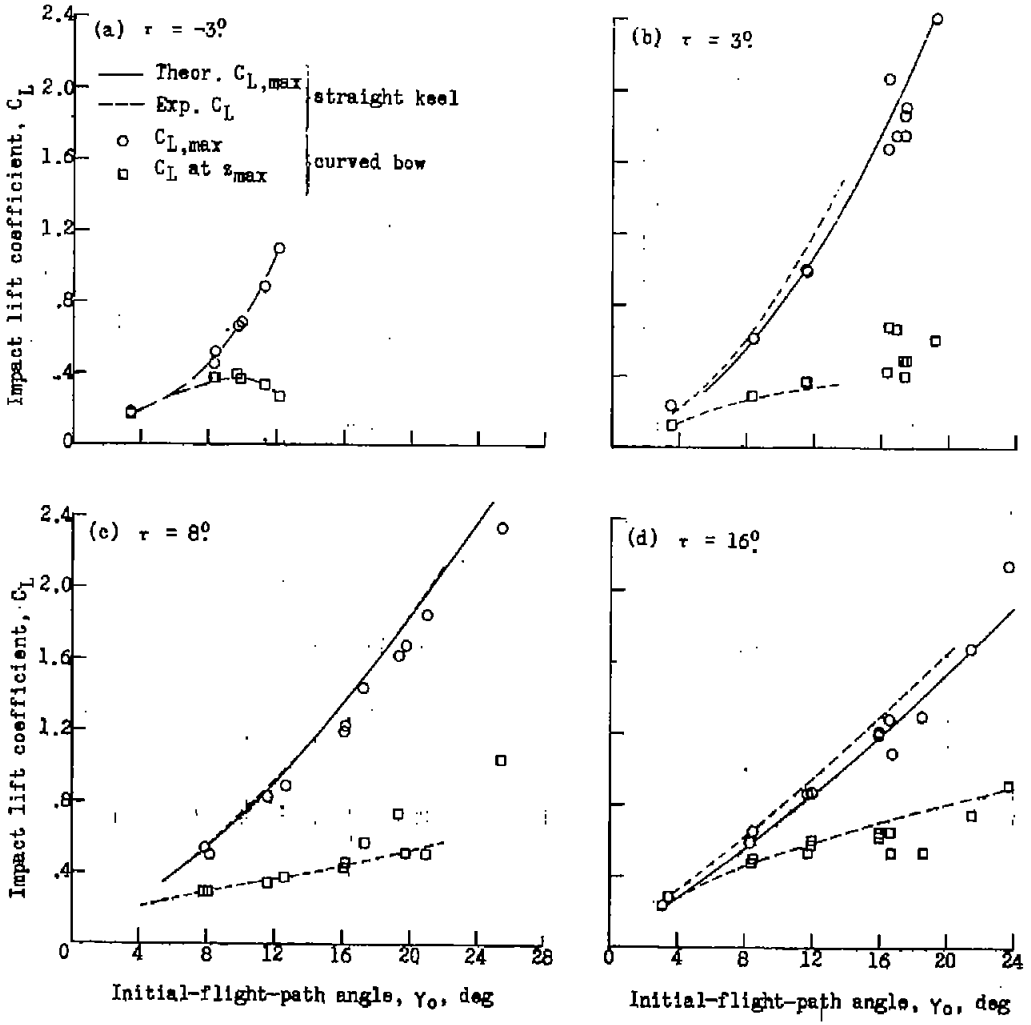

Figure 25.- Experimental variation of lift coefficient with initial-flight-path angle for curved-bow model in smooth water. $C_\Delta = 18.77$.

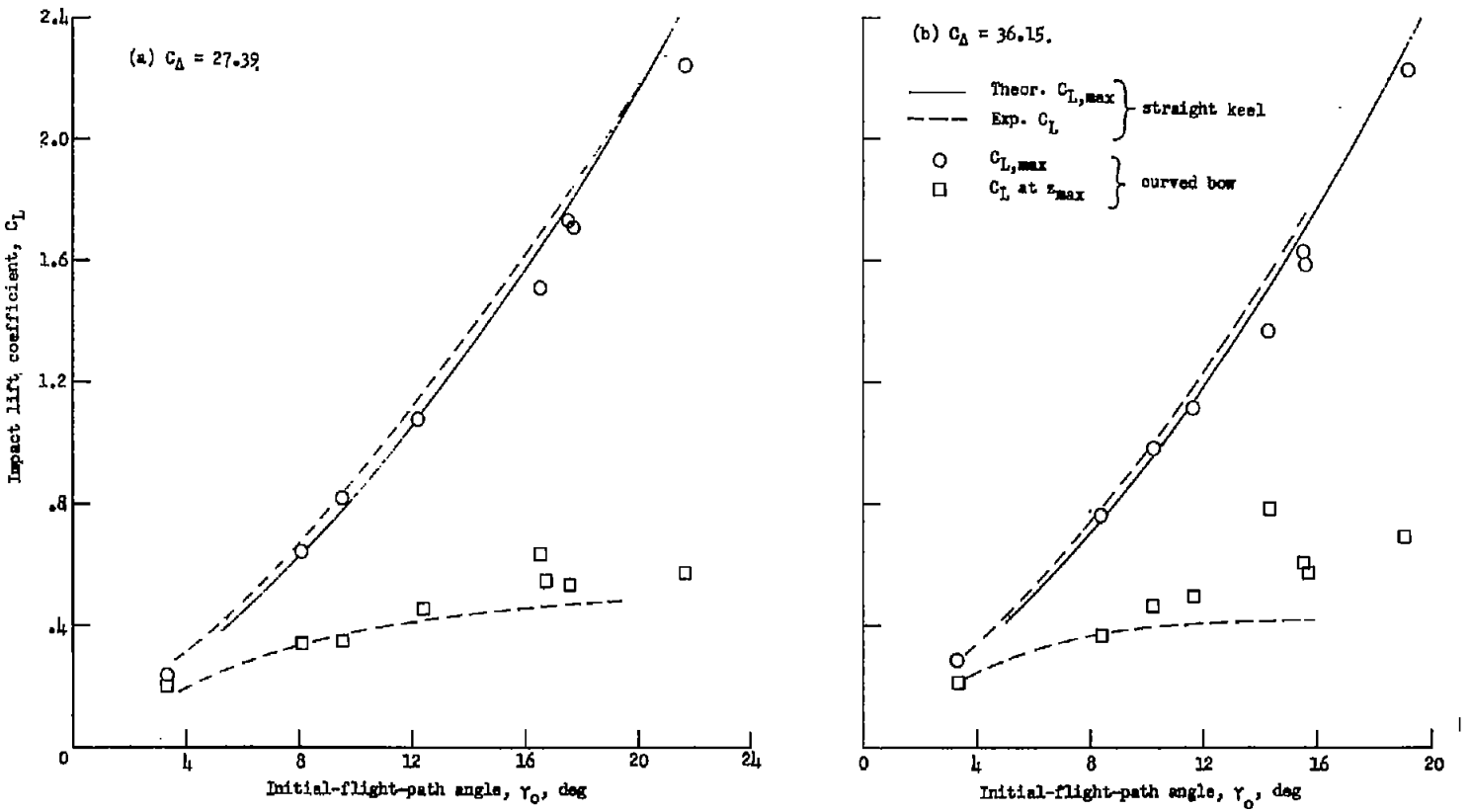

Figure 26.- Variation of lift coefficient with initial-flight-path angle for curved-bow model in smooth water. $\tau = 8^\circ$; $C_\Delta = 27.39$ and 36.15.

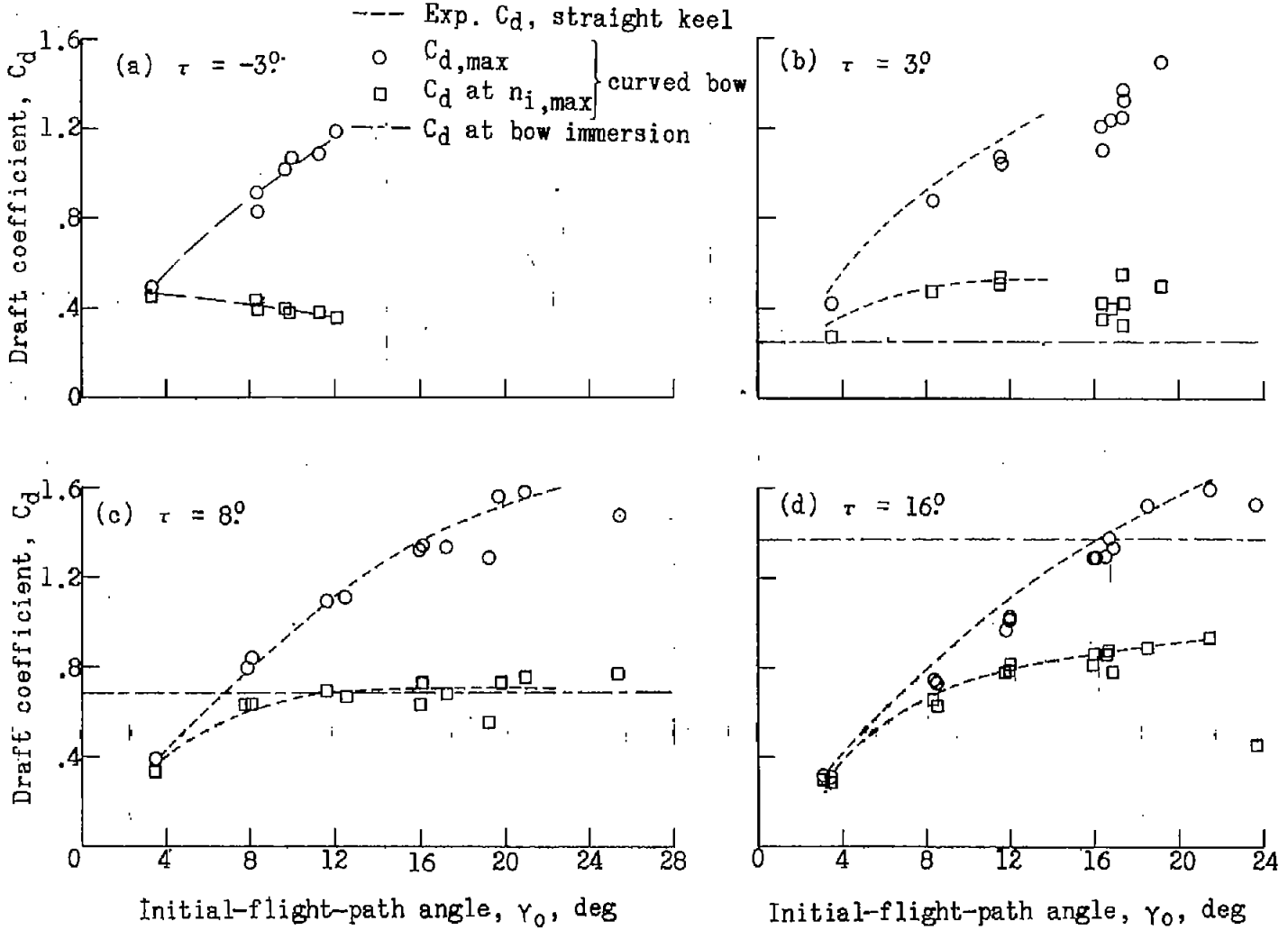

Figure 27.- Experimental variation of draft coefficient with initial-flight-path angle for curved-bow model in smooth water. C_Δ = 18.77.

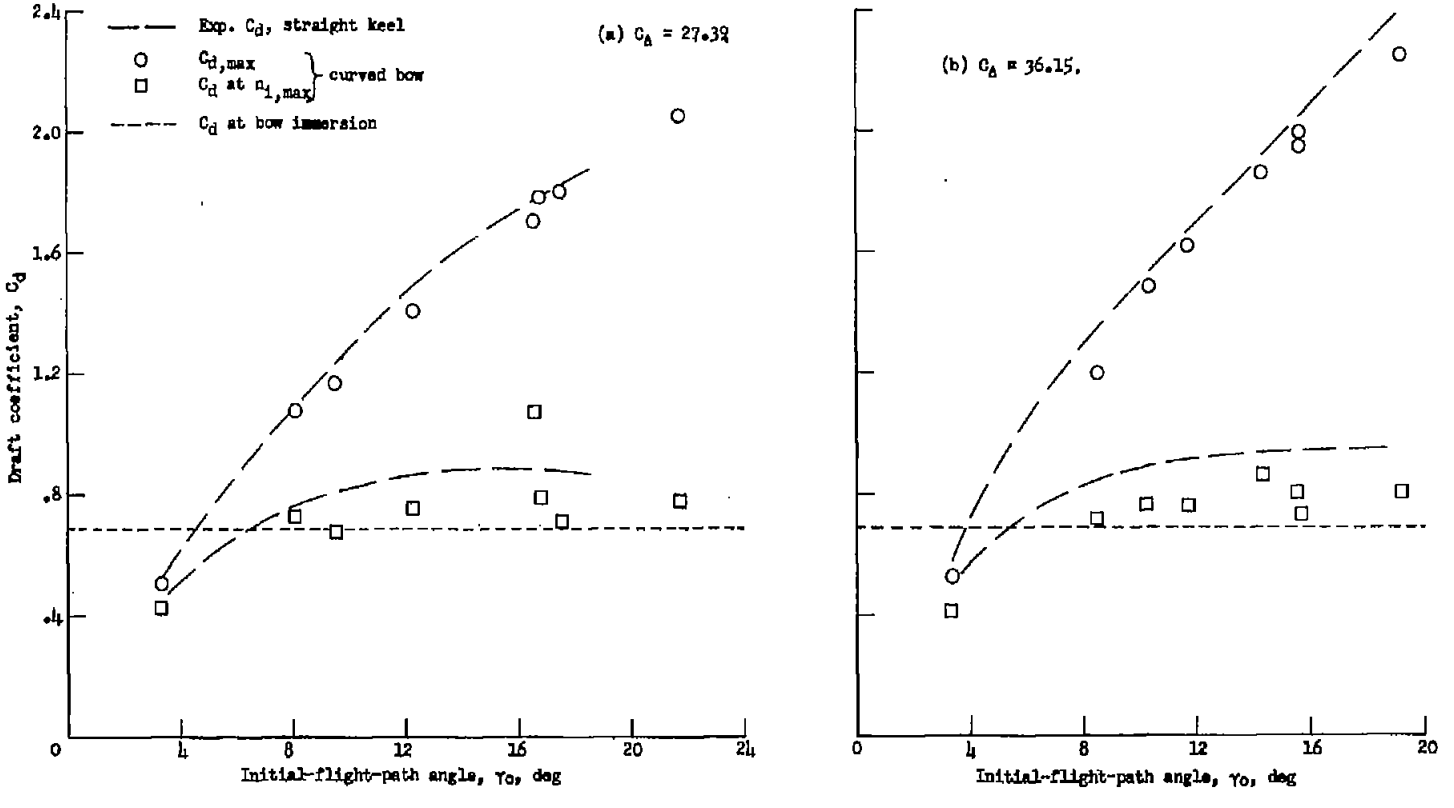

Figure 28.- Experimental variation of draft coefficient with initial-flight-path angle for curved-bow model in smooth water. $\tau = 8^\circ$; $C_\Delta = 27.39$ and 36.15.

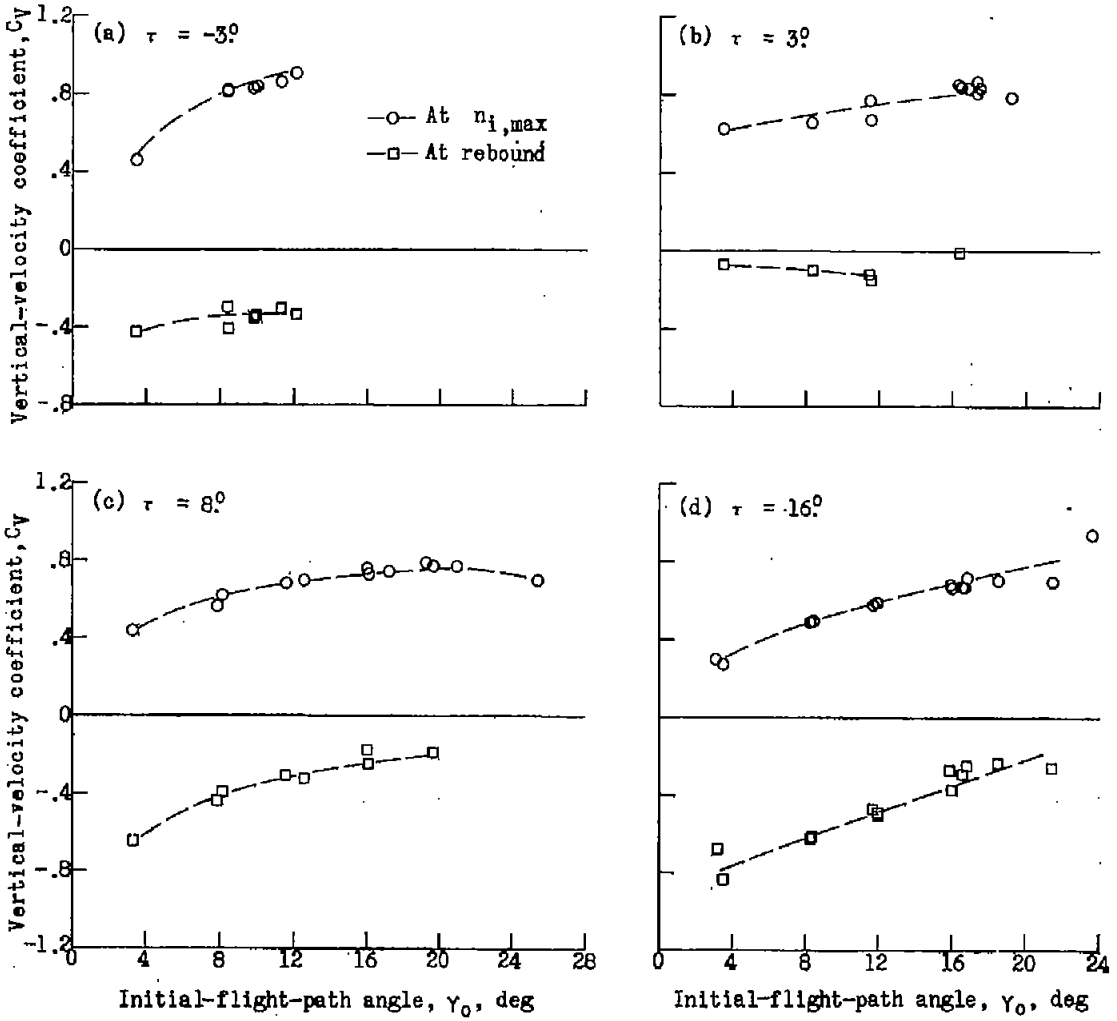

Figure 29.- Experimental variation of vertical-velocity coefficient with initial-flight-path angle for curved-bow model in smooth water. $C_\Delta = 18.77$.

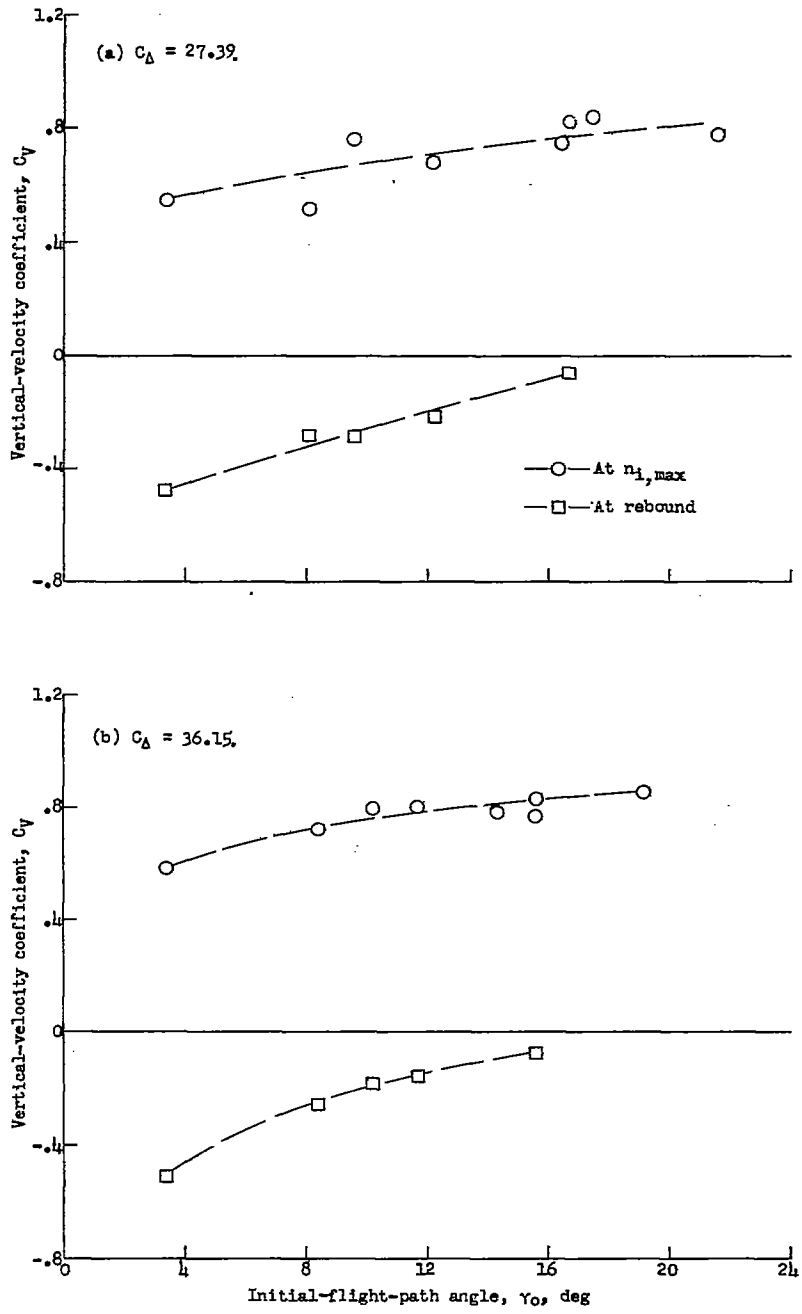

Figure 30.- Experimental variation of vertical-velocity coefficient with initial-flight-path angle for curved-bow model in smooth water. $\tau = 8^\circ$; C_Δ = 27.39 and 36.15.

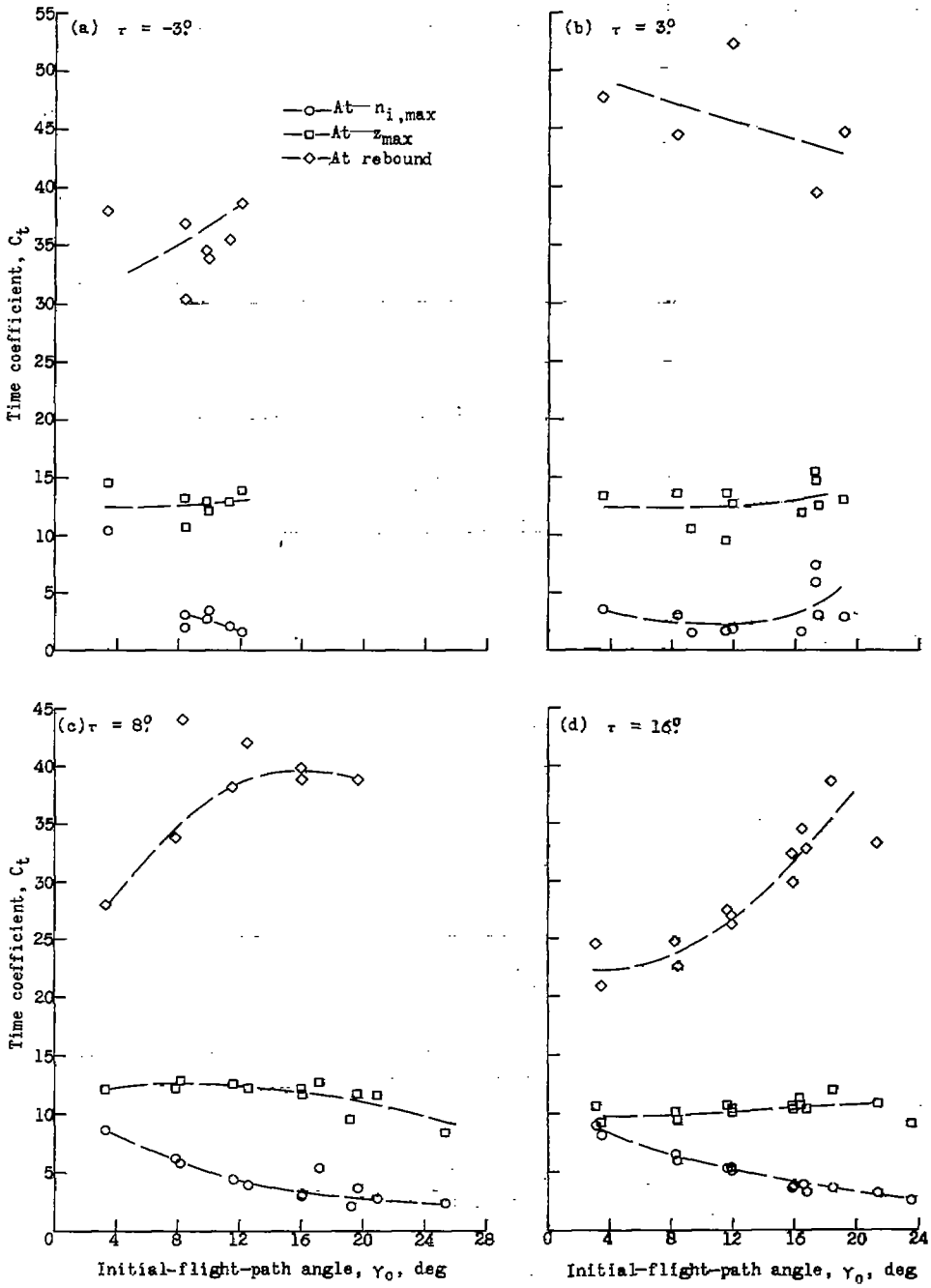

Figure 31.- Experimental variation of time coefficient with initial-flight-path angle for curved-bow model in smooth water. C_Δ = 18.77.

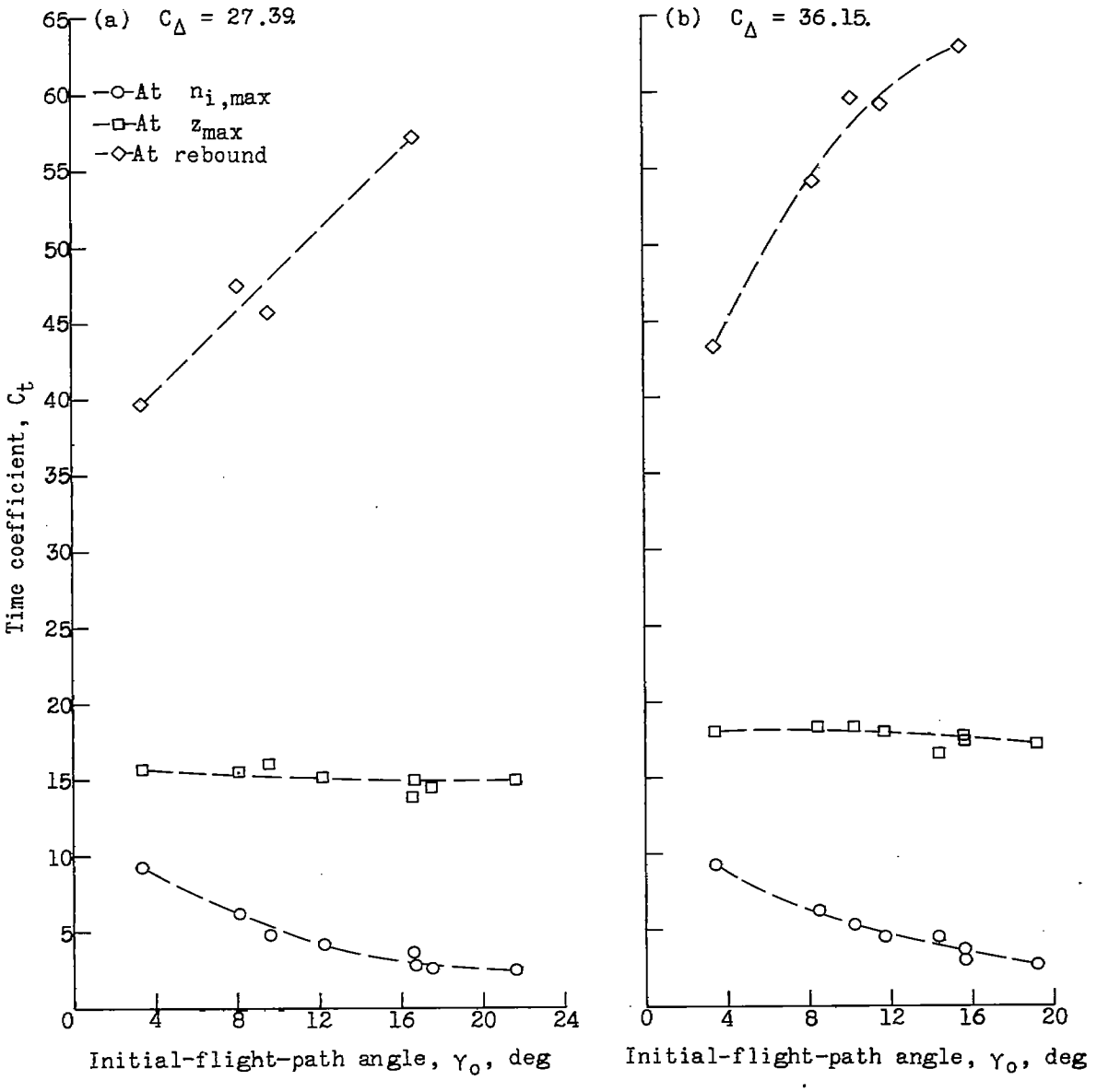

Figure 32.- Experimental variation of time coefficient with initial-flight-path angle for curved-bow model in smooth water. $\tau = 8^\circ$; C_Δ = 27.39 and 36.15.

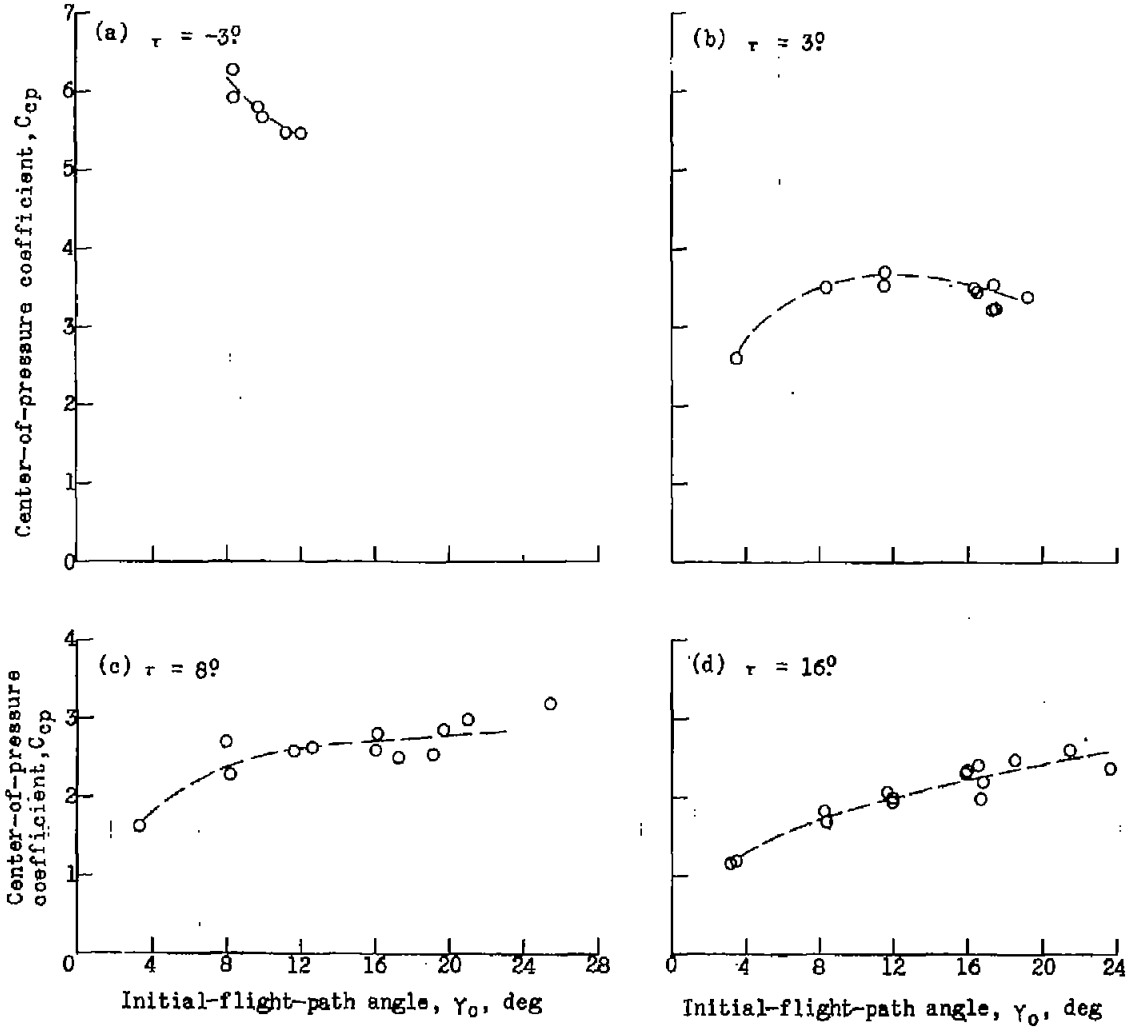

Figure 33.- Experimental variation of center-of-pressure coefficient at $n_{1,max}$ with initial-flight-path angle for curved-bow model in smooth water. $C_\Delta = 18.77$.

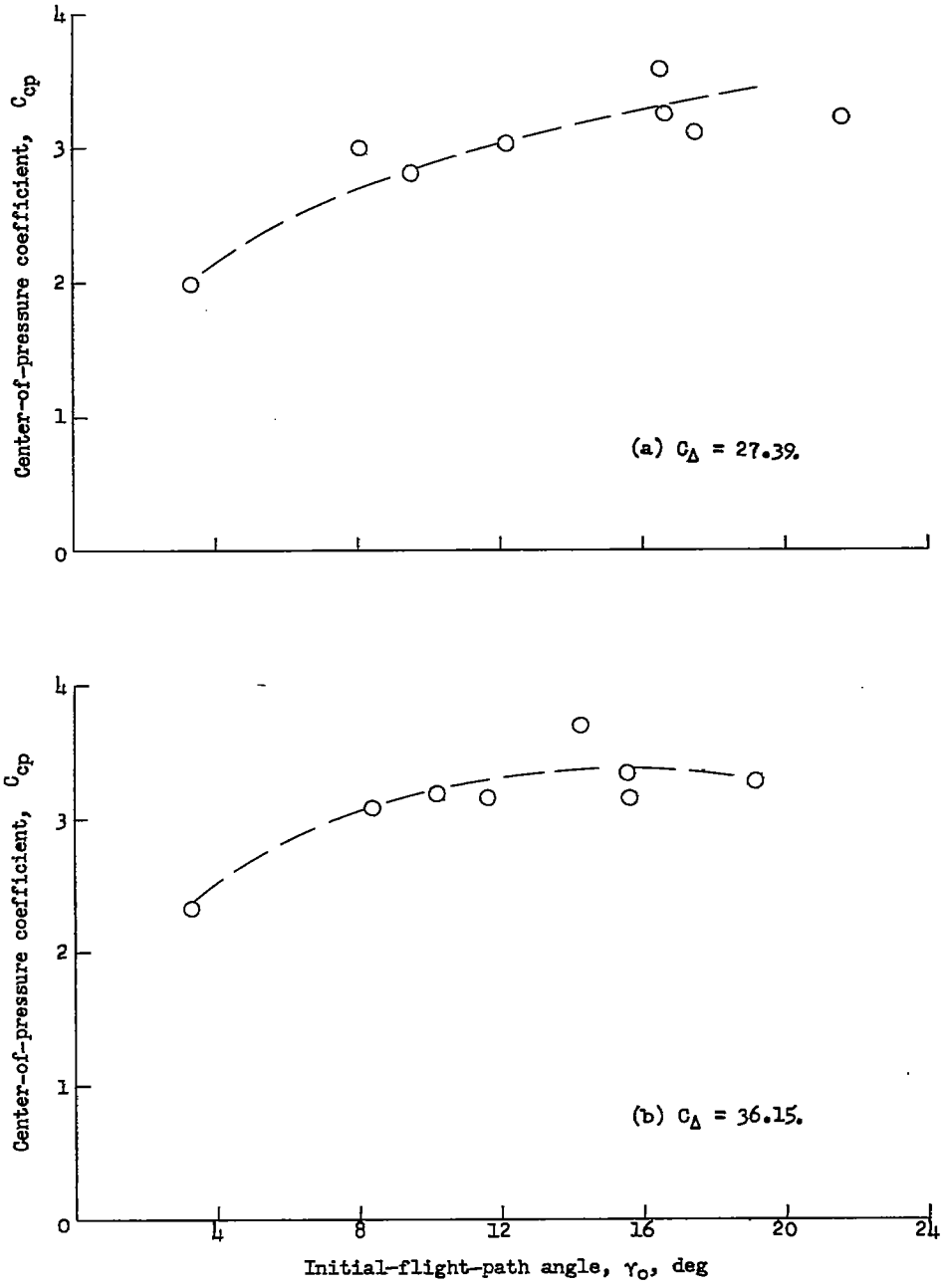

Figure 34.- Experimental variation of center-of-pressure coefficient at $n_{i,max}$ with initial-flight-path angle for curved-bow model in smooth water. $\tau = 8^\circ$; C_Δ = 27.39 and 36.15.

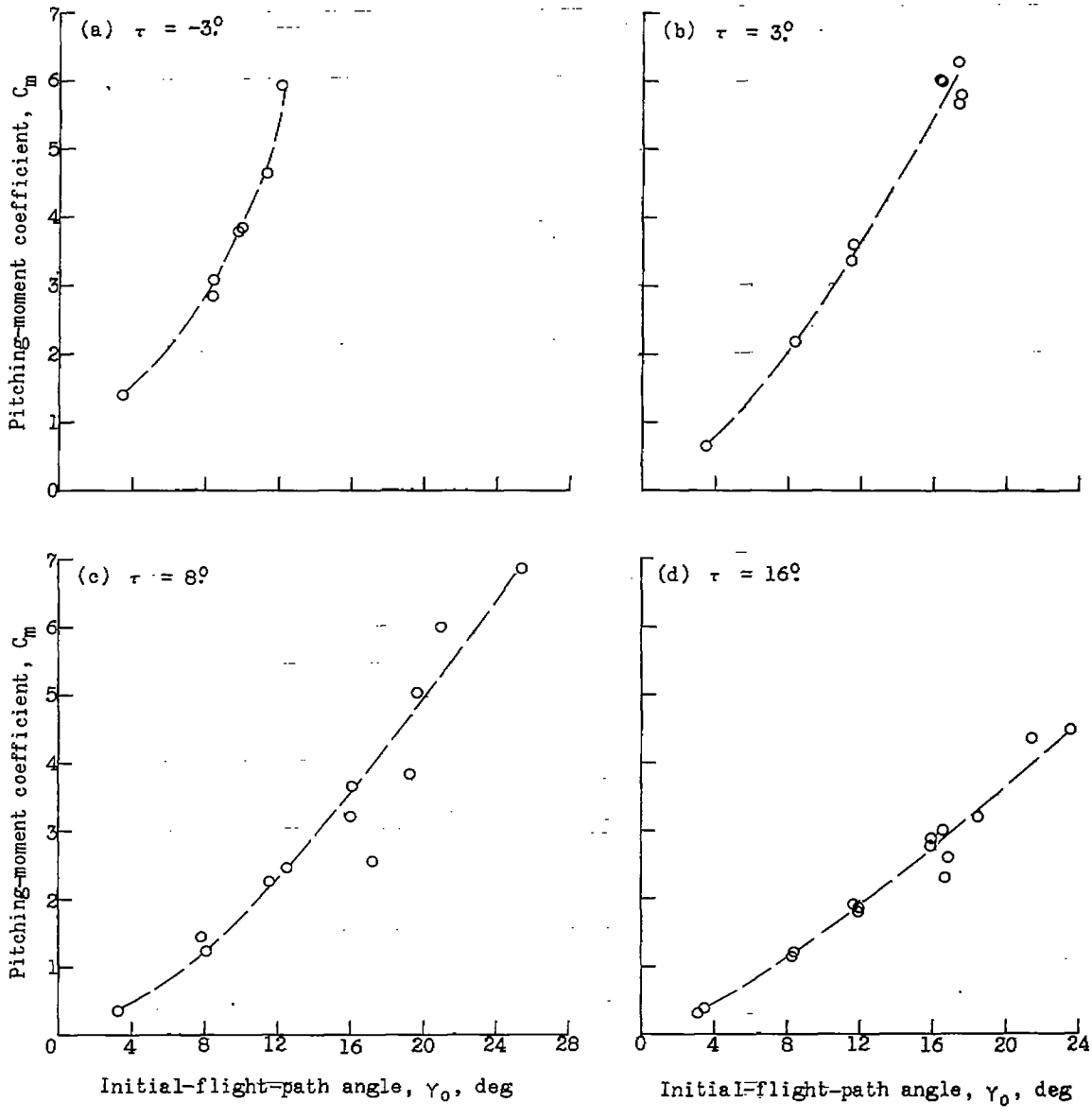

Figure 35.- Experimental variation of pitching-moment coefficient at $n_{i,max}$ with initial-flight-path angle for curved-bow model in smooth water. $C_\Delta = 18.77$.

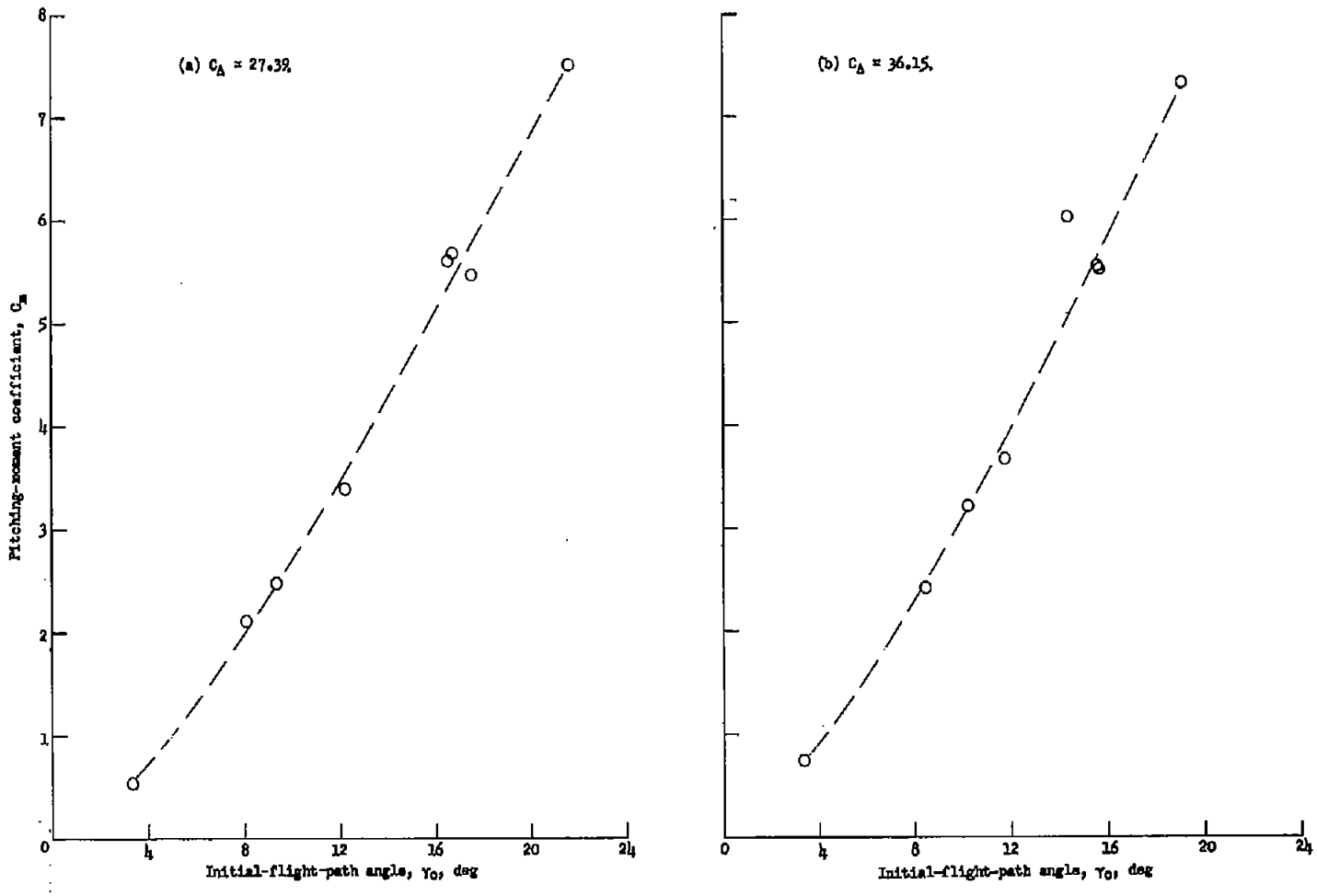

Figure 36.- Experimental variation of pitching-moment coefficient at $n_{i,max}$ with initial-flight-path angle for curved-bow model in smooth water. $\tau = 8^\circ$; $C_\Delta = 27.39$ and 36.15.

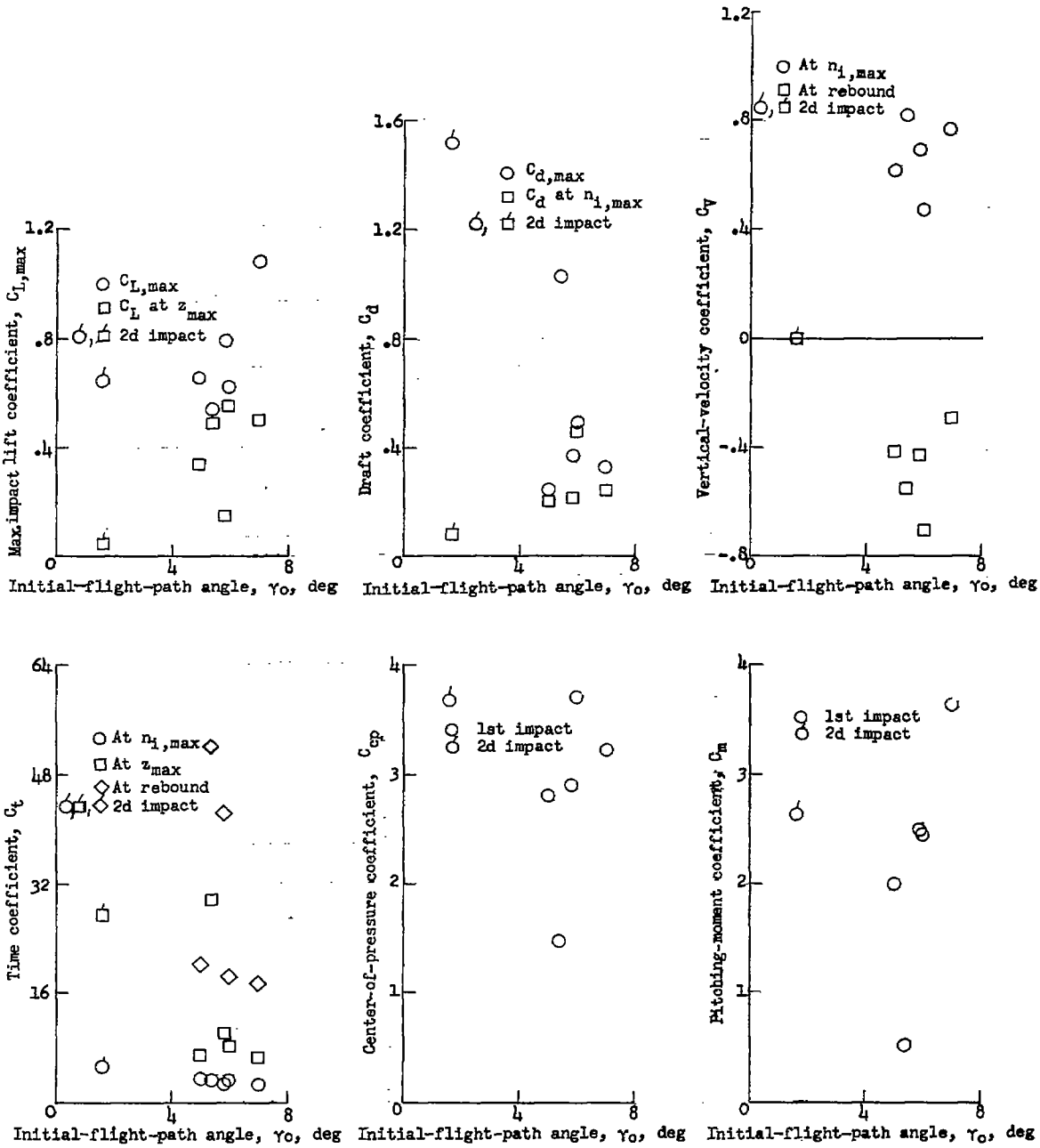

Figure 37.- Variation of the coefficients with initial-flight-path angle for the curved-bow model in rough water. $\tau = 8°$; $C_\Delta = 18.77$.

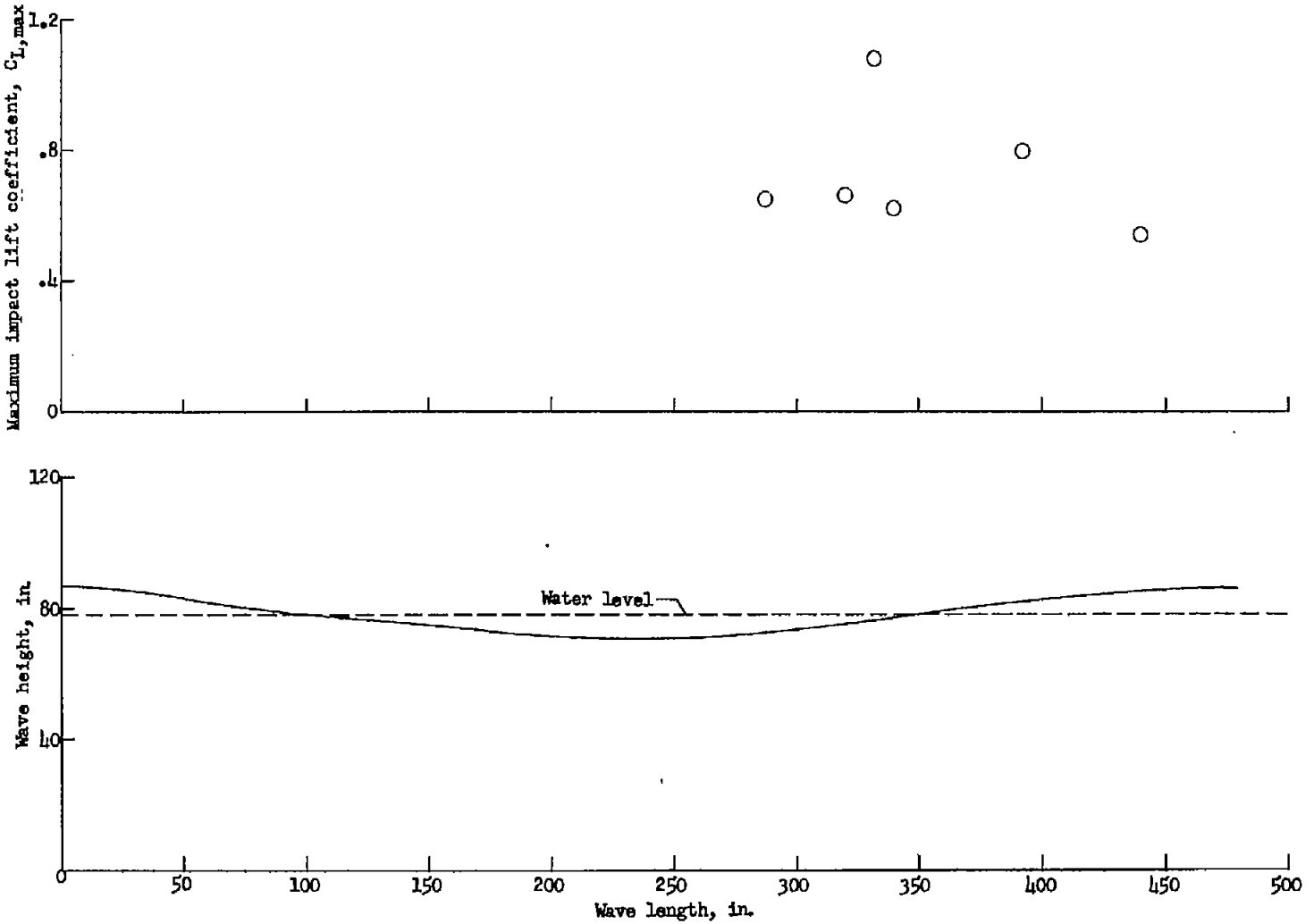

Figure 38.- Variation of maximum impact lift coefficient with location of impact on wave.

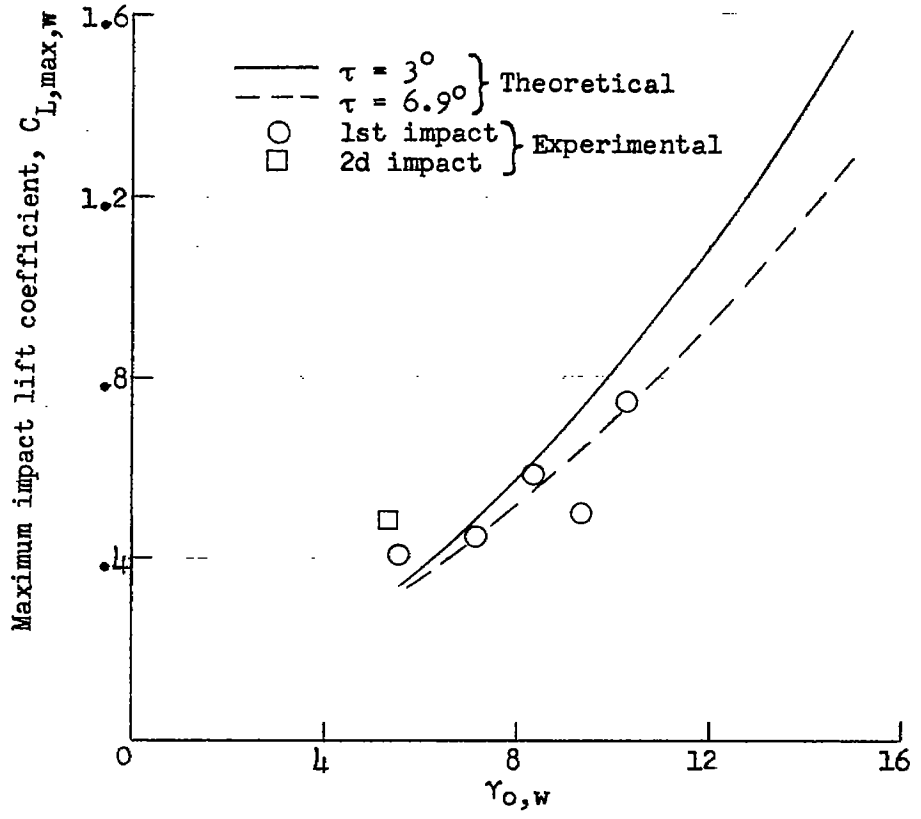

Figure 39.- Variation of maximum impact lift coefficient relative to wave with initial-flight-path angle relative to wave.

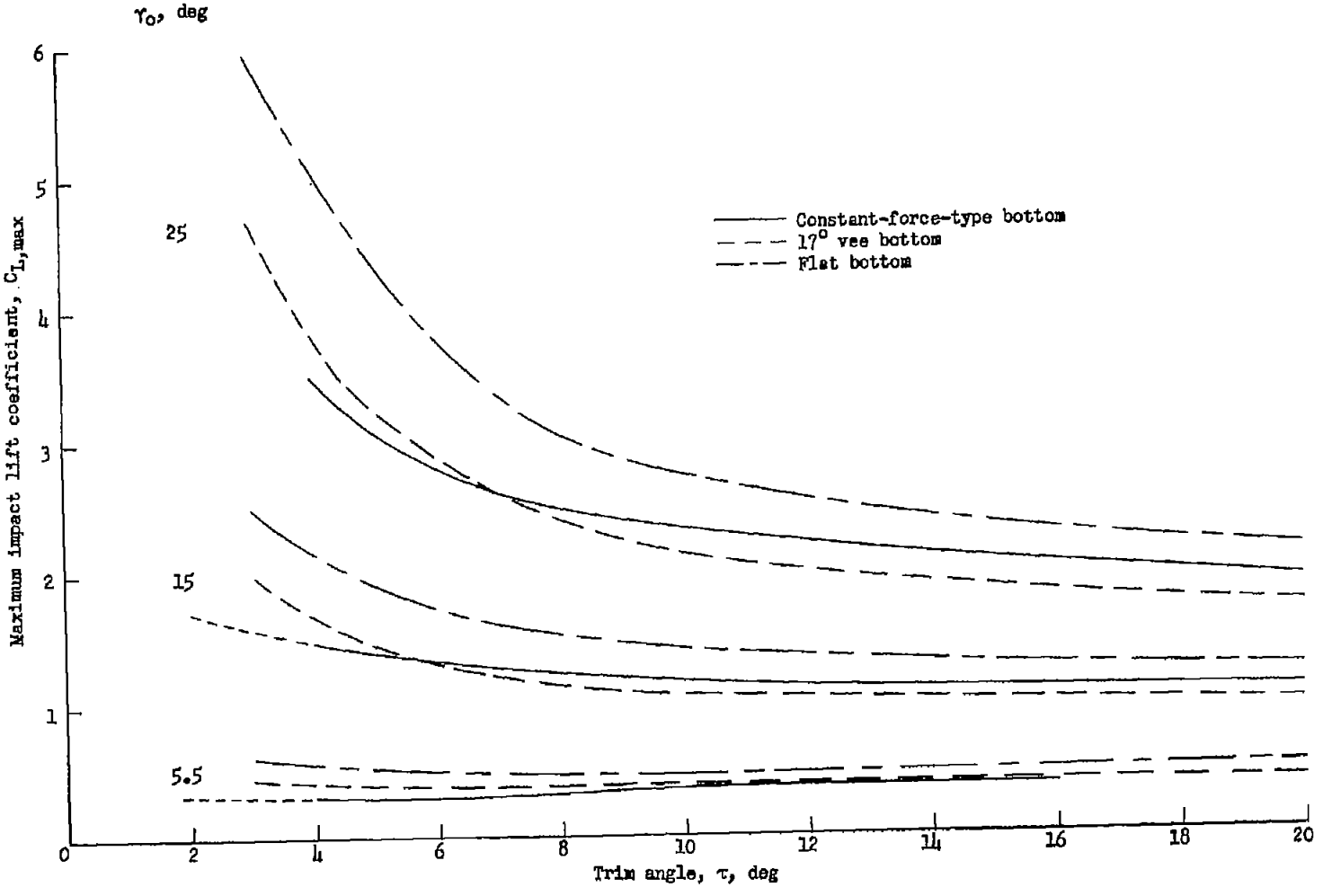

Figure 40.- Theoretical variation of maximum impact lift coefficient with trim angle for the constant-force-type-bottom, vee-bottom, and flat-bottom transverse shapes.

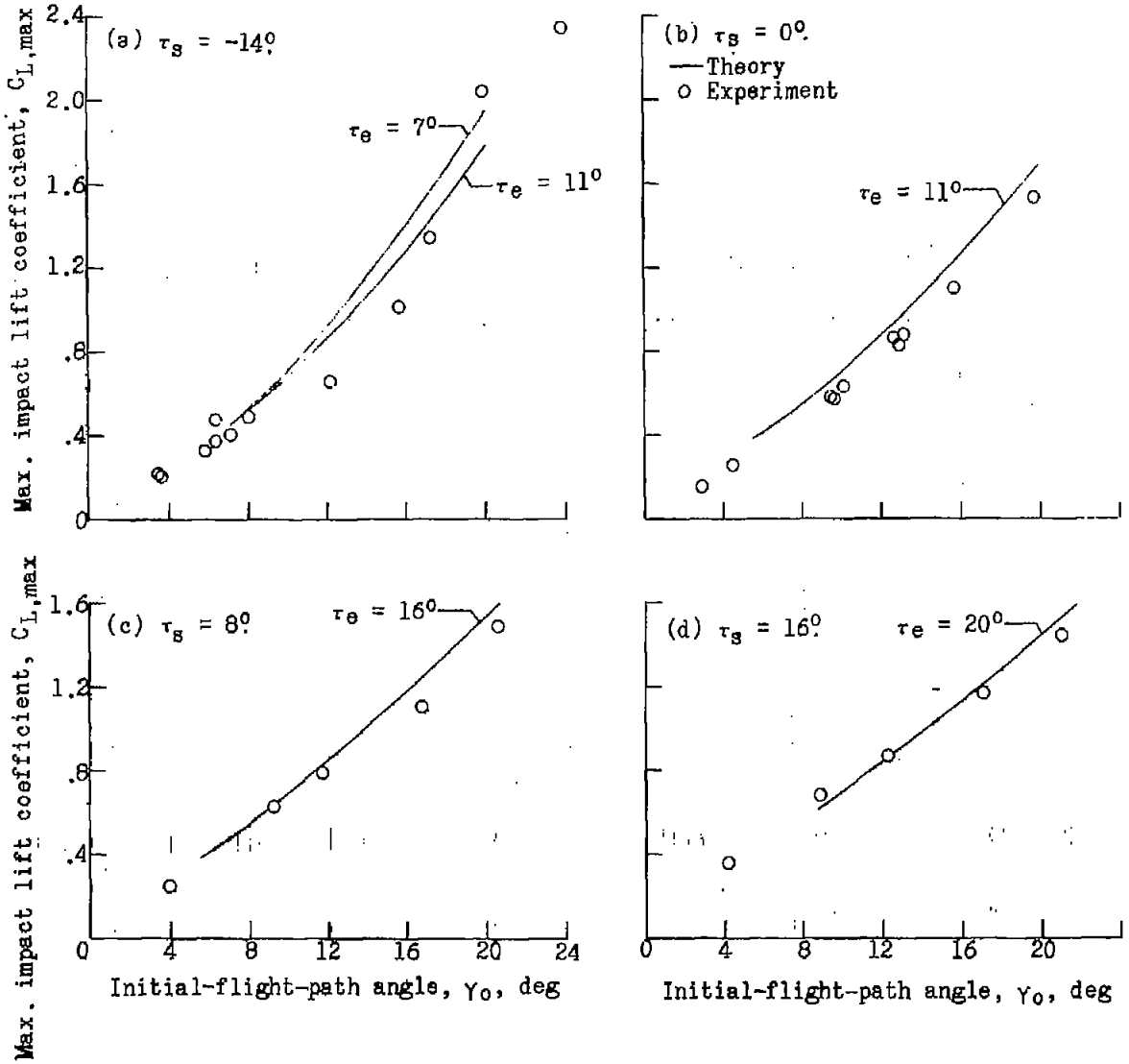

Figure 41.- Comparison of experimental maximum impact lift coefficient with theoretical impact lift coefficient based on an equivalent angle of trim.

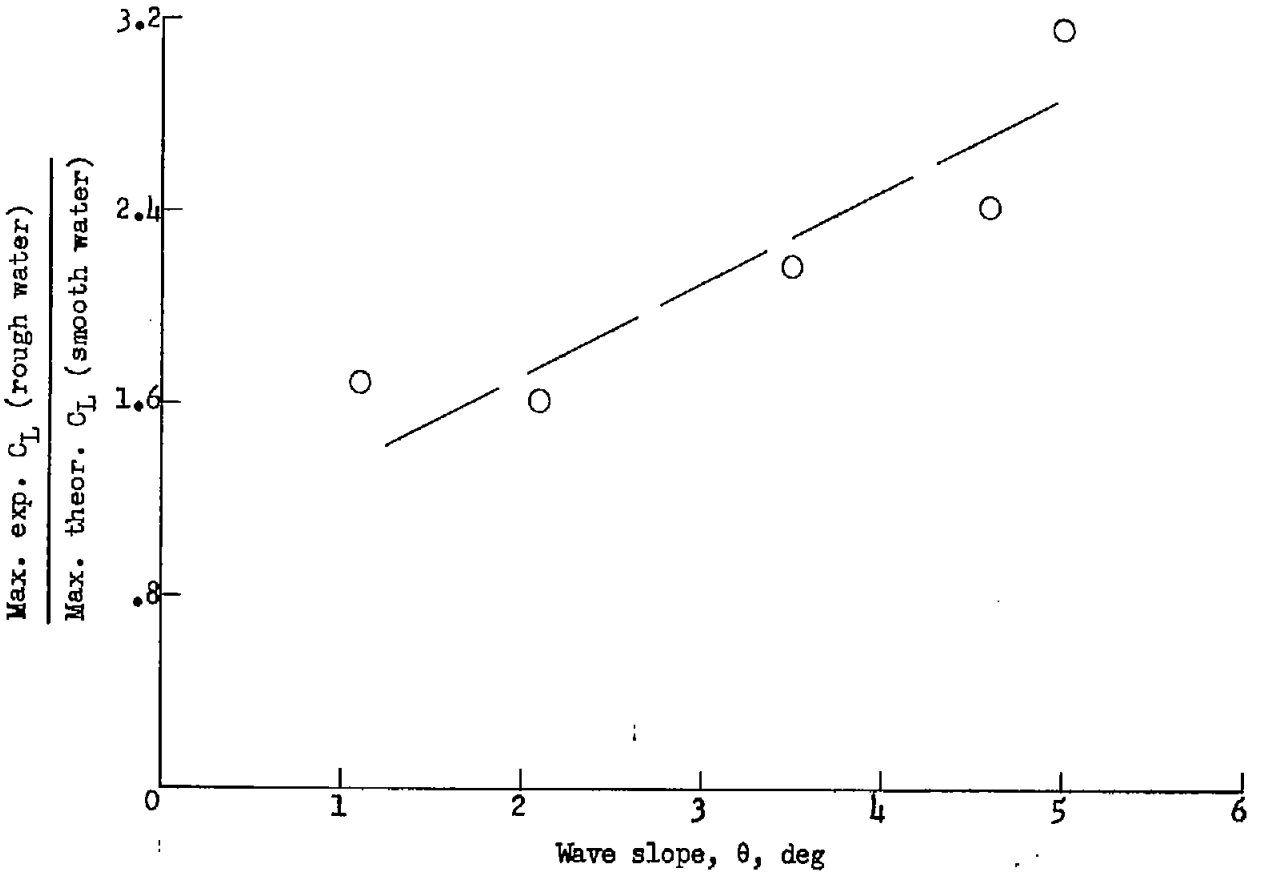

Figure 42.- Variation of the ratio of loads in waves to those in smooth water with wave slope.

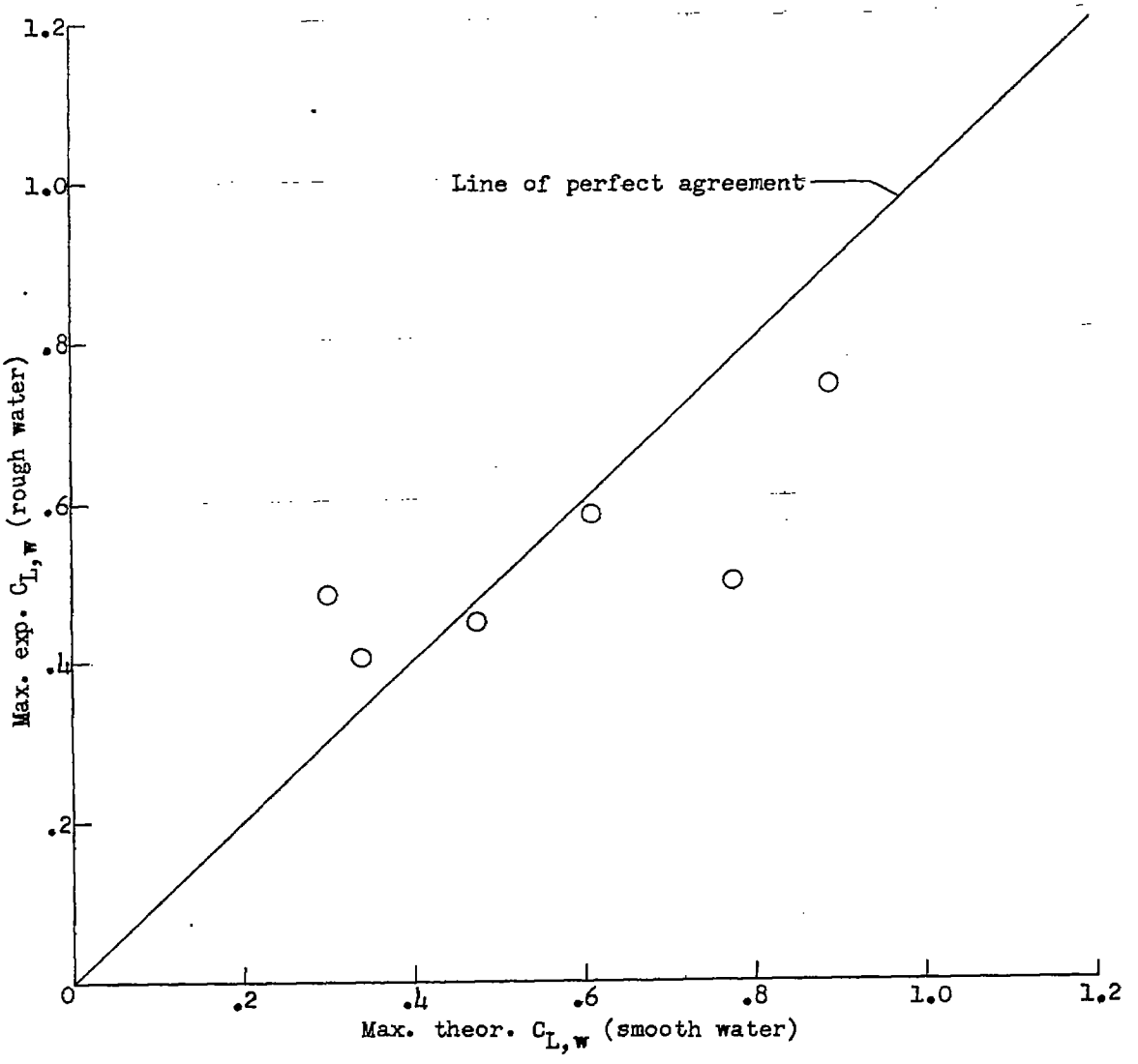

Figure 43.- Comparison of experimental maximum impact lift coefficient with theoretical maximum impact lift coefficient predicted by inclined-axis method.